THE
PHYSICAL REVIEW
A journal of experimental and theoretical physics established by E. L. Nichols in 1893

SECOND SERIES, VOL. 64, NOS. 9 AND 10 NOVEMBER 1 AND 15, 1943

Rotational Analysis of the Emission Spectrum of CuF

L. H. WOODS
Ryerson Physical Laboratories, University of Chicago, Chicago, Illinois
(Received August 21, 1943)

The emission spectrum of gaseous HF at pressures of about 0.1 mm in a copper hollow cathode has been examined from 7000 to 2000A and an unknown band spectrum of widely spaced lines lying in the region 2450–2600A thought to be the $^2\Sigma \rightarrow {}^2\Pi$ transition of HF^+ has been found. From the same source the emission spectrum of CuF has been obtained and was photographed on the 30,000-lines-per-inch Chicago grating spectrograph. The spectrum consists of 3 band systems lying at 5700A, 5060A, and 4920A. A rotational analysis of the spectrum has shown the three systems to have the same lower state, and to be of the type $^1\Pi \rightarrow {}^1\Sigma$, $^1\Sigma \rightarrow {}^1\Sigma$, and $^1\Pi \rightarrow {}^1\Sigma$. The constants of these states are given in the following table:

State	Transition	ν_0	B_0 cm^{-1}	D_0 cm^{-1}	r_0(A)	ν_1	B_1	r_1
$C\ ^1\Pi$	$C \rightarrow X$	20,269.62	0.3748	5.06×10^{-7}	1.755			
$B\ ^1\Sigma$	$B \rightarrow X$	19,734.66	0.3700	4.8×10^{-7}	1.769	19769.92	0.3650	1.779
$A\ ^1\Pi$	$A \rightarrow X$	17,556.40	0.3675		1.773			
$X\ ^1\Sigma$			0.3780	5.6×10^{-7}	1.749		0.3734	1.759

The calculated rotational isotope effect has been found to check very well that measured experimentally.

I. INTRODUCTION

THE emission spectrum of CuF was first described by Mulliken,[1] who obtained very weak exposures of the bands by heating CuF_2 in active nitrogen. He inferred that the bands obtained from CuF_2 are emitted by the diatomic molecule CuF, on the basis that (1) the bands of other copper halides are excited from either cupric or cuprous salts, and (2) the vibrational analysis and isotope effects of the bands of the other copper halides indicate them to belong to the diatomic molecules CuX. The vibrational analysis of the absorption spectrum of CuF was published by Ritschl[2] in 1927. He photographed the spectrum from vapor at 2000°C on a seven meter grating, obtaining resolution of the vibrational but not the rotational structure. The spectrum consists of three band systems, whose rotational structure is degraded to the red and whose vibrational structure is degraded to the violet, lying at 5700A, 5060A, 4920A, with increasing intensity in this order, and respectively referred to as A, B, and C. Using the frequencies of the band heads, Ritschl was able to make a vibrational analysis which showed that the B and C systems had the same lower state, and he assumed the A system also to have, an hypothesis supported by the conclusions reached in this paper.

The present study of the CuF bands is a by-product of a search for the emission spectrum of HF, which has been sought unsuccessfully in the past by many experimenters. In the present ex-

[1] R. S. Mulliken, Phys. Rev. **26**, 1 (1925).
[2] R. Ritschl, Zeits. f. Physik **42**, 172 (1927).

FIG. 1. The group of lines around 2500A of the $^2\Pi \rightarrow {}^2\Sigma$ system of HF^+.

periments there has been obtained an unknown spectrum with very widely spaced lines, such as would be emitted by a diatomic hydride molecule. This is thought to belong to HF^+. It lies in the region 2450A–2600A, which agrees well with the position predicted from the location of the known HCl^+ and HBr^+ $^2\Sigma \rightarrow {}^2\Pi$ spectra. The identification is not complete, however, because the spectrum has not been analyzed.

In looking for possible bands of HF, the spectral region from 2000A to 6600A was examined, and in this way were obtained the present photographs of the CuF band system. In these, both the rotational structure and rotational isotope splitting were resolved and the following rotational analysis was made. Previously, the nature of some of the electronic states of CuCl had been deduced by Terrien[3] from the appearance of the emission spectrum. He identified a $^1\Sigma$ ground state and a $^1\Pi$ and a $^1\Sigma$ excited state.

II. EXPERIMENTAL

The spectra were obtained from a small water-cooled hollow cathode made of copper, through which flowed gaseous HF at pressures of about 0.1 mm of mercury. The cathode was run from a 2000 volt d.c. generator at a current of about 0.3 ampere. The anode was insulated from the cathode by a thick glass ring, and the edges where copper met glass were sealed with Apiezon Q wax. The design of the cathode is very like that used by Mrozowski[4] for the HgH^+ and HgD^+ spectra with the exception that (1) there is no long glass sleeve running far down between anode and cathode, (2) the gas is introduced into the cathode through an opening at the end, and (3) the window opening is small. This last condition was necessary because the window of the discharge tube was a small flat crystal of artificial white sapphire (Al_2O_3; alundum) about $1\times1\frac{1}{2}$ mm in size. Its valuable properties, described by Freed, McMurry, and Rosenbaum,[5] are enthusiastically supported by these experiments. After several hundred hours of contact with flowing anhydrous HF gas, although it has been cleaned several times of sputtered copper, the crystal is as clear as glass and shows no corrosion. Its transmitting properties seem equally as good as those of quartz to 2000A, so far as these experiments could detect.

The HF was generated in a copper oven, a tube about $1\frac{1}{2}''$ in diameter and 16″ long, by decomposition of anhydrous KHF_2 at about 275°C according to the equation $KHF_2 \rightarrow KF + HF$. The lower end of the oven was closed with a screwed-in plug of copper and sealed with silver solder. At the upper end, the lid and delivery tube which led to the cathode were sealed with soft solder to facilitate recharging with fresh KHF_2. To prevent this seal from softening when the oven was heated, the seal was water-cooled with a copper coil. The HF gas flowed through the delivery tube, through the cathode, passed through a copper to glass seal, and was condensed in two successive glass traps at liquid nitrogen temperatures. After an exposure the traps were removed and washed with large quantities of water to dissolve and dilute the liquid HF (boiling point =19.5°C). The traps prevented the HF from flowing into the oil and mercury pumps, which were run continuously during the long exposures to prevent accumulation of impurities.

The group of lines around 2500A believed to belong to HF^+ (Fig. 1) was excited only in the

[3] Jean Terrien, Theses, University of Paris, 1937.

[4] S. Mrozowski, Phys. Rev. **58**, 332 (1940).

[5] Freed, McMurry, and Rosenbaum, J. Chem. Phys. **7**, 853 (1939).

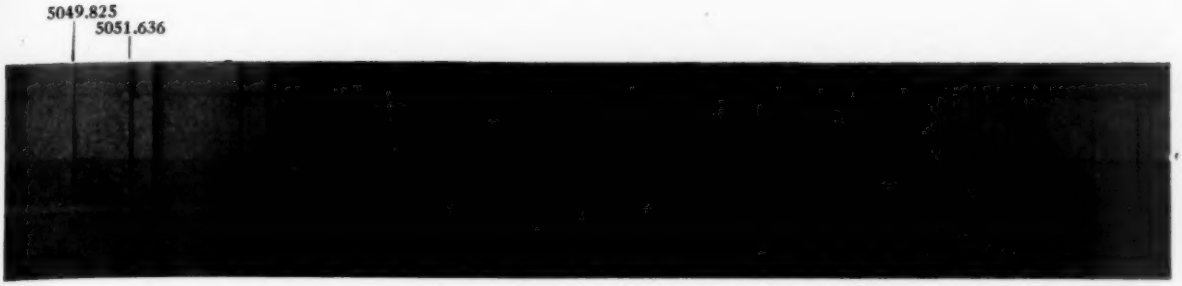

FIG. 2. An enlargement of the $(0'-0)$ and $(1-1)$ bands of the $^1\Sigma \rightarrow {}^1\Sigma$ system at 5060A.

flowing gas. Under these conditions the discharge was deep red with a bluish cast. In stagnant gas the bands of CO, CO_2, and SiF became very strong, the color of the discharge turned blue, and the 2500A band disappeared presumably because the pressure increased and the electrons were slower. The glass ring which insulated the anode from the cathode provided a constant source of SiF, but this impurity was not present in large amounts in the flowing gas. The CuF bands were excited even in the stagnant gas discharge; however under these conditions their analysis was interfered with by many overlapping bands of impurities. The CuF bands were obtained quite free from foreign spectra when excited in the flowing gas. Presence of helium did not increase the intensity of the bands.

TABLE I. $^1\Sigma \rightarrow {}^1\Sigma$ transition of CuF [0→0]. $\nu_0 = 19{,}734.66$.

J	P	R	Pi	J	P	R	Pi
0	—	—	—				
1	19733.89	19736.01		41	19691.01	—	10691.20
2	3.12	6.88		42	89.65		89.88
3	2.36	7.62		43	8.25		8.48
4	1.60	8.25		44	6.80		7.09
5	0.80	8.87		45	5.42		5.69
6	19729.91	19739.48	—	46	19684.03	—	19684.26
7	9.09	40.11		47	2.59		2.80
8	8.22	0.72		48	1.11		1.80
9	7.28	1.37		49	79.66		79.96
10	6.41	1.98		50	8.17		8.42
11	19725.52	19742.55	—	51	19676.70	19752.50bh	19677.01
12	4.60	3.09		52	5.23	—	5.55
13	3.67	3.60		53	3.68		4.03
14	2.70	4.10		54	2.15		2.51
15	1.73	4.61		55	0.62		0.98
16	19720.71	19745.10	—	56	19669.05	—	19669.43
17	19.69	5.60		57	7.53		7.86
18	8.66	6.04		58	5.95		6.31
19	7.65	6.46		59	4.36		4.79
20	6.61	6.87		60	2.77		3.16
21	19715.55	19747.27	—	61	19661.18	—	19661.59
22	4.45	7.66		62	59.54		0.02
23	3.34	8.04		63	7.97	19750.53	58.39
24	2.22	8.40		64	6.27	0.29	6.75
25	1.09	8.76		65	4.65	0.02	5.11
26	19709.96	19749.08	—	66	19652.98	19749.73	19653.45
27	8.93	49.40		67	1.29	9.40	1.80
28	7.62	9.73		68	49.64	9.08	0.15
29	6.41	50.02		69	7.96	8.76	48.51
30	5.23	0.28		70	6.24	8.39	6.85
31	19704.00	19750.53	—	71	19644.51	19748.04	19645.06
32	2.75	—		72	2.83	7.67	3.33
33	1.48			73	1.13	7.27	1.73
34	0.23			74	39.32	6.87	39.91
35	698.92		19699.14	75	7.48	6.46	—
36	19697.60	—	19697.84	76	19635.93	19746.04	—
37	6.36		6.56	77	4.18	5.60	
38	5.03		5.27	78	2.42	5.10	
39	3.75		3.99	79	0.55	4.61	
40	2.36		2.63	80	28.81	4.10	
				81	19626.65	19743.60	—
				82	5.18	3.09	

By use of a slit width of 20 microns, the B and C bands were photographed on Eastman 144-B plates in the first order of the 30-foot Chicago grating. Photographs of these bands in the higher orders could not be obtained because the second and third orders at 5000A are too weak. Unfortunately the A system at 5700A, which is the least intense of the three, fell on the position of the slit, and it was necessary to photograph this band with an older grating which has about one-third the intensity of the new grating. In order to obtain a picture, it was therefore imperative to photograph this band system on Eastman 103-D plates, with a wide slit and a current of 1.6 amperes, but even under these conditions, the photograph obtained, although adequate, is not impressive, and the analysis of this band has consequently suffered.

III. ANALYSIS

B System

The B system at 5060A is a $v'=v''$ vibrational sequence of bands of the type $^1\Sigma \rightarrow {}^1\Sigma$ (Fig. 2). Although Ritschl observed both $v'=v''$ and $v''+1=v'$ sequences in absorption, only the $v'=v''$ sequence appeared in the emission spectrum. Even after a 56-hour exposure, the $v'=v''+1$ sequence did not appear on the plates. The zero gap is clearly visible. $P(J)-P(J-1)$ and $R(J)-R(J-1)$ were plotted along the same

Fig. 3. An enlargement of the C system ($^1\Pi \rightarrow {}^1\Sigma$) at 4920A.

line against J. From the slope of this line, which is equal to $2(B_0' - B_0'')$, was obtained the value $B_0' - B_0'' = -0.00805$ cm^{-1}. The J numbering given here (Table I), which classifies the three unobserved central lines as the true missing line, the $R(0)$ line, and the $P(1)$ line, was assumed correct, with the reservation that it may err by one unit because of the faintness of P and R lines of low J values. From plots of the $\Delta_2 F$ values based on this numbering, the values $B_0'' = 0.3780 \pm 0.0005$ cm^{-1} and $B_0' = 0.3700 \pm 0.0005$ cm^{-1} were obtained. These figures are consistent with the value for $(B_0' - B_0'')$. The value of B_0'' is corroborated by the analysis of system C. For this reason the J numbering as given here is believed to be correct. The only possible alternative J numbering, namely that which increases the J value of each R line and decreases that of each P line by one unit, gives values $B_0'' = 0.3850$ cm^{-1} and $B_0' = 0.3770$ cm^{-1}. From the theoretical relation $D_v = 4B_v^3/\omega_v^2$, and Ritschl's ω_v values, $D_0' = 4.8 \times 10^{-7}$ and $D_0'' = 5.6 \times 10^{-7}$ cm^{-1} were calculated. The slopes of the curves $[R(J-1) - P(J+1)]/(4J+2)$ and $[R(J) - P(J)]/(4J+2)$ plotted against J^2 gave the approximate values $D_0' = 10 \times 10^{-7}$ cm^{-1} and $D_0'' = 11 \times 10^{-7}$ cm^{-1}.

C System

The C system at 4920A is a $v' = v''$ vibrational sequence of bands (Table II) of the type $^1\Pi \rightarrow {}^1\Sigma$ (Fig. 3). The intense band heads are Q branches, the strong edge of each band being the origin of the Q branch. The P branch of the $0 \rightarrow 0$ band is easily traced toward decreasing wave-lengths until it becomes too faint to be seen, but the R branch, which starts with low intensity from the origin, runs through the $1 \rightarrow 1$ P branch into the intense $1 \rightarrow 1$ Q branch overlapped by $2 \rightarrow 2$ P and Q branches. It cannot be traced through this thicket of lines. At approximately $J = 74$ where the Intensity is no longer large, i' is calculated to reach a head which cannot be seen because it is covered by the intense $1 \rightarrow 1$ Q head. The slopes of the two lines $P(J) - P(J-1)$ and $Q(J) - Q(J-1)$ plotted against J gave the values $B_0'(P) - B_0'' = -0.0027$ cm^{-1} and $B_0'(Q) - B_0'' = -0.0037$ cm^{-1}.

TABLE II. $^1\Pi \rightarrow {}^1\Sigma$ transition of CuF ($0 \rightarrow 0$). $\nu_0 = 20{,}269.62$ cm^{-1}.

J	P(cm^{-1})	Q(cm^{-1})	Pi(cm^{-1})	J	P(cm^{-1})	Q(cm^{-1})	Pi(cm^{-1})
8	20263.05	—	—	51	20224.05	20258.58	20224.33
9	2.37			52	3.04	8.21	3.33
10	1.65			53	2.02	7.72	2.27
11	20260.96	—	—	54	0.97	7.36	1.25
12	0.21			55	219.91	6.87	0.17
13	59.41			56	20218.86	20256.48	20219.21
14	8.61			57	7.88	5.99	8.15
15	7.73			58	6.77	5.53	7.13
16	20256.88	—	—	59	5.76	5.01	6.03
17	6.07	—		60	4.72	4.61	4.96
18	5.22	20268.29	—	61	20213.57	20254.05	20213.93
19	4.36	8.07		62	2.52	3.60	2.86
20	3.53	7.89		63	1.41	3.09	1.88
21	20252.63	20267.67	—	64	0.44	2.66	0.73
22	1.80	7.50		65	09.36	2.08	09.65
23	0.90	7.35		66	20208.24	20251.63	20208.68
24	49.99	7.10		67	7.21	1.10	7.49
25	9.10	6.90		68	6.10	0.64	6.41
26	20248.17	20266.65	—	69	4.96	0.04	5.30
27	7.28	6.45		70	3.88	49.63	4.21
28	6.37	6.18		71	20202.76	20248.98	20203.14
29	5.49	5.99		72	1.65	8.79	2.07
30	4.56	5.71		73	0.62	7.88	0.95
31	20243.58	20265.45	—	74	199.50	7.31	199.84
32	2.64	5.14		75	8.39	6.77	8.73
33	1.75	4.91		76	20196.86	20246.22	20197.71
34	0.80	4.54		77	6.21	5.67	—
35	39.83	4.34		78	5.09	5.04	—
36	20238.91	20263.96	—	79	3.98	4.50	—
37	7.93	3.70		80	2.85	4.33	3.22
38	7.00	3.37		81	20191.73	20243.31	20192.01
39	6.00	3.11		82	0.62	2.70	0.90
40	5.05	2.66		83	89.43	2.17	89.82
41	20234.05	20262.43	—	84	8.31	1.51	—
42	3.08	1.99		85	7.23	0.93	—
43	2.09	1.77		86	20186.10	20240.28	—
44	1.11	1.29		87	4.98	39.59	
45	0.12	1.00		88	3.80	—	
46	20229.17	20260.51	—	89	2.56	8.48	
47	8.13	0.20	—				
48	7.09	59.72	20227.31				
49	6.08	9.36	6.40				
50	5.07	8.95	5.30				

Because it was impossible to measure the R branch, the exact Δ_2F's for the lower state could not be obtained independently. But the quantity $Q(J)-Q(J-1)-P(J)-P(J+1)$, which is equal to the $\Delta_2F(J)$ for the lower state plus the quantum defect of the $^1\Pi$ state, was plotted against J for several possible J numberings of the Q and P branches. The slopes of the curves were computed at low J values, where the possible error due to the quantum defect was small, and compared with the slopes of the Δ_2F curves obtained for the two possible J numberings of the 5060A band. In one and only one way of numbering was it possible to get equal slopes for the curves of the two bands, indicating that the J numberings which they represented gave the same B_0'' for the lower states of transitions C and B, and the J numberings thus found are those given here. $\{Q(J)+Q(J+1)-P(J)-P(J+1)\}/(4J+2)$, plotted against J and extrapolated to $J=0$ gave $B_0'(Q)=0.373$ cm^{-1}. $\{Q(J)+Q(J-1)-P(J)-P(J-1)\}/(4J+2)$ similarly treated gave $B_0''=0.3775$ cm^{-1}, in agreement with the value of B_0'' obtained from the analysis of the 5060A $^1\Sigma\rightarrow{}^1\Sigma$ band. One concludes from this value that the two transitions have the same lower state, confirming the results of Ritschl's vibrational analysis. The lower state must be a $^1\Sigma$ state. There are two upper states, a $^1\Pi$ and a $^1\Sigma$, whose separation is 534.96 cm^{-1}.

TABLE III. $^1\Pi\rightarrow{}^1\Sigma$ transition of CuF (0→0). Band head at 17556.40.

J	P(cm^{-1})	Pi(cm^{-1})	J	P(cm^{-1})	Pi(cm^{-1})
1			41	17509.06	17509.44
2	17555.08	——	42	7.57	7.96
3	4.30		43	6.08	6.50
4	3.43		44	4.62	4.97
5	2.49		45	3.08	3.48
6	17551.59	——	46	17501.55	17502.03
7	0.68		47	0.02	0.53
8	49.73		48	498.54	498.97
9	8.81		49	6.96	7.45
10	7.88		50	5.32	5.84
11	17546.94	——	51	17493.91	17494.31
12	5.91		52	2.30	2.81
13	4.88		53	0.76	1.17
14	3.83		54	89.13	89.65
15	2.80		55	7.60	8.11
16	17541.71	——	56	17486.98	17486.44
17	0.54		57	4.40	4.91
18	39.46		58	2.77	3.26
19	8.36		59	1.14	1.71
20	7.16		60	79.51	——
21	17535.96	——	61	17477.91	17478.41
22	4.79		62	6.28	6.77
23	3.53		63	4.69	4.97
24	2.33		64	3.00	——
25	1.07		65	1.44	——
26	17529.79	——	66	17469.75	——
27	8.52		67	8.06	
28	7.16		68	6.40	
29	5.86		69	4.74	
30	4.52		70	3.09	
31	17523.22	——	71	17461.42	——
32	1.85		72	59.73	
33	0.51		73	8.14	
34	19.08		74	6.39	
35	7.72		75	4.71	
36	17516.36	——	76	17453.05	——
37	4.86		77	——	
38	3.39				
39	1.97				
40	0.53	17511.00			

FIG. 4. The A system of CuF at 5690A of the type $^1\Pi\rightarrow{}^1\Sigma$.

From the quantities $B_0'(P)-B_0''=-0.0027$, $B_0'(Q)-B_0''=-0.0037$, and $B_0''=0.3775$ cm^{-1}, the values $B_0'(P)=0.3748$ and $B_0'(Q)=0.3738$ cm^{-1} are readily obtained. Unfortunately, $B_0'(Q)$ differs somewhat from the value obtained by extrapolation given above.

Kronig[6] and Van Vleck[7] have shown that the splitting of the rotational levels caused by the interaction of rotation and electronic motion may be expressed by a term of the form $qJ(J+1)$ where $q=B_0'(P)-B_0'(Q)$. In this case the experimental value of q, the difference of the B's, is 0.0010 cm^{-1}. For the case of Van Vleck's pure precession between a $^1\Pi$ and a $^1\Sigma$ state, the theoretical value of q is given by $q=2B_v^2l(l+1)/\nu(\Pi,\Sigma)$, which in this case has the value 0.0011 cm^{-1}. The experimental value 0.0010 cm^{-1} was tested in the following equation $P(J+1)-Q(J)+2B_0''(J+1)+2D_0''(J+1)^2=qJ(J+1)$ over a

[6] R. de L. Kronig, Zeits. f. Physik **50**, 347 (1928).
[7] J. H. Van Vleck, Phys. Rev. **37**, 733 (1929).

TABLE IV. $^1\Sigma \rightarrow {}^1\Sigma$ transition of CuF (1→1).

J	R(cm^{-1})	P(cm^{-1})	J	R(cm^{-1})	P(cm^{-1})
0	——	——			
1	19771.75	——	16	19780.30	19756.09
2	2.47	——	17	0.79	5.11
3	3.19	19768.11	18	1.23	4.15
4	3.81	6.72	19	1.61	3.06
5	4.42	6.01	20	1.99	——
6	19775.05	19765.13	21	19782.37	——
7	5.79	4.26	22	2.74	
8	6.20	3.47	23	3.12	
9	6.79	2.56	24	3.45	
10	7.29	1.71	25	3.72	
11	19777.87	19760.77	26	19784.08	——
12	8.39	59.90	27	4.36	
13	8.87	8.90	28	4.67	
14	9.36	7.97			
15	9.84	7.08			

range of 80 units of J with satisfactory results. The values $D_0' = 5.06 \times 10^{-7}$ and $D_0'' = 5.60 \times 10^{-7}$ were calculated from the equations $D_0' = 4B_0'^3/\omega_0^2$ and $D_0'' = 4B_0''^3/\omega_0^2$, where $B = \frac{1}{2}B(P) + \frac{1}{2}B(Q)$.

A System

Band *A* at 5690A (Table III) is also of the type $^1\Pi \rightarrow {}^1\Sigma$ (Fig. 4). The band edges are heads of Q branches, but unfortunately the Q lines cannot be measured. At low J values they merge into the gray background which forms the head, and at high J values they are too faint. The R branch, lost in the overlapping lines of the 1→1 and 2→2 transitions, cannot be measured either. The slope of the curve $P(J) - P(J-1)$ plotted against J gives the value of $B_0'(P) - B_0'' = -0.00849$ cm^{-1}. The P branch can be traced close enough to ν_0, whose position is given by the Q head, to fix the J numbering of the lines. The intercept of $P(J) - P(J-1)$ at $J = 0$ gives $B_0'(P) = 0.367$ cm^{-1} and $B_0'' = 0.378$ cm^{-1}, in poor agreement with the more exact value of the difference of the B values given above, but still agreeing within the limits of the experimental error attending this determination. Within the limits of experimental error, then, it may be concluded that all three transitions have the same lower state. Since the R branch has not been obtained for this band it is not possible to check this conclusion by obtaining the $\Delta_2 F$'s and comparing them with those of the 5060A $^1\Sigma \rightarrow {}^1\Sigma$ transition.

B System

Enough of the P and R lines of the 5060A (1→1) vibrational transition (Table IV) have been found to allow the difference of the B values to be obtained: $(B_1' - B_1'') = -0.0084$ cm^{-1}. The J values are not fixed accurately enough to give the B values with certainty, but the quantities $B_1' = 0.3650$ and $B_1'' = 0.3734$ cm^{-1} are probably correct.

The rotational isotope effect in the P branch was calculated from the equation $\Delta P_i(J) = (1 - \rho^2)(B_0' - B_0'')J(J+1) - 2JB_0'$, where $\rho^2 = \mu/\mu_i = 0.99287$, and was found to check very well the experimentally measured isotope splitting within the limits of experimental error of determination of the B's. μ and μ_i are the reduced masses $(m_1 - m_2)/m_1 m_2$ of the molecules $Cu^{63}F^{19}$ and $Cu^{65}F^{19}$, respectively.

ACKNOWLEDGMENTS

The author expresses deepest appreciation to Professor R. S. Mulliken whose keen interest in the progress of this problem and whose many helpful suggestions greatly speeded the progress of the work. Grateful acknowledgment is also made to Dr. S. Mrozowski for his unfailing enthusiasm and generous advice.

PHYSICAL REVIEW VOLUME 64, NUMBERS 9 AND 10 NOVEMBER 1 AND 15, 1943

The Energies of the γ-Rays from Sb^{122}, Cd^{115}, Ir^{192}, Mn^{54}, Zn^{65}, and Co^{60}

C. E. MANDEVILLE*
The Rice Institute, Houston, Texas
AND
H. W. FULBRIGHT
Washington University, St. Louis, Missouri

(Received August 27, 1943)

The energies of the γ-rays emitted in the disintegration of some radioelements have been determined by means of a magnetic spectrograph. The results may be summarized as follows:

Radioelement	Sb^{122}	Cd^{115}	Ir^{192}	Mn^{54}	Zn^{65}	Co^{60}
Quantum energies (Mev)	0.80 ± 0.02	0.65 ± 0.02	0.63 ± 0.02	0.86 ± 0.02	1.14 ± 0.02	1.33 ± 0.03

The quantum energies were obtained from the end points of distributions in momentum of Compton secondaries arising from the several γ-rays. Qualitative results obtained from observations on several other γ-ray emitters are briefly discussed.

INTRODUCTION

THE distributions in momentum of Compton recoils arising from γ-rays emitted in the disintegration of several radioelements have been obtained by coincidence counting in a magnetic spectrograph.[1] From the end points of the distributions, the quantum energies of the γ-rays may be calculated. The Compton recoil method did not resolve the two quanta at 1.10 ± 0.02 Mev and 1.30 ± 0.02 Mev which have been previously reported[2] to be emitted in the disintegration of Co^{60}.

In addition to a specific discussion of measurements on the gamma-radiation emitted by the radioelements given in the title of this paper, some qualitative remarks are also made with regard to radiations from some other radioactive isotopes which were surveyed only briefly.

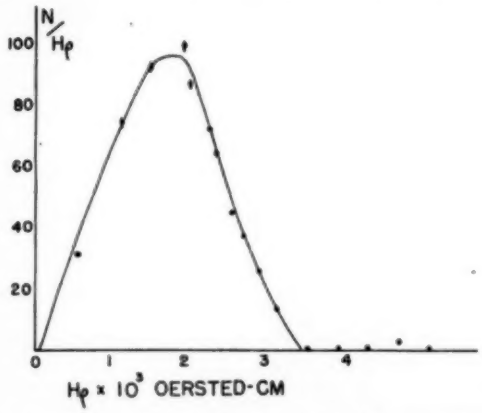

FIG. 1. Momentum distribution of the Compton recoils of the γ-rays from Sb^{122}. This distribution arises from a γ-ray of energy 0.80 ± 0.02 Mev.

Sb^{122}

The gamma-radiation of the 63-hour Sb^{122} has been previously investigated by Mitchell, Langer, and McDaniel.[3] Coincidence absorption experiments by those authors revealed the presence of a γ-ray of energy 0.96 Mev. Their $\beta-\gamma$ and $\gamma-\gamma$ coincidence experiments on Sb^{122} suggested that the γ-ray at 0.96 Mev is the only one emitted in the disintegration of that element. The momentum distribution of the Compton recoils of the γ-rays from Sb^{122} is given in Fig. 1, and the end point of the distribution is found to correspond to a gamma-ray energy of 0.80 ± 0.02 Mev, a somewhat lower value than the previously determined one. From the shape of the curve, it is clear that a single γ-ray is present, confirming in general the conclusions of the Indiana University group.

The Sb^{122} of the curve of Fig. 1 was obtained when pure metallic antimony was irradiated by slow neutrons from the reaction $Be-d-n$ for a period of about 48 hours.

Cd^{115}

Gamma-radiation from Cd^{115} at 0.8 Mev has been reported by Cork and Lawson,[4] employing

* At present at the Radiation Laboratory, the Massachusetts Institute of Technology, Cambridge, Massachusetts.

[1] C. E. Mandeville, Phys. Rev. **62**, 309 (1942); **63**, 387 (1943).

[2] M. Deutsch and L. G. Elliott, Phys. Rev. **62**, 558 (1942).

[3] A. C. G. Mitchell, L. M. Langer, and P. W. McDaniel, Phys. Rev. **57**, 1107 (1940).

[4] J. M. Cork and J. L. Lawson, Phys. Rev. **56**, 241 (1939).

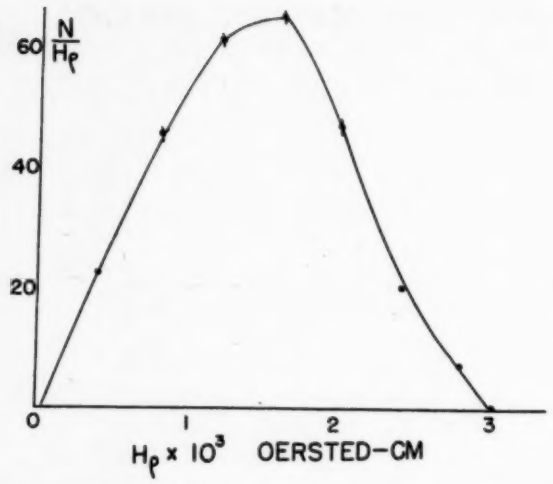

FIG. 2. Momentum distribution of the Compton recoils of the γ-rays from Cd^{115}. The energy of the γ-ray is 0.65 ± 0.02 Mev.

the method of cloud chamber recoils. Later cloud chamber and absorption experiments by Lawson and Cork[5] resulted in the value 0.55 Mev. The momentum distribution of the Compton recoils of the γ-rays from Cd^{115} is given in Fig. 2. The end point of the distribution corresponds to a quantum energy of 0.65 ± 0.02 Mev. The Cd^{115} of Fig. 2 was produced by an irradiation of pure metallic cadmium by slow neutrons. Observations were begun about sixty hours after cessation of bombardment, and the ordinates of the curve of Fig. 2 appeared to decay with a half-period between fifty-four and sixty hours, in good agreement with other values[4, 6] obtained for the half-period of Cd^{115}.

Ir^{192}

Pure metallic iridium was irradiated by slow neutrons. The sixty-day Ir^{192} was found to be produced with great intensity. The momentum distribution of the Compton secondaries arising from the γ-rays emitted in the disintegration of Ir^{192} is given in Fig. 3. The shape of the distribution is characteristic of a single γ-ray, and the energy taken from the end point is 0.63 ± 0.02 Mev. It was also observed that γ-rays of low energy (less than 0.5 Mev) and high intensity are emitted by the sixty-day iridium. γ-rays of an energy less than 0.5 Mev are not measurable with the spectrograph.[7] The presence of the intense radiation of low energy is not inconsistent with the view that isomeric transitions may be occurring in iridium.[8]

[5] J. L. Lawson and J. M. Cork, Phys. Rev. **57**, 982 (1940).
[6] M. Goldhaber, R. D. Hill, and L. Szilard, Phys. Rev. **55**, 47 (1937).

Mn^{54}, Zn^{65}, and Co^{60}

The distributions in momentum of the Compton recoils of the γ-rays emitted in the disintegration of Mn^{54}, Zn^{65}, and the five-year Co^{60} are given in Figs. 4, 5, and 6. The energies of these γ-rays were found to be 0.86 ± 0.02 Mev, 1.14 ± 0.02 Mev, and 1.33 ± 0.03 Mev, respectively. The energies of these γ-rays have been previously measured by the group at the Massa-

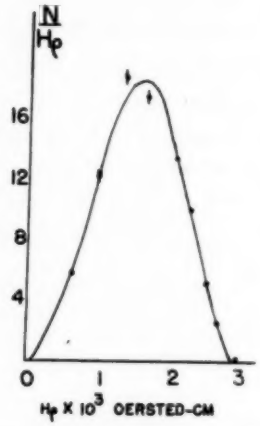

FIG. 3. Momentum distribution of the Compton recoils of the γ-rays from Ir^{192}. The quantum energy is 0.63 ± 0.02 Mev.

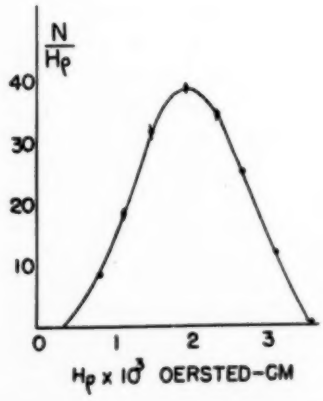

FIG. 4. Momentum distribution of the Compton recoils of the γ-rays from Mn^{54}. The energy of the γ-ray is 0.86 ± 0.02 Mev.

[7] C. E. Mandeville, Phys. Rev. **64**, 147 (1943).
[8] E. McMillan, M. Kamen, and S. Ruben, Phys. Rev. **52**, 375 (1937).

chusetts Institute of Technology,[2,9,10] and our results are in good agreement with the values obtained by them. It is to be noted that the Compton recoil method does not resolve the two γ-rays[2] at 1.10±0.02 Mev and 1.30±0.02 Mev emitted in the disintegration of Co^{60}.

OTHER MEASUREMENTS

Observations begun about 48 hours after cessation of bombardment seemed to indicate that Sm, Nd, Os, and Ge, when irradiated by slow neutrons, emitted gamma-radiation of too low an energy or too low an intensity to be measured by the spectrograph. The twenty-hour Re^{188} was produced when ReO_2 was irradiated by slow neutrons. A γ-ray of low intensity and of energy about 0.8 Mev appeared to be emitted in the disintegration of Re^{188}. A γ-ray of low intensity and of energy about 1.35 Mev appeared to be associated with the nineteen-hour Ir^{194}.

Prevailing conditions unfortunately did not permit a continuation of the study of radiations from these various radioelements. The results mentioned in this section are therefore to be regarded as only tentative.

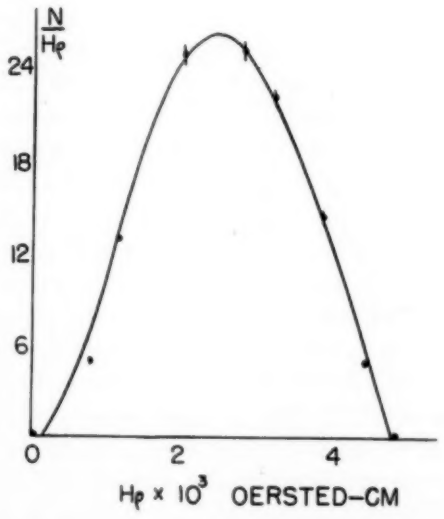

FIG. 5. Momentum distribution of the Compton recoils of the γ-rays from Zn^{65}. The quantum energy is 1.14±0.02 Mev.

[9] M. Deutsch and A. Roberts, Phys. Rev. **60**, 362 (1941); M. Deutsch, A. Roberts, and L. G. Elliott Phys. Rev. **61**, 389 (1942).

[10] L. G. Elliott and M. Deutsch, Phys. Rev., to be published in near future.

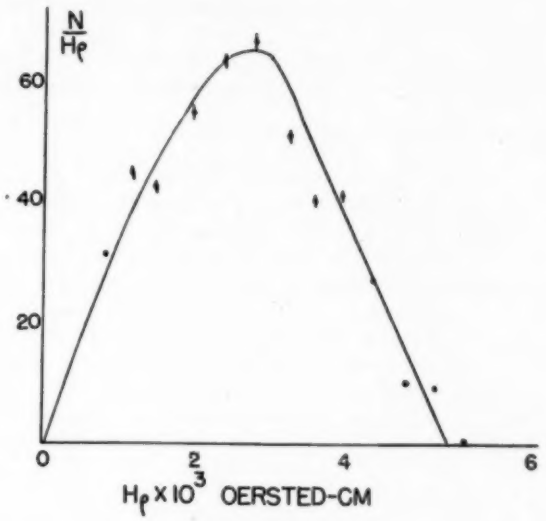

FIG. 6. Momentum distribution of the Compton recoils of the γ-rays from the five-year Co^{60}. The quantum energy is 1.33±0.02 Mev. The two γ-rays previously reported at 1.10±0.02 Mev and 1.30±0.02 Mev were not resolved by the Compton recoil method.

ACKNOWLEDGMENTS

The writers wish to acknowledge the interest in these experiments of Professor A. L. Hughes of Washington University, St. Louis, Missouri, and Professor H. A. Wilson of the Rice Institute. We wish also to express appreciation for the preparation of many of the radioactive sources by the members of the Washington University cyclotron group. The sources of radioactive Mn^{54}, Zn^{65}, and Co^{60} were very kindly sent to us by Dr. Martin Deutsch of the Massachusetts Institute of Technology.

ADDED NOTE

The γ-rays from the sixty-day Ir^{192} have been recently studied by Dr. Martin Deutsch of the Massachusetts Institute of Technology. With the magnetic lens spectrometer, photoelectric lines were observed corresponding to γ-rays of energies 0.307 Mev, 0.467 Mev, and 0.603 Mev. The γ-ray of energy 0.603 Mev (reported in this paper at 0.63±0.02 Mev.) appeared to be less intense than the two softer γ-rays.

The source used in the measurements with the magnetic lens spectrometer was also employed by us.

Disintegration Schemes of Radioactive Substances. V. I^{130}

A. ROBERTS,* L. G. ELLIOTT,** J. R. DOWNING,*** W. C. PEACOCK, AND M. DEUTSCH
Massachusetts Institute of Technology, Cambridge, Massachusetts

(Received July 26, 1943)

The disintegration of I^{130} was studied by spectrometer and coincidence techniques. The decay proceeds by two modes of negatron emission of maximum beta-ray energy 0.61 ± 0.02 Mev and 1.03 ± 0.02 Mev, respectively. The high energy spectrum represents 60 ± 10 percent of the disintegrations and is accompanied by three gamma-rays of energies 0.537 ± 0.005 Mev, 0.667 ± 0.008 Mev, 0.744 ± 0.010 Mev. The low energy spectrum is accompanied by these same three gamma-rays and, in addition, by a gamma-ray of energy 0.417 ± 0.005 Mev. The coefficients of internal conversion in the K shell are 0.0031, 0.0038, 0.0069, 0.012, (±20 percent) in order of decreasing gamma-ray energy. The conversion in the L shell is much smaller. It is shown that the Fermi plot of the complex spectrum can be separated into straight lines which may be extrapolated to obtain the correct disintegration energies.

INTRODUCTION

THE radioactive species of iodine of 12.6 hour half-life, obtained by bombarding tellurium with protons or deuterons, is definitely assigned to I^{130} because it is produced by fast neutron bombardment of the single stable isotope of cesium, Cs^{133}. The only previous published results on the radiations from this species were the absorption measurements of Livingood and Seaborg[1] and the cloud-chamber observations of Tape.[2] The former gave 1.05 Mev and 0.6 Mev for the beta- and gamma-ray energies, respectively, while Tape reported 0.83 Mev and 0.59 Mev, respectively.

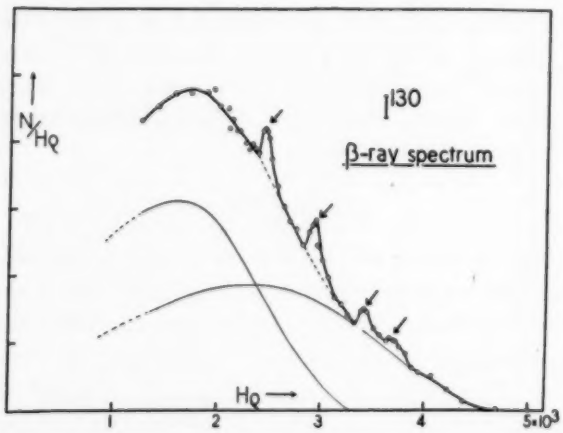

FIG. 1. The beta-ray spectrum of I^{130}. Arrows mark internal conversion lines.

We have studied the radiations and the disintegration scheme of I^{130} by means of the methods described in the preceding papers of this series.[3] A brief report on some preliminary results was presented before the Physical Society.[4] The present paper extends, and in some details supersedes those results.

Radioactive iodine has been produced and used in this laboratory extensively, particularly for experimental and clinical studies of iodine metabolism, using both tracer and therapeutic irradiation doses.[5] The 12.6 hour species has been used largely for radiation treatment. It is important for the proper calculation of dosage to have a full knowledge of the radiations emitted. For this reason I^{130} was chosen as one of the activities to be studied in this series.

When tellurium is bombarded with deuterons, at least four radioactive species of iodine are formed, with half-lives of 25 minutes, 12.6 hours, 8 days, and 13 days.[1] In the case of the bombarding energy used in the Massachusetts Institute of Technology cyclotron (about 11.5 Mev when these experiments were performed), for thick targets, and for bombardments of a few hours duration, the 25-minute activity becomes

* Now at the Massachusetts Institute of Technology Radiation Laboratory.
** Now with the Radiological Committee, Canadian National Research Council, Montreal.
*** Now at National Research Corporation, Boston.
[1] J. J. Livingood and G. T. Seaborg, Phys. Rev. **54**, 775 (1938).
[2] G. F. Tape, Phys. Rev. **56**, 965 (1939).
[3] Phys. Rev. **60**, 470; 544 (1941); **61**, 672, 686 (1942); **62**, 3 (1942). They will be referred to by the roman numerals I to IV.
[4] J. R. Downing, M. Deutsch, and A. Roberts, Phys. Rev. **61**, 389 (1942).
[5] E.g., S. Hertz, A. Roberts, J. H. Means, and R. D. Evans, Am. J. Physiol. **128**, 565 (1940).

negligible about four hours after the end of the bombardment. At that time about 10 percent of the disintegrations are due to the 8-day species I^{131}, about one percent is due to the 13-day species I^{126}, and the rest to I^{130}. These percentages refer to the number of disintegrations. The activity ratios as observed on most instruments, except those with very thin windows tend to overestimate the amount of I^{130} because of the higher beta-ray energy and the larger number of gamma-rays per disintegration. No trace[1] of the 4-day positron activity reported to be due to I^{124} was found although it might be expected to be formed both by (d, n) and $(d, 2n)$ reactions if the assignment is correct. It was necessary to correct all measurements for effects due to radiations from I^{131}, which are well understood (paper III), and, occasionally for the effects of the 13-day activity.

A. Preparation of Sources

Tellurium was bombarded in the form of cobalt telluride by the circulating beam of the Massachusetts Institute of Technology cyclotron. Iodine was separated from the targets by distillation from a nitric acid solution. Since the sources used usually consisted of a small fraction of very strong preparations (about ten millicuries), used for therapeutic doses, and since only a total amount of about one-half milligram of iodine was used as inactive carrier in the separation, the specific activity was always very satisfactory for all purposes.

Beta-ray sources were prepared by evaporating a small drop of active NaI solution on a microscope cover slip or a flake of mica on which a drop of dilute $AgNO_3$ solution had been deposited previously.

Gamma-ray sources for the study of secondary electron spectra were obtained by sealing active NaI or AgI into suitable brass or copper capsules.

All measurements were made within 24 hours of the separation. The decay of each source was followed for several days in order to correct for the longer period activities.

B. The Beta-Ray Spectrum

The beta-ray spectrum obtained in the short lens spectrometer, corrected for long period radiations, is shown in Fig. 1. Besides the continuous spectrum there appear four weak internal conversion lines (marked with arrows). When the K binding energy of Xe is added to the energies of these lines, the following gamma-ray energies are obtained:

0.416 ± 0.005 Mev, 0.538 ± 0.007 Mev,
0.665 ± 0.008 Mev, 0.747 ± 0.010 Mev.

These values are in excellent agreement with

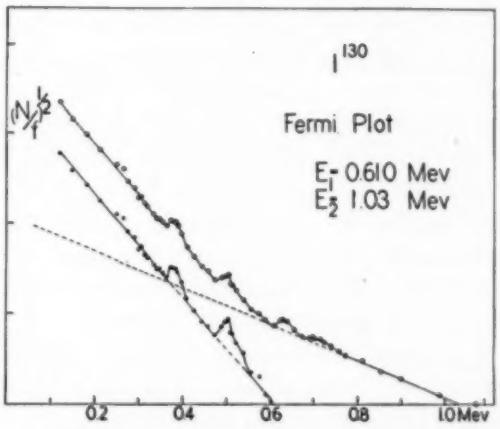

FIG. 2. Fermi plot of the beta-ray spectrum of I^{130}.

the values previously obtained by us from secondary electron spectra.[6]

These conversion lines will be further discussed below, but it should be pointed out here that the heights of the lines appearing in Fig. 1 do not represent the true intensities of the conversion lines, because of the correction for momentum interval, applied to the spectrum.

The shape of the continuous spectrum indicates that it is complex. Indeed, when the data are plotted as a "Fermi plot" the resulting curve (Fig. 2) clearly breaks into two straight lines, indicating two spectra of maximum energies 0.61 ± 0.02 Mev and 1.03 ± 0.02 Mev, respectively. These two spectra are indicated in Fig. 1. The areas under the two curves are very nearly equal. The low energy spectrum represents 53 ± 10 percent of all the disintegrations. The energy difference between the two end points appears to be 0.42 ± 0.02 Mev. The splitting of the Fermi plot into straight lines is not necessarily significant since it is known that at least

[6] M. Deutsch and A. Roberts, Phys. Rev. **60**, 362 (1941).

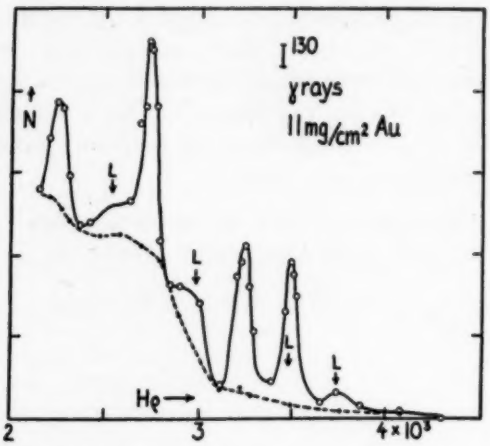

FIG. 3. Typical photoelectron spectrum due to gamma-rays of I^{130}. Dotted line indicates background due to recoil electrons from brass capsule.

some spectra do not show a simple Fermi distribution.[7] However, it will appear in the further discussion that in the case of I^{130} this procedure is almost certainly justified. It will be noted immediately that the energy difference between the two beta-ray spectra corresponds, well within the probable error, to the energy of the 0.417-Mev gamma-ray found in the internal conversion spectrum. We shall show further on that this agreement is significant and that the gamma-ray corresponds to a transition between the two levels to which beta-ray transitions take place.

The slightly larger energy difference between the two end points of I^{130} reported previously[4] was due to the fact that the earlier data were obtained with the spectrometer adjusted for lower resolution. Ordinarily this does not affect the study of continuous spectra very seriously, but in this case the presence of four unresolved internal conversion lines led to an apparent change in the slope of the Fermi plot.

C. The Gamma-Ray Spectrum

The gamma-rays from the disintegration of I^{130} were investigated by studying the energy distribution of secondary electrons produced in various radiators. The spectrometer and the general technique used are the same as in the previous papers of this series and in our preliminary report on gamma-ray energies.[6] However certain improvements in technique now permit greater resolution, and an investigation of the effects of radiator thickness allows us to estimate relative intensities of various gamma-rays with some accuracy.

Figure 3 shows a typical secondary electron spectrum obtained with a gold radiator of 11.0 mg/cm² thickness placed on top of the relatively thick brass capsule containing the active material. Only the energy range 0.35 Mev to 0.80 Mev is shown because no gamma-rays were found outside this range. Similar curves were obtained with various thicknesses of gold and lead radiators. The points marked by full circles in Fig. 3 were obtained without any radiator except the brass capsule itself. It should represent the background of Compton electrons on which the photoelectron lines are superimposed. However it was necessary to normalize the data obtained without radiator to those obtained with gold because of the different intensity of the Compton groups in the two cases.[8]

The lines shown in Fig. 3 correspond to gamma-rays of energies 0.417 ± 0.008, 0.535 ± 0.010, 0.670 ± 0.013, 0.740 ± 0.015 Mev.

The difference in energy of the two highest energy lines is very nearly equal to the difference between the K and L binding energies of gold so that the L photoelectrons due to the 0.667-Mev gamma-ray are hidden by the K photoelectrons due to the 0.744-Mev gamma-ray. This complication was avoided in another experiment by using a tin radiator. Since the results thus obtained did not reveal any different information than was obtained by the use of gold radiators, they are not presented here. In order to obtain the relative intensities of the gamma-rays, it is necessary to subtract the number of Compton recoil electrons from the data of Fig. 3 and to correct the heights of the photoelectron lines for the effect of finite radiator thickness. The procedure for this correction will be published in a separate paper dealing with spectrometer technique. In the case of the 0.744-Mev gamma-ray, the height of the line must also be corrected for the presence of the L photoelectrons

[7] E. J. Konopinski and G. E. Uhlenbeck, Phys. Rev. 60, 308 (1941).

[8] L. G. Elliott, M. Deutsch, and A. Roberts, Phys. Rev. 63, 386 (1943).

due to the 0.667-Mev gamma-ray. Figure 4(A) shows the relative heights of the K photoelectron lines thus corrected. The curve marked "τ" shows the variation of the photoelectric cross section with energy in this region, obtained from Gray's empirical formula,[9]

$$\log \tau = \text{const.} + \log \lambda + 0.48(\log \lambda)^2.$$

It should be noted that the energy scale in Fig. 4(A) represents the energy of the photoelectrons from the K shell rather than the energy of the gamma-rays.

As is easily seen in Fig. 4(A), the three high energy gamma-rays are of equal intensity (within the experimental error), but the 0.417-Mev gamma-ray is only about half as intense as the others. The value of its intensity, deduced from Fig. 4(A) is 0.3 ± 0.1 of the average intensity of the other three gamma-rays. The relatively large probable error is due to the fact that all of the corrections mentioned above are comparatively large for this gamma-ray.

D. Coincidence Studies

Observations of coincidences between radiations from I^{130} are complicated somewhat by the necessity for correcting all measurements for the effects due to the longer lived activities. These corrections must be determined separately for each source since the ratio of the several activities varies somewhat from target to target.

Figure 5 shows the number of beta-gamma coincidences per recorded beta-ray as a function of the amount of absorbing material between source and beta-ray counter. The data are corrected for chance and cosmic-ray coincidences, for long period radiations, for gamma-rays recorded in the beta-ray counter, and for gamma-gamma coincidences. For most of the points the corrections are fairly small. The gamma-ray counter used in these measurements was a platinum screen cathode type counter described in paper III, but the geometry used was slightly different.

Figure 5 shows that the fraction of the beta-rays which causes coincidences is independent of beta-ray energy above about 0.6 Mev. This means that all beta-rays having more than this energy are accompanied—at least on the average—by the same gamma-rays or at least by gamma-rays for which the gamma-ray counter has the same total detection efficiency. Similarly, the rise in the fractional coincidence rate as more absorber is removed shows that some of the beta-rays of less than 0.6-Mev energy are accompanied by gamma-rays of greater total detection efficiency; i.e., either by a greater number or by more energetic gamma-rays.

Coincidences between gamma-rays were measured in an experimental arrangement in which their number could be directly compared with the number of beta-gamma coincidences, as shown in Fig. 6. In this arrangement we observed $(2.93 \pm 0.15) \times 10^{-3}$ beta-gamma coincidence per recorded high energy (above 0.6 Mev) beta-ray and $(2.57 \pm 0.2) \times 10^{-3}$ gamma-gamma coincidence per recorded gamma-ray, after all corrections. The large ratio of gamma-gamma to beta-gamma fractional coincidence rate signifies—even without any knowledge of the efficiency

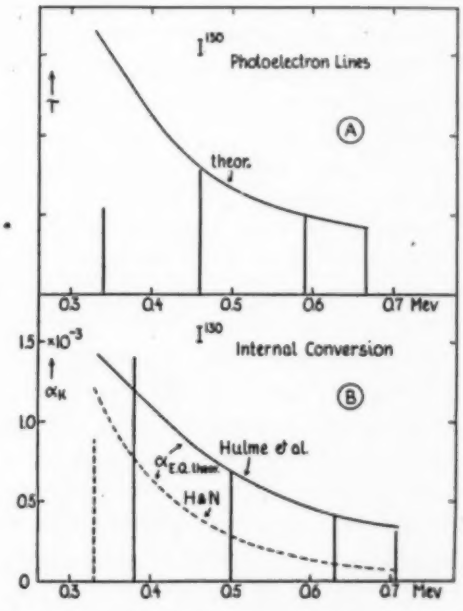

FIG. 4. (A) Relative intensity of photoelectron groups due to gamma-rays of I^{130}. Curve shows variation of photoelectric cross section according to Gray's formula. (B) Internal conversion coefficients for I^{129} (solid) and I^{131} (dotted). Curves show theoretical values for electric quadrupole transitions. Energy scale refers to electron (not gamma-ray) energies.

[9] L. H. Gray, Proc. Camb. Phil. Soc. **27**, 103 (1931). This formula is in close agreement with the theoretical results of Hulme *et al.*, Proc. Roy. Soc. **149**, 131 (1935). It was derived for lead. However the effect of the slight difference of atomic number between gold and lead should be only a small change in the value of the constant.

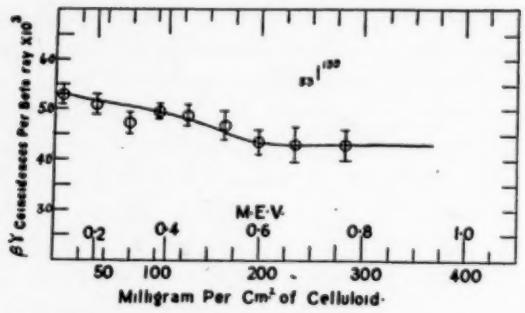

FIG. 5. Beta-gamma coincidences per recorded beta-ray as a function of beta-ray absorber.

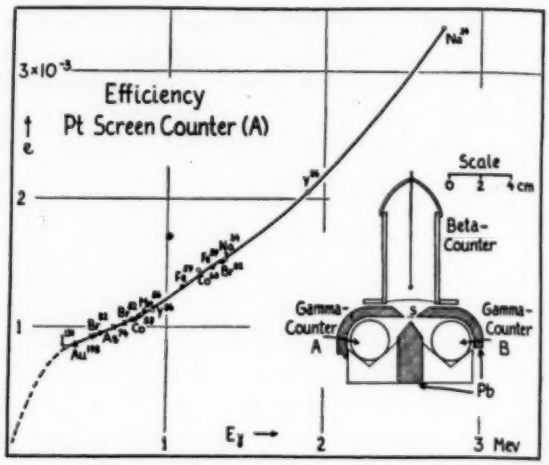

FIG. 6. Net efficiency of gamma-ray counter. Crosses show gamma-rays of I^{130}. For calibration points see papers I–IV, also reference 10. Dotted part of curve is doubtful. Insert: Experimental arrangement used.

of the gamma-ray counter—that either (a) the majority of the beta-rays is accompanied by several (more than two) gamma-rays, or (b) a large fraction of all the gamma-rays is emitted in cascade transitions *unaccompanied by beta-rays*. The latter alternative cannot be excluded a priori since I^{130} could decay by orbital electron capture to Te^{130} as well as by negatron emission to Xe^{130}, or the emission of some of the gamma-rays might be delayed.

The two possibilities may be distinguished without any assumptions concerning the disintegration scheme. The number of beta-gamma coincidences per recorded beta-ray gives the probability of detecting, in the gamma-ray counter, any of the gamma-rays accompanying an average beta-ray. On the other hand the total number of beta-rays emitted by a given source may be determined since the efficiency of our beta-ray counters is fairly well known from previous results on other substances. By multiplying this total number of beta-rays by the detection efficiency for gamma-rays found from the coincidence rate, we can predict the number of gamma-ray counts due to *the gamma-rays accompanying the beta-rays*. If the number of gamma-ray counts actually observed is greater than this predicted number, some of the gamma-rays must be emitted in processes not accompanying the beta-rays. Actually it was found that the number of gamma-rays emitted by I^{130} agreed with the predicted number within the experimental uncertainty of about 10 percent.

Fortunately the fact that the efficiency of the gamma-ray counter for radiations of the energies involved is known allows an independent determination of the number of gamma-rays accompanying each beta-ray. Figure 6[10] shows the efficiency (including geometrical factors) as a function of gamma-ray energy as determined from known disintegration schemes. From this curve, each point of which should be reliable to a few percent, we obtain the following values for the efficiencies of the counter for the gamma-rays of I^{130}, in order of increasing gamma-ray energy:

$$\epsilon_1=0.90\times10^{-3},\quad \epsilon_2=0.95\times10^{-3},$$
$$\epsilon_3=1.02\times10^{-3},\quad \epsilon_4=1.06\times10^{-3}.$$

From these values we may conclude that whatever the exact disintegration scheme of I^{130} may be, each high energy beta-ray is accompanied by three gamma-rays and that each gamma-ray is accompanied, on the average, by more than two and less than three other gamma-rays.[11] The fact that the efficiency varies so little in this energy range makes these conclusions particularly reliable.

E. The Disintegration Scheme

The complexity of both the beta- and gamma-

[10] For calibration points see: Phys. Rev. **62**, 558 (1942); **63**, 219, 321, 386 (1943).

[11] For complex disintegration schemes the formula for the gamma-gamma coincidence rate (papers II and III) becomes

$$N_{\gamma\gamma}/N_\gamma=\Sigma_k\,(a_k\Sigma_{ij}\,\epsilon_i\epsilon_j)/\Sigma_k\,(a_k\Sigma_i\,\epsilon_i),$$

where the a_k are the fraction of the disintegrations proceeding by the kth mode and the summations over i and j are carried out for the gamma-rays accompanying this mode. A similar formula holds for the beta-gamma coincidences, the ϵ_i being replaced by the efficiency of the beta-ray counter for the various beta-ray spectra.

ray spectra indicates that the disintegration of I^{130} must follow a more complicated scheme than any yet discussed in this series. Both the Fermi plot (Fig. 2) and the coincidence data (Fig. 5) indicate clearly that the beta-decay leads to two levels in the product nucleus, differing in energy by about 0.42 Mev. There are two ways in which the four gamma-ray energies could be arranged to give a scheme consistent with this separation. If the high energy spectrum were accompanied by a 0.416 Mev and a 0.537-Mev gamma-ray in cascade and the low energy spectrum by a 0.667-Mev and a 0.744-Mev gamma-ray, an energy balance could be obtained just within the combined experimental errors of the energy determinations. On the other hand all energy measurements are in excellent agreement with the scheme shown in Fig. 7 in which the high energy spectrum is accompanied by the three gamma-rays of higher energies and the low energy spectrum by the same and in addition by a 0.416-Mev gamma-ray. The decision between the two possible schemes is readily made by considering the beta-gamma coincidence rate, as discussed in the preceding section. It was shown there that each high energy beta-ray is accompanied by *three* gamma-rays, consistent with the scheme shown in Fig. 7, but not with the alternative scheme mentioned above. In fact, the fractional coincidence rates predicted by the scheme of Fig. 7 are $N_{\beta\gamma}/N_\beta = 3.03\times10^{-3}$ and $N_{\gamma\gamma}/N_\gamma = 2.54\times10^{-3}$ compared with the experimental values of 2.93×10^{-3} and 2.57×10^{-3}, respectively, showing excellent agreement. For the alternative scheme the predicted rates would be 1.85×10^{-3} and 0.98×10^{-3}, respectively. Finally, the relative intensities of the gamma-rays are consistent only with the scheme of Fig. 7, since the 0.416-Mev gamma-ray is only half as intense as any one of the other three gamma-rays. We are therefore led to conclude that the scheme shown in Fig. 7 represents the main modes of disintegration of I^{130}. Other rare processes may, of course, have escaped detection. However, the emission of high energy gamma-rays in "cross-over" transitions between the several levels of Xe^{130} cannot occur in more than about 7 percent of the disintegrations, if at all, since the spectrometer observations as well as absorption measurements over a wide range of thickness of lead absorber failed to show any sign of higher energy gamma-rays. Also the number of gamma-gamma coincidences is quite sensitive to such transitions.

An attempt was made to verify the proposed disintegration scheme directly by a modification of the method used to determine the conversion coefficient of the 0.367-Mev gamma-ray of I^{131} (paper III). According to the proposed scheme conversion electrons due to the 0.417-Mev gamma-ray should coincide only with the soft beta-ray spectrum. Measurements were made of coincidences between these conversion electrons, focused in the spectrometer and beta-rays recorded in a counter placed behind the source, with and without absorber between source and counter. The results were consistent with the proposed disintegration scheme, i.e., such coincidences were not found when only high energy beta-rays were admitted to the counter. However the conversion coefficient is so low and the number of gamma-rays accompanying both the continuum and the conversion electrons is so large that the background of chance and beta-gamma coincidences is large compared with the number of conversion line-beta coincidences and the statistical counting error of the results almost completely masks the effect studied.

While the location of the 0.416-Mev gamma-ray in the disintegration scheme appears quite certain, the order of emission of the other three gamma-rays is not known, and the particular order shown in Fig. 7 is entirely arbitrary.

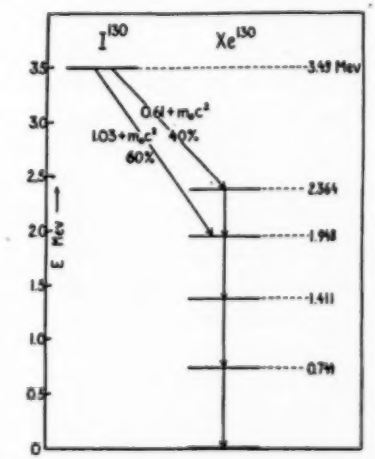

FIG. 7. Disintegration scheme of I^{130}. Arrangement of the first two excited states is in doubt since the order of emission of the gamma-rays involved is not known.

Although it has been shown in Section D that orbital electron capture accompanied by gamma-rays does not occur with appreciable abundance, the possibility of orbital electron capture leading directly to the ground state of Te^{130} remains. A search for Te x-rays expected to accompany such a process was undertaken by means of an argon-filled counter. No x-ray activity was found to decay with the 13-hour period although very intense x-radiation was found to be emitted by an activity of longer life, probably the 13-day I^{126}. Since we have, as yet, no measurement of the efficiency of our counter for x-rays of this wave-length, we cannot set a definite upper limit to the possible abundance of orbital electron capture leading to the ground state of Te^{130}, but if it does occur at all, it is certainly considerably less frequent than negatron emission.

F. Conversion Coefficients

Because of the difficulties pointed out in the preceding section, it was not possible to determine the coefficients of internal conversion directly by the coincidence method used for I^{131} (paper III) with sufficient accuracy. Therefore we followed the usual procedure of comparing the actual number of conversion electrons in each line with the total number of beta-rays obtained by integrating the distribution shown in Fig. 1. In order to perform this integration, it is necessary to know the mean width of the transmitted momentum band. In this case this width was about three percent of the momentum. It is also assumed that the Fermi theory gives the correct shape of the spectrum at low energies. Any error in the ratio introduced by this assumption would be small. The number of electrons counted in each line should, of course, *not* be divided by the momentum as is done in the case of the continuous distribution. The data shown in Fig. 1 were so divided, and the height of the peaks appearing in that figure is not a true measure of the internal conversion.

In Fig. 4(B) the vertical lines indicate the observed conversion coefficients for the gamma-rays of I^{130}. The dotted line indicates the conversion coefficient for the 0.367-Mev gamma-ray of I^{131} (paper III).

Besides counting errors and errors in the integration of the beta-ray spectrum, the ejection of photoelectrons from the source material might introduce an error of several percent.

The coefficients of internal conversion shown in Fig. 4(B) are 12×10^{-3}, 6.9×10^{-3}, 3.8×10^{-3}, 3.1×10^{-3} in the order of increasing energy.

The solid curve shows the internal conversion coefficients obtained from the calculations of Hulme *et al.*[12] for electric quadrupole transitions, in which we assume α to vary as Z^3. The dotted line was computed from the non-relativistic calculations of Hebb and Nelson,[13] which are, however, probably not applicable in this case. The rather close agreement between theory and experiment should not be considered unduly significant until more accurate calculations are available for this range of Z. However, the fact that the conversion coefficients of all four gamma-rays fall on a smooth curve of the general shape predicted by theory suggests that all of the transitions are of the same type. Some considerations presented in the next section indicate that if this is true, they are probably all electric quadrupole transitions.

The conversion in the L shell is too weak to be detected in our experiment, in agreement with all theories.

G. Discussion

With exception of the order of emission of the higher energy gamma-rays, the disintegration scheme of I^{130} (Fig. 7) may be considered well established. The relative probabilities of the two beta-ray transitions have the largest probable error of the various features—their ratio being uncertain to about 15 percent. The most interesting feature of the scheme is the fact that the highest excited state involved decays by the emission of four successive gamma-rays with no observed cross-over transition. This is the longest chain of cascade transitions observed so far, at least in induced radioactivities. Also this is the second case in which it has been shown that the extrapolation and separation of the Fermi plot leads to the correct assignment of energy levels in the product nucleus even for forbidden

[12] H. R. Hulme, N. F. Mott, F. Oppenheimer, and H. M. Taylor, Proc. Roy. Soc. **A155**, 315 (1936).
[13] M. H. Hebb and E. Nelson, Phys. Rev. **58**, 486 (1940).

spectra.[14] The first case (Fe^{59}), discussed in paper IV involved much lower beta-ray energies and nuclei of much lower atomic number. A third case[15] (Mn^{56}) will be discussed in a subsequent paper of this series.

It is customary at this point to propose angular momenta for the various states involved in the disintegration. While this is only of doubtful value it may be worth while to show that it is possible to make assignments which are consistent with the few known selection rules, even in this relatively complicated disintegration.

The ground state of Xe^{130} probably has no angular momentum since this nucleus consists of an even number of protons and an even number of neutrons. If we admit that the only selection rules governing gamma-ray emission concern angular momenta and parity, then we find that the minimum possible angular momentum values are 1, 1, 2, 3, for the successive excited states. With this arrangement all of the gamma-rays would be electric dipole radiation, and no electric dipole cross-overs would be allowed. However, electric quadrupole and magnetic dipole radiations could cause cross-overs, and it is thought that these types of radiation are about equally probable as dipole radiation. It is possible to construct a scheme in which the angular momenta are 1, 2, 3, 4, and the parity assignments such that the radiations would be alternately electric dipole and electric quadrupole or magnetic dipole radiations. In this scheme the lowest multipole orders that can cause cross-over transitions are magnetic quadrupole or electric octupole radiations. Such a scheme would, however, probably show a different behavior of the conversion coefficients than is actually observed. If we specify that all of the transitions should be of the same type (electric quadrupole and/or magnetic dipole) and that no cross-overs involving lower multipole orders than electric 2^4 pole or magnetic octupole should be allowed, the lowest possible angular momentum quantum numbers are 2, 3, 5, 6, and all states have the same parity. These values of the angular momenta appear rather high. Otherwise it is probably the scheme least open to objections since it predicts a multipole order for cross-over transitions which would have to be greater by *two* than that of the transitions actually taking place.

From the general trend of decay constants in this region of the periodic table one may conclude that both of the beta-ray transitions may be first forbidden. The ratio of the two transition probabilities is such that both may be equally forbidden or the higher energy spectrum may be forbidden by one more order. The lowest possible angular momentum of the decaying state of I^{130} is 3, for the first of the quantum number schemes proposed above, or 6, for the scheme considered most satisfactory in the above discussion. It is not to be taken for granted that the decaying state is the ground state of I^{130}, particularly because of the probably high angular momentum.

Guggenheimer[16] has pointed out that there seem to be some whole number relationships between the gamma-ray energies of some radioactive substances. Although sufficient data are not yet available to decide whether these relations are significant or fortuitous, it may be pointed out that the multiples $4\times106=424$, $5\times106=530$, $7\times106=742$ correspond, within the experimental errors, to three of the four gamma-rays of I^{130}.

Acknowledgments

The authors wish to express their gratitude to Professor R. D. Evans for his continued help and encouragement and to Professor M. S. Livingston and the cyclotron crew for making the bombardments. Dr. J. W. Irvine, Jr. performed the chemical separations.

This research was supported in part by a grant from the John and Mary R. Markle foundation.

[14] The so-called "K-U plot" still occasionally applied to cloud-chamber data has no physical significance as has been shown by all careful studies in recent years.

[15] L. G. Elliott and M. Deutsch, Phys. Rev. **63**, 321 (1943).

[16] K. M. Guggenheimer, Proc. Roy. Soc. **A181**, 169 (1942).

Theory of the Continuous X-Ray Spectrum: Short Wave Limit

ROBERT WEINSTOCK
Stanford University, Stanford University, California

(Received August 21, 1943)

An earlier result for the intensity distribution of continuous x-radiation is reduced to applicability at the short-wave limit; this is accomplished by passing to the limit of zero velocity for the scattered electron.

IN an earlier work[1] the results of the theory of the continuous x-ray spectrum—relativity and retardation of potential neglected—were given in a form reasonably convenient for numerical computation of intensity distributions. The results as given, however, are not directly applicable to the special case of the short wave (Duane-Hunt) limit—i.e., where the incident electron loses all its energy in the production of an x-ray quantum. Also, experience has shown that whenever one attempts to carry out the computations near the short wave limit—i.e., when the emergent electron speed is small compared with the incident speed—the numerical work is unwieldy to the point of uselessness, so that extrapolation to the short wave limit is not feasible. In the present work the difficulty is overcome by a reduction of the earlier results to direct applicability to the short wave limit.

ANALYTICAL TREATMENT

The absolute intensity of continuous x-radiation observed at an angle Θ (made with the direction of bombardment, taken as the x direction) is given by[2]

$$I_\nu(\Theta)=\frac{(8\pi^2e^2h^2/m^2c^3)n_1^4}{[\exp(2\pi i n_1)-1][1-\exp(-2\pi i n_2)]}\times(L_x^2\sin^2\Theta+L_z^2\cos^2\Theta+L_y^2) \quad (1)$$

ergs per unit solid angle per unit frequency range per bombarding electron per atom-per-square-centimeter of target area. Here,

$in_{1,2}=(Ze^2/\hbar v_{1,2})$;
$v_{1,2}=$ initial, final electron velocities;
$Z=$ atomic number of target element;

$$L_x^2=(-1/\xi_0)\Big\{B^2\sum_{r=0}^{\infty}\frac{s_r w_0^{r+1}}{r+1}-\xi_0+\sum_{r=1}^{\infty}t_r[(1-\xi_0)w_0^r-rI_{r-1}]-B\sum_{r=0}^{\infty}I_r(u_r+u_r^*)\Big\}; \quad (2)$$

$$L_y^2=L_z^2=[(1-n_1^2)/2\xi_0]\times\sum_{r=0}^{\infty}p_r\{(\xi_0-r-2)I_{r+1}+(1-\xi_0)w_0^{r+2}\}; \quad (3)$$

$$\xi_0=-4n_1n_2/(n_1-n_2)^2;$$
$$B=(n_1+n_2)/(n_1-n_2); \quad w_0=\xi_0/(\xi_0-1);$$
$$s_r=\sum_{\nu=0}^{r}g_{1\nu}g_{1,r-\nu}^*; \quad t_r=\sum_{\nu=0}^{r}g_{2\nu}g_{2,r-\nu}^*;$$
$$u_r=\sum_{\nu=0}^{r}g_{1\nu}g_{2,r-\nu}^*; \quad p_r=\sum_{\nu=0}^{r}g_{3\nu}g_{3,r-\nu}^*; \quad (4)$$
$$I_r=\int_0^{w_0}[w^r/(1-w)]dw;$$

the $g_{s\nu}$ are given through the recursion formulae:

$$g_{2,\nu+1}=\frac{\nu^2-n_1n_2+\nu(n_1-n_2)}{(\nu+1)^2}g_{2\nu},$$

$$g_{1\nu}=(1+\nu/n_1)g_{2\nu},\ g_{3\nu}=g_{1\nu}/(\nu+1); \quad g_{s0}=1.$$

Close to the short wave limit, $in_2\gg in_1$, $in_2\gg 1$, whence important simplifications are found to occur. In this limiting case[3]

[1] R. Weinstock, Phys. Rev. **61**, 584 (1942).

[2] Here the y direction is taken perpendicular to both the direction of incident electron and direction of observation. As given here, the expression for $I_\nu(\Theta)$ differs somewhat in appearance from that given in reference 1: Use has been made of the fact that $(Z/ak_1)^2=-n_1^2$; also, $(\mathfrak{M}_z^2/|A|^2)$ has been replaced by $(-16\pi n_1^2/\xi_0^2)L_z^2$ (etc.).

[3] The limiting values of rI_{r-1} and I_{r+1} are taken to an extra power of w_0, as is required by the occurrence of cancellations among the lower power terms when substitution is made into (2) and (3).

$$\xi_0=-4n_1/n_2,\quad w_0=4n_1/n_2,$$
$$B=-1,\quad I_r=w_0^{r+1}/(r+1),$$
$$rI_{r-1}=w_0^r+rw_0^{r+1}/(r+1),$$
$$I_{r+1}=[w_0^{r+2}/(r+2)]+[w_0^{r+3}/(r+3)].$$

The first recursion formula for the $g_{\sigma\nu}$ becomes

$$g_{2,\nu+1}=\frac{-n_2(n_1+\nu)}{(\nu+1)^2}g_{2\nu},$$

while the others remain unaltered. With these changes, we have

$$L_z^2=-\frac{w_0}{\xi_0}\sum_{r=0}^{\infty}\frac{w_0^r(s_r+t_r+u_r+u_r^*)}{r+1}$$
$$=\sum_{r=0}^{\infty}\frac{w_0^r}{r+1}\sum_{\nu=0}^{r}(g_{1\nu}+g_{2\nu})(g_{1,r-\nu}^*+g_{2,r-\nu}^*),$$

from (2) and (4);

$$L_z^2=\sum_{r=0}^{\infty}\frac{\sum_{\nu=0}^{r}(f_{1\nu}+f_{2\nu})(f_{1,r-\nu}^*+f_{2,r-\nu}^*)}{r+1}. \quad (5)$$

Also, by virtue of the above simplifications, (3) becomes

$$L_y^2=L_z^2=(n_2^2w_0^3/2\xi_0)\sum_{r=0}^{\infty}\frac{p_rw_0^r}{(r+2)(r+3)}$$
$$=-8n_1^2\sum_{r=0}^{\infty}\frac{\sum_{\nu=0}^{r}f_{3\nu}f_{3,r-\nu}^*}{(r+2)(r+3)}, \quad (6)$$

where, for $\sigma=1, 2, 3$, $f_{\sigma\nu}=w_0^rg_{\sigma\nu}=(4n_1/n_2)^rg_{\sigma\nu}$. The recursion relations among the $f_{\sigma\nu}$ are thus found to be

$$f_{2,\nu+1}=\frac{-4n_1(n_1+\nu)}{(\nu+1)^2}f_{2\nu},\quad f_{1\nu}=(1+\nu/n_1)f_{2\nu},$$
$$f_{3\nu}=f_{1\nu}/(\nu+1);\quad f_{\sigma 0}=1.$$

Finally, (1) reduces to

$$I_\nu(\Theta)=\frac{(8\pi^2e^2\hbar^2/m^2c^3)n_1^4}{\exp(2\pi in_1)-1}\times(L_z^2\sin^2\Theta+L_x^2\cos^2\Theta+L_y^2)$$

for the absolute intensity at the short wave limit [in the units given for (1)]. Now the $L_{x,y,z}^2$ are given by (5) and (6).

In terms of the tube voltage V we have, since in our non-relativistic approximation $\frac{1}{2}mv_1^2=eV/300$,

$$in_1=Ze^{\frac{1}{2}}(150m)^{\frac{1}{2}}/\hbar V^{\frac{1}{2}}=[Ze^2m^{\frac{1}{2}}/(4\pi\hbar^3c)^{\frac{1}{2}}]\lambda_0^{\frac{1}{2}}, \quad (7)$$

where λ_0 is the minimum wave-length for given V, consistent with energy conservation. (The latter expression holds at the short wave limit only, since only there does $\frac{1}{2}mv_1^2=2\pi\hbar c/\lambda_0$.) Since for a given angle of observation $I_\nu(\Theta)$ depends upon n_1 alone, (7) reveals that pairs of values of Z, λ_0 satisfying $Z\lambda_0^{\frac{1}{2}}=$constant should yield the same absolute intensity at the limit.

NUMERICAL CHECK

Just as in the case of computations carried out far from the short wave limit, a numerical check is desirable to effect an estimate of the error involved in the breaking off of the expansions (5) and (6) after a finite number of terms. The desired check is here also provided by the ingeniously attained result of Sommerfeld and Maue[4]—a relatively simple expression for the sum $L^2=L_x^2+L_y^2+L_z^2$. Although the check itself converges no more rapidly than do (5) and (6), the simplicity of their result renders the numerical calculation of L^2 much easier than the individual $L_{x,y,z}^2$ to the same number of terms.

According to Sommerfeld-Maue,

$$L^2=-\frac{\xi_0}{2n_1^2}\frac{d}{d\xi_0}|\mathfrak{F}|^2,$$

where $\mathfrak{F}=F(-n_1, -n_2, 1, \xi_0)$, the hypergeometric function of indicated parameters. That is, $\mathfrak{F}$ is expressible as a power series $\sum_{\nu=0}^{\infty}a_\nu\xi_0^\nu$ whose coefficients are defined through

$$a_{\nu+1}=\frac{(-n_1+\nu)(-n_2+\nu)}{(\nu+1)^2}a_\nu,\quad a_0=1.$$

Now, $|\mathfrak{F}|^2=\sum_{r=0}^{\infty}\sum_{\nu=0}^{r}a_\nu a_{r-\nu}^*\xi_0^r$; we find, therefore, upon differentiation,

$$L^2=(-1/2n_1^2)\sum_{r=0}^{\infty}r\sum_{\nu=0}^{r}a_\nu a_{r-\nu}^*\xi_0^r.$$

For $in_2\gg in_1$, $in_2\gg 1$, whence $\xi_0=(-4n_1/n_2)$, we

[4] A. Sommerfeld and A. W. Maue, Ann. d. Physik **23**, 589 (1935).

find at length

$$L^2=(-1/2n_1^2)\sum_{r=0}^{\infty} r \sum_{\nu=0}^{r} f_{2\nu} f^*_{2,r-\nu},$$

where $f_{2\nu}$ is the quantity defined in the preceding section.

LIMITATIONS OF THE RESULTS

It is well to keep in mind the limits to the applicability of the results of this paper; these consist, briefly, of the following. In addition to the neglect of relativity and retardation of potential, there is inherent the neglect of screening by the atomic electrons of the target material —i.e., the assumption of a pure Coulomb field as seen by the incident electron during the emission process. "This is only strictly justified for an electron whose de Broglie wave-length is small compared with the radius of the K shell of the scattering atom. For $Z=28$ and $V=15$ kilovolts, for example, these lengths are of the same order of magnitude, so that at best the assumption of a pure Coulomb field is only approximate—the higher the voltage and the smaller Z, the better the approximation."[5] Finally, the x-radiation upon which measurement is made for comparison with the theory must originate from a *thin* target; the theory takes no account of multiple scattering within the target.

[5] Quoted from reference 1.

PHYSICAL REVIEW VOLUME 64, NUMBERS 9 AND 10 NOVEMBER 1 AND 15, 1943

The Relative Abundance of the Isotopes of Potassium in Pacific Kelps and in Rocks of Different Geologic Age

KENNETH L. COOK
Ryerson Physical Laboratory, University of Chicago, Chicago, Illinois
(Received May 19, 1943)

The Dempster double focusing mass spectrograph has been used to determine the K^{39}/K^{41} isotope ratio in certain Pacific kelps, fossils, and rocks of different geologic age. Within the 1 percent accuracy obtainable, the potassium isotope ratio for the kelps and two Upper Cambrian fossils examined is the same as that of rocks. Rocks whose ages vary from Early pre-Cambrian to Tertiary show no measurable difference in the potassium isotope ratio, within 1 percent error. The average value of the potassium isotope ratio was found to be 14.12 ± 0.28. Fluctuations in the ratio are attributed to isotope effects of the hot-filament ion source.

INTRODUCTION

DURING the past seven years there have been reported variations in the relative abundance of the stable isotopes of three elements. Variations in the relative abundance of the stable isotopes of oxygen were found by Dole[1] in his careful measurements of the density of water in different localities. Variations of 5 percent in the isotope ratio of the stable isotopes of carbon (C^{12}/C^{13}) have been observed by Nier[2] and his collaborators.[3] Variations of as much as 15 percent in the ratio of the relative abundance of the stable isotopes of potassium (K^{39}/K^{41}) have been reported by Brewer.[4] As emphasized by Brewer, variations of this order of magnitude are too small to be detected by any of the present chemical techniques of measuring atomic weights of the above elements. Therefore, more precise determinations, such as those obtainable with the modern mass spectrograph or by careful density measurements, must ordinarily be employed.

It seemed desirable to have the above observations substantiated and supplemented by further studies. Goodman[5] has already pointed out the

[1] M. Dole, J. Chem. Phys. **4**, 268, 778 (1936).
[2] A. O. Nier and E. A. Gulbransen, J. Am. Chem. Soc. **61**, 697 (1939).
[3] B. F. Murphy and A. O. Nier, Phys. Rev. **59**, 771 (1941).
[4] A. K. Brewer, J. Am. Chem. Soc. **58**, 365 (1936).
[5] C. Goodman, J. App. Phys. **13**, 276 (1942).

importance of carrying on such studies of the isotopes of potassium because of its widespread occurrence on the earth's crust (2.5 percent of the earth's crust and the seventh most abundant element) as well as its importance in essentially all biological processes.

The present paper contains measurements of the relative abundance of the potassium isotopes in certain potassium-bearing plants and rocks and observations of the ratio in rocks of different geologic age.

EXPERIMENTAL DETAILS

I. The Ion Source

The use of a hot filament as a source of alkali ions has been a standard practice for many years in mass spectrograph work. Recently it has been demonstrated by Blewett and Jones[6] that alumino-silicates of the alkali metals are the best thermionic sources of ions yet tried and that ternary compounds of alkali oxide, alumina, and silica are, in general, better emitters of the alkali ions than binary compounds. They further noted that the synthetic alumino-silicates of each of the five alkali metals of composition $R_2O \cdot Al_2O_3 \cdot 2SiO_2$ are ion-emitters and are as good as, or in some ways superior to, the natural minerals (spodumene, jadeite, leucite, pollucite) which have ordinarily been used in the past.

Throughout the course of the present work potassium alumino-silicates were used. The potassium alumino-silicate to be studied was powdered and mounted on a filament of 0.0005-inch-thick platinum (plus 10 percent iridium) foil cut in the form of a strip 15 mm by 1 mm. Distilled water was used as a binder. Enough powder was always used so that, after fusion, a thin layer of glass completely covered the platinum strip throughout about 6 mm of its central portion. Before putting on the powder each platinum strip was heated at white heat for a few minutes to drive off any volatile potassium impurities incorporated in the platinum foil. Brewer noted that most commercial platinum has some potassium impurities in it.[7] To ascertain that the technique of pre-heating the filaments was effective, a clean platinum strip was once put into the apparatus after pre-heating; it was found that no detectable potassium ions were emitted even near the melting point of the platinum.

The composition of the alumino-silicates used in the present investigation varied with the particular material under examination. In the case of the modern plants under study, their ash was combined with alumina and silica to make artificial potassium alumino-silicates. Details of the technique for this will be described below. In the case of the rocks under study, the investigation was confined chiefly to those igneous rocks containing one or more of the following natural minerals: orthoclase ($K_2O \cdot Al_2O_3 \cdot 6SiO_2$); microcline ($K_2O \cdot Al_2O_3 \cdot 6SiO_2$); muscovite ($2H_2O \cdot \cdot K_2O \cdot 3Al_2O_3 \cdot 6SiO_2$); perthite (a mixture of orthoclase and albite [$Na_2O \cdot Al_2O_3 \cdot 6SiO_2$]); microcline-perthite (a mixture of microcline and albite). It will be noted that all of these minerals are potassium-bearing alumino-silicates. That these minerals, when heated, are good emitters of potassium ions was discovered during the preliminary experiments incident to the present investigation.[8] All of them proved to be essentially as good emitters as the mineral leucite. The fact that all of them melt at temperatures considerably below the melting point of platinum make them superior to leucite, whose melting point is so near that of platinum that melting of the platinum filament often accidentally occurred in fusing the leucite to the filament. It was possible to find examples of all geologic ages among these minerals.

Preliminary experiments with leucite and perthite showed that the *comparison* of the potassium isotope ratio of different specimens with the present apparatus could be made with errors not exceeding 1 percent. It was decided, therefore, to turn to some material whose potassium ratio was thought to vary more than this amount and carry on an intensive study of that material. The kelps of the Pacific were studied, since variations of some 6 percent were reported by Brewer to be customary[9] and variations up to 15 percent had been claimed.[10]

The kelp specimens were collected and dried at room temperature. No chemicals were added to

[6] J. P. Blewett and E. J. Jones, Phys. Rev. **50**, 464 (1936).
[7] A. K. Brewer, see reference 4.
[8] Orthoclase and muscovite were originally tried at the suggestion of Professor Bowen.
[9] A. K. Brewer, Ind. and Eng. Chem. **30**, 896 (1938).
[10] A. K. Brewer, J. Am. Chem. Soc. **58**, 365 (1936).

contaminate them. They were then cut into small pieces and burned to an ash in a clean, open platinum crucible.[11] Enough kelp was used to form about 0.5 g of the ash for each specimen. A brief examination of the kelp ash of *Macrocystis* was made with the aid of a petrographic microscope and standard oils for determining index of refraction. Among the various crystals present, potassium chloride was dominant and potassium sulfate was a minor constituent.[12] Stewart's[13] thorough examination of the chemical composition of three of the most common Pacific kelps, *Macrocystis pyrifera*, *Nereocystis leutkeana*, and *Pelagophycus porra*, led him to conclude that 85 percent by weight of the total ash is water-soluble, and that of this water-soluble part, 75 percent consists of potassium salts, chiefly potassium chloride and potassium sulfate. His report indicates that the element potassium is present in the ash of these kelps to the extent of about 30 percent by weight. As shown by the exhaustive treatments of the chemical composition of Pacific kelps by Burd,[14] Balch,[15] and Turrentine,[16] the potassium content in some kelps varies considerably from this figure; but by and large, 30 percent may be taken as an average value for the potassium content in the ash of Pacific kelps.

The extensive work by Bondy and his collaborators[17] on hot-filament ion sources showed that chlorides and sulfates of the alkali metals are not desirable to use as ion-emitters because they volatilize so easily that the vacuum becomes bad even at very low temperatures of the filament. Furthermore, the rapid volatilization of the salts readily impoverishes the source of potassium and renders it useless as an ion-emitter after only a short time of heating. For these reasons, Bondy turned to glasses in which various compounds of the alkali metals were incorporated chemically into the alumino-silicate lattice.

For the present investigation it was therefore decided that, just as Bondy had done in the case of potassium hydroxide, potassium chloride could be used in preparing an alumino-silicate glass. Using as a guide the ternary system $NaAlSiO_4$-$KAlSiO_4$-SiO_2, which was investigated by Schairer and Bowen,[18] it was found that a glass of the approximate composition 57 percent (by weight) $KAlSiO_4$, 26 percent $NaAlSiO_4$, 17 percent SiO_2 could be made by fusing 0.10 g KCl, 0.05 g NaCl, 0.11 g Al_2O_3, and 0.18 g SiO_2 in a furnace at 1450°C.[19] An estimation of the relative amounts of kelp ash, Al_2O_3, and SiO_2 that would be mixed together to give a glass of a composition similar to that above was then made. In calculating the amount of the oxides formed from the alkalis in the chemical reaction of the chlorides and sulfates in the kelp ash with the alumina and silica (and also the oxygen in the air), it was assumed that potassium and sodium are present in kelp ash to the extent of 30 percent and 10 percent, respectively, and that calcium and magnesium together constitute 7 percent of the ash.[20] The chlorine, which in the kelp is in chemical union with the alkalis, was liberated in the reaction that formed the alkali alumino-silicates. In making a glass from the kelp ash the actual amounts used for each specimen were: 0.08 g of kelp ash; 0.06 g Al_2O_3; and 0.11 g SiO_2. Since the exact chemical composition of each kelp specimen was not available, these amounts were not critical.

Each mixture was thoroughly stirred in an agate mortar and then heated in a clean platinum crucible in a furnace at 1450°C. The melting point of essentially all of the glasses made was between 1300° and 1400°C. The furnace used was similar to those employed in the Geophysical Laboratories in Washington, D. C. The mixture was heated 20 minutes to permit the complete liberation of chlorine gas and also to assure a rather uniform mixture of the constituents. The crucible holding the melt was then quenched in water to give the glass, which, after being powdered, was applied directly to the filament in the manner previously described. As pointed out

[11] The platinum crucibles were always cleaned by (1) fusing 10 min. with sodium carbonate, (2) dissolving this away with dilute hydrochloric acid, and (3) heating the crucible for 10 min. at a white heat over a high temperature gas burner.

[12] Personal communication from Professor N. L. Bowen.

[13] G. R. Stewart, J. Agr. Research **4**, 21 (1915).

[14] J. S. Burd, Calif. Agr. Exp. Sta. Bull. **248**, 183 (1915).

[15] D. M. Balch, Ind. and Eng. Chem. **1**, 777 (1909).

[16] J. W. Turrentine, Ind. and Eng. Chem. **4**, 431 (1921).

[17] H. Bondy, G. Johannsen, and K. Popper, Zeits. f. Physik **95**, 46 (1935); H. Bondy and V. Vanicek, Zeits. f. Physik **101**, 186 (1939).

[18] N. L. Bowen, Am. J. Sci. **33**, 11 (1937).

[19] The sodium compound was included in order to make a glass of much lower melting point than would result if the sodium were not present.

[20] Calcium and magnesium were neglected in writing the above formula but were reckoned into the detailed computations that were made.

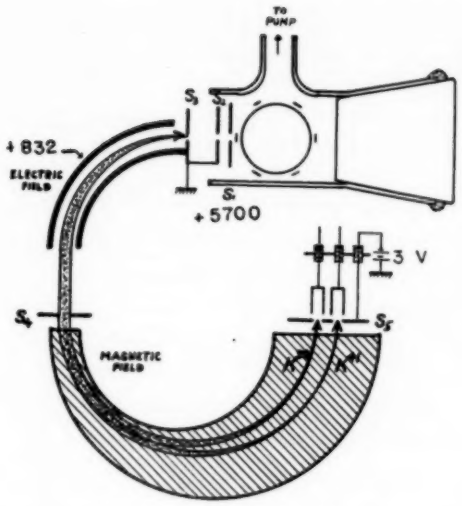

FIG. 1. Arrangement of rotating filament mechanism and collecting unit used on the Dempster double focusing mass spectrograph.

by Blewett and Jones,[21] the repeated vitrification technique used in phase diagram studies is not necessary for such isotope work.

II. The Apparatus

A. The Mass Spectrograph

In the present investigation Professor Dempster's mass spectrograph of the double focusing type, which has already been completely described by him,[22] was used (see Fig. 1). The potassium ions after emission from the hot filament passed through a circular hole of 1-mm diameter in the diaphragm. The diaphragm was at a high potential equal to that of the filament itself and was situated 2 mm from the heated filament. The ions were then accelerated a distance of 7 mm before entering the collimating slit system. Collimation was effected by two slits, the first being $\frac{3}{4}$ mm in width and located 9 mm from the filament and the second being $\frac{1}{2}$ mm in width and located 29 mm from the filament. After passing through the collimating system, the ions were deflected 90° during their passage through the electrostatic field, supplied by two quadrant condenser plates, and then bent 180° in the magnetic field. Upon leaving the magnetic field, the two distinct beams of the K^{39} and K^{41} isotopes were separated by a distance of $4\frac{3}{4}$ mm between the centers of the respective beams. The width of each beam at this point was found from photographs to be about 1 mm. Each kind of potassium ions then passed through a slit in the collecting unit and entered a separate Faraday chamber. Its arrival was registered by a quadrant electrometer.

The thermionic ion current coming off the filament was of the order of 10^{-6} amp. The potassium ion current entering the collector was between 5×10^{-10} and 5×10^{-11} amp. No trouble with Ca^{40} ions was experienced with the filament temperatures employed.

B. Current and Voltage Sources

The source of the heating current was the $\frac{1}{2}$-volt secondary of a step-down transformer. The accelerating potential of 5700 volts, which was used throughout the present investigation, was obtained from a transformer and rectified by a kenotron and condenser. An electrostatic deflecting potential of 832 volts was supplied by *B*-batteries. A 2-microfarad condenser was connected across the charged plates. The magnetic field of 7300–7700 oersteds necessitated a current of 4.15–4.65 amp., which was obtained from lead storage cells. An electromagnet, which was used to compensate for the stray magnetic field in the region of the plates, almost completely prevented any pre-separation of the isotopes before they reached the magnetic field.

C. The Collecting Unit

The slit system in the collecting unit consisted of two 3-mm-wide slits whose centers were placed $4\frac{3}{4}$ mm apart (see Fig. 1). The slits were cut in a $1'' \times 1''$ phosphorbronze plate, which was placed 8 mm above the edge of the magnetic field—this distance being necessarily chosen in order to leave room for the insertion of a photographic plate for supplementary photographic determinations. The phosphorbronze plate was kept at a potential of 3 volts below ground (the cathode was at ground potential) to mitigate effects caused by secondary electron emission. The open end of each Faraday chamber was 1 mm above the phosphorbronze plate. Each chamber was made of 0.005-inch Nichrome foil and was $12\times8\times3.15$ mm in size. Each was made rather deep to help nullify effects from secondary emission in that most of

[21] J. P. Blewett and E. J. Jones, reference 6.
[22] A. J. Dempster, Proc. Am. Phil. Soc. **75**, 762 (1935).

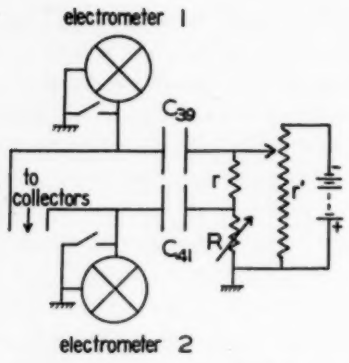

FIG. 2. Circuit used in the null method for measuring the K^{39} and K^{41} ion currents received by the two collectors.

the secondary electrons formed with the chamber would, in the presence of the stray magnetic field, be bent back to the inner sides of the chamber. It was found that the deep collectors alone, without the additional benefit provided by the phosphorbronze plate at a negative potential, were not adequate insurance against noticeable secondary electron effects. By means of Nichrome wire and nickel strips, the plate and collecting chambers were rigidly fastened to three $\frac{3}{16}$-inch brass rods which passed through amber bushings to the outside of the apparatus. From here electric contact with the electrometers was made through polystyrene-insulated, coaxial cable.

D. The Electrometer Circuit and Null Method

A null method was employed to measure the number of ions entering each collector. The method is identical with that developed by V. A. Bailey[23] and Vanderberg,[24] and employed in mass spectrograph work by Straus[25] and Sherwin and Dempster.[26] Each collector is connected to an electrometer and to one side of a condenser whose other plate is connected to a source of potential, as in Fig. 2. As the charge due to the incoming ions accumulates, the two electrometers are kept at approximately zero potential by adjusting potentiometer r', it having been previously observed what approximate values to use for r and R. After sufficient charge has been collected and the filament current shut off, an exact null reading of the two electrometers is obtained by adjusting r' and also the dial box R—resistance r being a dial box maintained at 4000 ohms.

The ratio of the charges on the two systems, and hence of the relative abundance of the isotopes coming in, is given by

$$\text{Ratio of } K^{39}/K^{41}=Q_{39}/Q_{41}=k(R+r)/R. \quad (1)$$

Here $k=C_{39}/C_{41}$ and was 1.298, as determined by capacity bridge measurement. Since r is held constant, it is seen that

$$K^{39}/K^{41}=1.298(R+4000)/R. \quad (2)$$

Thus, by drawing a curve of K^{39}/K^{41} *vs.* R, one can readily translate the measured value of R into a measure of the relative abundance of the isotopes.

An electrometer of the Dolezalek type registered the arrival of the K^{39} ions; that registering K^{41} ions was of the Compton type. The Dolezalek instrument had by far the longer period of the two, and it proved advantageous to use it to collect the more abundant K^{39} ions.

E. Comparisons by Rotating Filaments

In the preliminary work on leucite, only one filament at a time was put into the apparatus. It was observed that the same leucite specimen, when left in the apparatus overnight, might show a different K^{39}/K^{41} ratio by as much as 2.5 percent the following day. Sometimes, but not usually, the isotope ratio observed in the afternoon would differ from that in the evening by as great a percentage. These changes were observed in spite of the fact that, insofar as could be detected, all operative conditions were identical. During the course of about one-half hour of making measurements, the ratio usually remained constant within one percent.

These results indicated that in order to compare the isotope ratio of two specimens with an accuracy within 1 percent, it was imperative that they be examined in turn within the time that the same experimental conditions prevailed. A two-electrode arrangement was therefore employed in which the two sources to be compared could alternately be brought in front of the first slit. This arrangement was not entirely satisfactory because the design necessitated that both filaments be heated at the same time. Though they were separated by a distance of 1 cm from each

[23] V. A. Bailey, Phil. Mag. **50**, 381 (1929).
[24] R. M. Vanderberg, Phys. Rev. **59**, 114A (1941).
[25] H. A. Straus, Phys. Rev. **59**, 430 (1941).
[26] C. W. Sherwin and A. J. Dempster, Phys. Rev. **59**, 114 (1941).

other, it was observed that the heated filament which was not in front of the slit, would, nevertheless, contribute some of its ions in addition to those from the heated filament that was at the moment under study and directly in front of the slit.

The above results demonstrated the need for a rotating-filament device which would permit two or more specimens to be examined in turn under essentially identical experimental conditions and allow only one filament to be heated at any one time.

F. Mechanism for Rotating Filaments

The rotating-filament device was comprised of three main units: (1) the unit holding the filaments; (2) the brass plate; and (3) the Wilson seal.[27] (See Fig. 3.)

The unit holding the filaments consisted of a central $\frac{1}{8}$-inch brass shaft to which was attached six pure nickel wires (0.040-in. diam.) which radiated out from the shaft at angles of 60° from each other in the form of spokes of a wheel. The six wires were soldered into small holes in the shaft at $\frac{1}{16}$-in. intervals and were bent so that their ends, which in each case supported one end of the six platinum filaments, fell in the plane of a circle perpendicular to the shaft. Thus each of these six wires, rigidly fixed to the shaft, served to conduct the current to one end of each of the six platinum filaments. Also rigidly affixed to the shaft by means of two nuts and a spring washer, was a Lavite disk.[28] Six screws were placed near the outer rim of the Lavite disk at angles of 60° from each other. These screws served two purposes: (1) looped around each screw was a small length of nickel wire which was bent in such a fashion that one end of it could support an end of the platinum filament; (2) the head of each screw was cut down on a lathe to a flat surface, and it served to make electric contact with a contact-screw in the brass plate. Since at a given instant only one of the screws on the Lavite disk was in contact with the contact-screw in the brass plate, only one filament could be heated at any one time. After the removal of the male part of the ground-glass joint, the complete filament unit could be removed from the apparatus (see Fig. 1). As fresh platinum strips were put onto the filament unit, one end of the platinum filament was soldered to the tip of the nickel-wire spoke, and the other end was soldered to the tip of the nickel wire attached to the Lavite disk.

The brass plate, besides holding the contact-screw already mentioned, carried four screws spaced near the outer rim in such a way that whenever the contact-screw was in contact with a screw on the Lavite disk, they all touched the Lavite disk at points in between the screws in the Lavite disk. In this manner the brass plate resisted the small force offered it by the atmospheric pressure. The side of the brass plate facing the filament unit was counterbored to permit a yoke on the Lavite disk to fit into it. This feature, as well as helping in the alignment of the filament in front of the first slit, also served as an interior support to the filament unit and thus took some strain off the gasket of the Wilson seal. By means of a nickel wire soldered to it, the brass plate supported a circular Nichrome diaphragm ($1\frac{1}{4}$-in. diam.) in the center of which was cut the first slit.

The Wilson seal was essentially the same as that originally described by Wilson.[29] The metal parts of the seal were made of brass. The dimensions used in the single metal part facing the low pressure side were identical to those given in Wilson's paper: the 30° angle was used; since a $\frac{3}{16}$-in. rod was used, the rubber gasket was made to have an inner diameter of $\frac{3}{32}$-in. and an outer diameter of $\frac{15}{16}$-in. The gasket was made with one-sixteenth-in. thick Garlock 353 rubber. In making the metal part on the high pressure side to hold the rubber gasket in place, a simpler design—originally suggested by Mr. Thomas O'Donnell—

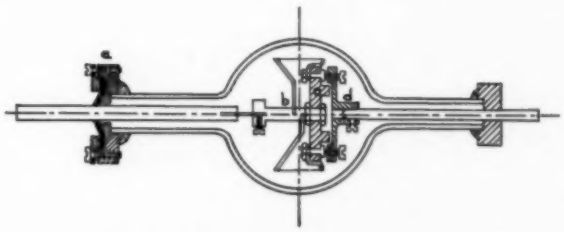

FIG. 3. Rotating filament mechanism.

[27] The writer is greatly indebted to Professor Dempster for designing the mechanism for the rotating filaments.

[28] Lavite was chosen as the insulating material because it can be easily fashioned to the desired shape on a lathe and then baked in a furnace at 800–1000°C for a few hours to give a sturdy unit.

[29] R. A. Wilson, Rev. Sci. Inst. 12, 91 (1941).

was employed. It consisted of one piece of brass fashioned so that the inner circular part fitted down on the gasket while the outer rim rested over the low pressure metal part so that screws could be used to force down the gasket tightly against the latter. The whole Wilson seal unit was held in position by waxing the low-pressure metal part to the extended glass tubing, as shown in Fig. 3. The hole, through which the rod could be either slid or rotated, was drilled slightly large in order to give about $\frac{1}{8}$-in. freedom of movement of the rod at its end inside the apparatus. This necessary play compensated for the slight discrepancy in the alignment of the two glass tubes inherent in any glass-blown apparatus. The nickel wire, soldered to the end of the rod and made fast to the filament unit by a setscrew, also helped to mitigate this discrepancy by giving the filament unit opportunity to turn so that the face of the Lavite disk would conform to the screws of the fixed brass plate.

RESULTS AND DISCUSSION

I. Observations

To obtain the true value of R and hence the K^{39}/K^{41} ratio (see formula [2]) for any given specimen under study, the two isotope beams were moved across the two collectors by changing the current through the magnet. Figure 4 shows a plot of R against the voltage drop across the magnet obtained in this manner. The curve is characterized by a steep portion to the right, a plateau in the center, a gentle rise toward the left, and then a steep descent to the left. *Before* the central positions are reached by the ion beams as they are being swept, step by step, across the slits, there is an impoverishment of K^{39} ions entering the K^{39} collectors which is reflected by a higher value for R. In a similar manner—but with opposite results—*after* the central positions are reached by the ion beams and the ions are swept on toward the left (see Fig. 1), there is a diminution of the ions entering the K^{41} collector which is reflected by a lower value of R. These changes are rather critical and therefore cause a sharp rise or fall in the value of R. The gentle rise to the left before it finally drops off steeply is due to the fact that the distance between the edges of the slits in front of the collectors does not exactly conform to the distance between the edges of the two ion beams. During any given run of a specimen at least three, more commonly four, and oftentimes five points would lie along a straight line. Within a single run the points in the plateau region never varied from a straight line by as much as 1 percent of the value of R and usually did not vary by as much as 0.5 percent. A single run thus gave a single value for R and hence of K^{39}/K^{41}.

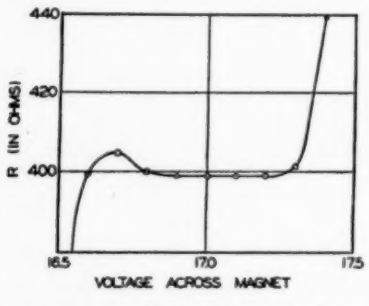

FIG. 4. Curve obtained for a single run.

One of the six specimens was always perthite, which, because of its low melting point, was used as a control sample in preference to leucite. After a run had been made with the control sample perthite, subsequent runs were made on each of the other five specimens of the rotating filament unit. Checks back to the control sample were made frequently. Since each run took about seven minutes, two or three runs on each of the six specimens could be made in one and one-half hours. Such a group of observations over a $1\frac{1}{2}$-hour period comprises what will be called in this paper a series of runs. After a separate series of runs had been taken, it would generally be followed by one or two subsequent series taken at daily or half-day intervals on the same group of specimens. Then six new filaments were introduced.

II. Discussion of Tables

Table I gives the names and sources of the specimens examined in the manner just described. Each specimen is assigned a definite number which is used to identify that same specimen in the subsequent tables. Specimens 36 and 3 to 12 are Pacific kelps; specimens 13, 28, and 37 are fossils; the remaining specimens are rocks. In the footnotes incident to this table are given the

TABLE I. Names of kelp, fossil, and rock specimens and their sources.

Number	Specimen and Source
1	Perthite A (control sample)[1] Lab. specimen, locality unknown
2	Leucite A[2] Civita Castellena, Italy
3	*Pelagophycus porra*[3] (kelp) La Jolla, Calif.
4	*Laminaria andersonii* stipe[4] (kelp) Pacific coast
5	*Macrocystis pyrifera* A[5] (kelp) La Jolla, Calif.
6	*Egregia laevigata*[3] (kelp) La Jolla, Calif.
7	*Nereocystis leutkeana* stipe A[4] (kelp) Pacific coast
8	*Nereocystis leutkeana* fronds B[6] (kelp) Friday Harbor, Wash.
9	*Pterygophora californica*[3] (kelp) La Jolla, Calif.
10	*Eisenia arborea*[3] (kelp) La Jolla, Calif.
11	*Nereocystis leutkeana* stipe C[6] (kelp) Friday Harbor, Wash.
12	*Nereocystis leutkeana* fronds D[7] (kelp) Friday Harbor, Wash.
13	*Cryptozoön proliferum* Hall A[8] (fossil) Saratoga County, N. Y.
14	Chelmsford granite A,[9,10] N. Chelmsford, Mass.
15	Columbia River basalt[9,11] Western part of U. S.
16	Triassic diabase[9,12] Centerville, Va.
17	Muscovite A[13] Ingersoll mine, Keystone, S. Dakota
18	Muscovite B[14] Mt. Mica, Paris, Me.
19	Microcline-antiperthite B[15] Wilberforce, Ont.
20	Milforde granite B[9,16] Milford, Mass.
21	Leucite B[17] Mt. Mikeno, Central Africa
22	Muscovite C[18] Spruce Pine, N. C.
23	Plagioclase feldspar A[19,20] Wm. Elliot dike, Butt Tp., Nippissing Dist., Ont.
24	Perthite[19,21] Villeneuve Tp., Papineau Co., Que.
25	Green microcline[19,22] Lyndoch Tp., Renfrew Co., Ont.
26	Perthite D[23,24] Pied des Monts, Charlevoix Co., Que.
27	Perthite E[23,25] Henvey Tp., concession B, lot 5, Parry Sound Dist., Ont.
28	*Cryptozoön undulatum* Bassler B[26] (fossil) 2½ mi. E. of East Galway, Saratoga quadrangle, N. Y.
29	Perthite F[23,27] Monteagle Tp., conc. VII, lot 18, Hastings Co., Ont.
30	Plagioclase feldspar B[23,28] West Portland Tp., range V, lot 2, Lièvre river section of Quebec
31	Microcline-perthite G[19,29] Mattawan Tp., Nipissing Dist., Ont.
32	Perthite H[19,30] March Tp., Carleton Co., Ont.
33	Microcline-perthite J[31] Whiteface Mt., Essex Co., N. Y.
34	Microcline-perthite K[31] Whiteface Mt., Essex Co., N. Y.
35	Perthite L[23,32] Huron claim, Winnipeg River, S. E., Manitoba, Canada
36	*Macrocystis* stipe B[33] Pacific coast
37	*Cryptozoön proliferum* Hall C[26] Ritchie Park, Saratoga, N. Y.

[1] From collection at Rosenwald Museum, University of Chicago, gift of Professor D. J. Fisher.
[2] From Ward collection. Gift of Professor D. J. Fisher.
[3] Collected Jan. 26, 1943, by Dr. J. F. Wohnus, of the Scripps Institution of Oceanography.
[4] Secured from California Botanical Material Company, Palo Alto, California.
[5] Collected Feb. 20, 1938, by Professor G. B. Rigg, of the Oceanographic Laboratories of the University of Washington.
[6] Collected Dec. 16, 1937, by Professor Rigg.
[7] Collected in August, 1935, by Professor Rigg.
[8] Obtained through M. S. Chappers from collection at Walker Museum, University of Chicago. H. P. Cushing and R. Ruedemann, N. Y. State Museum Bull. 169, 38 (1914).
[9] One of the standard specimens of the Committee on Standards of Radioactivity of the National Research Council being used for the international intercalibration of radioactivity measurements. Gift of Dr. Clark Goodman.
[10] Age: possibly Mississippian. R. D. Evans *et al.*, "Progress Report of National Research Council Committee of Standards of Radioactivity," p. 97. (Mimeographed.) B. K. Emerson, U. S. Geol. Survey Bull. 597, 188 (1917). C. Goodman and R. D. Evans, Bull. Geol. Soc. Am. 52, 491 (1941).
[11] Age: Middle Miocene. Evans *et al.*, reference 10, p. 99. R. D. Evans and C. Goodman, Bull. Geol. Soc. Am. 52, 483 (1941).
[12] Age: Triassic. Evans *et al.*, reference 10, p. 95.
[13] Age: Early pre-Cambrian, about 1465 million years old. Collected in summer of 1943 by Professor D. J. Fisher. Occurred in same pegmatites as those from which radioactive determinations of age have been made. A. F. Kovarik, Am. J. Sci. 20, 81 (1930). A. Holmes, "Age of the Earth," Nat. Res. Council Bull. 80, p. 338.
[14] Age: Late Silurian or Devonian. Obtained through Professor E. S. Bastin from collection of Rosenwald Museum, University of Chicago. E. S. Bastin, U. S. Geol. Survey Bull. 445, 15 (1911).
[15] Age: Middle pre-Cambrian. Gift of Professor Harry Berman. Holmes, reference 13, p. 325. H. V. Ellsworth, Econ. Geology Series No. 11, Geol. Survey, Canada, p. 54 (1932). H. S. Spence and R. K. Carnochan, Canadian Institute of Mining and Metallurgy Bulletin, pp. 1–37 (1930).
[16] Age: Devonian (?). Emerson, reference 10, p. 165.
[17] Age: Probably recent though perhaps Tertiary. Gift of Professor Bowen. N. L. Bowen and R. B. Ellestad, Am. Mineral. 22, 410 (1937).
[18] Age: late Carboniferous or early Permian (?). From a pegmatite specimen containing much altered uranium material. Gift of Professor Berman. Holmes, reference 13, pp. 340 ff.
[19] Age: Middle pre-Cambrian. Gift of Dr. H. V. Ellsworth.
[20] Ellsworth, reference 15, p. 188.
[21] Reference 15, p. 242.
[22] Reference 15, p. 228.
[23] Age: Middle pre-Cambrian. Gift of H. S. Spence.
[24] Associated with uraninite, thucholite, etc. H. S. Spence, Am. Mineral. 25, 711 (1940).
[25] Associated with uraninite, thucholite, etc. H. S. Spence, Am. Mineral. 15, 499 (1930). H. V. Ellsworth, Am. Mineral. 16, 576 (1931).
[26] Age: Upper Cambrian. Obtained through Dr. Winifred Goldring, N. Y. State Paleontologist, as a gift from the N. Y. State Museum.
[27] Associated with ellsworthite, thorite, etc. H. V. Ellsworth, Am. Mineral. 12, 368 (1927). T. L. Walker and A. L. Parsons, Univ. Toronto Studies 16, 13 (1923).
[28] Associated with monazite. H. S. Spence and O. B. Muench, Am. Mineral. 20, 726 (1935).
[29] Ellsworth, Econ. Geol. Series No. 11, p. 190.
[30] Reference 29, p. 238.
[31] Age: Middle pre-Cambrian, 1200 million years old. Associated with allanite. Gift of Dr. Marble. J. P. Marble, Am. J. Sci. 241, 32 (1943).
[32] J. S. DeLury and H. V. Ellsworth, Am. Mineral. 16, 569 (1931).
[33] Secured from General Biological Supply House, Chicago, Illinois.

names of the donors of the specimens, the ages of the specimens whenever known, and references which give the geologic occurrence of the rock specimens. The species of kelp examined include the most common ones of the Pacific coast. The fossil specimens examined are the same species as those previously investigated by Brewer and Baudisch.[30] Most of the rock specimens examined came from well-known localities and were once a part of pegmatites whose ages have been relatively well established not only by geologic evidence, but also by radioactive age determinations.

Tables IIA, IIB, and IIC give the values of the potassium isotope ratio obtained from the various specimens. A condensed form of the full name of the specimens occurring in Table I is given in these tables (in column 2) to facilitate interpretation of them. Within each individual vertical

[30] A. K. Brewer and O. Baudisch, J. Am. Chem. Soc. 59, 1578 (1937).

TABLE IIA. K^{39}/K^{41} isotope ratios for kelp, fossil, and rock specimens.

Number	Specimen	1	2A	2B	2C	3A	3B	3C	4A	4B	5A	5B
1	Perthite A	14.21(3)	14.03(3)	14.34(4)	14.25(2)	14.19(3)	14.29(4)	14.40(2)	14.33(3)	14.36(5)	14.33(4)	14.40(4)
2	Leucite A	.....	14.00(3)	14.31(1)	14.28(1)	.....	.....	.....	.....	.....	.....	.....
3	Pelagophycus	14.22(2)	14.00(2)	14.40(2)	14.28(2)	.....	.....	.....	.....	.....	14.40(4)	14.40(2)
4	Laminaria	14.19(2)	.....	.....	.....	.....	.....	.....	14.34(2)	14.31(2)	.....	.....
5	Macrocystis	.....	13.97(2)	14.38(2)	14.34(2)	.....	.....	.....	14.33(2)	14.37(1)	14.31(2)	14.46(2)
6	Egregia	.....	13.97(2)	14.37(1)	14.31(1)	.....	.....	.....	14.34(2)	14.34(2)	.....	.....
7	Nereocystis A	.....	14.09(1)	14.44(3)	14.28(2)	.....	.....	.....	.....	.....	.....	.....
8	Nereocystis B	.....	.....	.....	.....	14.12(1)	14.22(2)	14.42(1)	.....	.....	.....	.....
9	Pterygophora	.....	.....	.....	.....	14.15(1)	.....	14.37(1)	14.37(2)	14.42(2)	.....	.....
10	Eisenia	.....	.....	.....	.....	14.12(1)	14.25(2)	14.36(2)	.....	.....	14.28(2)	14.44(2)
11	Nereocystis C	.....	.....	.....	.....	14.28(1)	14.22(2)	14.48(1)	.....	.....	14.36(3)	14.37(3)
12	Nereocystis D	.....	.....	.....	.....	.....	.....	.....	14.37(2)	14.36(2)	.....	.....
14	Granite A	.....	.....	.....	.....	14.19(1)	14.28(1)	14.40(1)	.....	.....	.....	.....
	Average...	14.21	14.01	14.37	14.29	14.18	14.25	14.41	14.35	14.36	14.33	14.41

TABLE IIB. K^{39}/K^{41} isotope ratios for kelp, fossil, and rock specimens.

Number	Specimen	6A	6B	7A	7B	8A	8B	8C
13	Cryptozoön A	14.25(2)	14.46(3)	.....	.....	14.44(1)	14.28(4)	14.22(1)
14	Granite A	.....	.....	14.54(2)	14.63(2)	.....	.....	.....
15	Basalt	14.31(3)	14.49(3)	.....	.....	14.58(1)	14.43(2)	14.34(1)
16	Diabase	14.27(2)	14.48(2)	.....	.....	14.44(1)	14.37(2)	14.28(1)
17	Muscovite A	14.28(2)	14.51(2)	.....	.....	14.58(1)	14.43(2)	14.28(1)
1	Perthite A	14.27(4)	14.50(4)	14.58(4)	14.68(3)	14.57(2)	14.43(4)	14.33(2)
18	Muscovite B	14.28(2)	14.51(2)	.....	.....	14.58(1)	14.44(2)	14.33(1)
19	Perthite B	.....	.....	14.57(3)	15.51(4)	.....	.....	.....
20	Granite B	.....	.....	14.51(2)	14.54(2)	.....	.....	.....
21	Leucite B	.....	.....	14.53(2)	14.58(2)	.....	.....	.....
22	Muscovite C	.....	.....	14.53(2)	14.51(3)	.....	.....	.....
	Average.....	14.28	14.49	14.54	14.58	14.54	14.40	14.30

TABLE IIC. K^{39}/K^{41} isotope ratios for kelp, fossil, and rock specimens.

Number	Specimen	9A	9B	9C	10	11A	11B	12
3	Pelagophycus	14.28(2)	14.63(2)	14.25(1)	.....	.....	.....	.....
5	Macrocystis	14.27(1)	14.68(1)	14.31(1)	.....	.....	.....	.....
6	Egregia	.....	.....	.....	14.30(3)	.....	.....	.....
7	Nereocystis A	.....	.....	.....	14.40(1)	.....	.....	.....
10	Eisenia	.....	.....	.....	14.44(1)	.....	.....	.....
23	Feldspar A	14.22(1)	.....	14.28(2)	.....	.....	.....	.....
24	Perthite C	14.27(1)	.....	14.25(1)	.....	.....	.....	.....
25	Microcline	14.31(1)	.....	14.34(1)	.....	.....	.....	.....
1	Perthite A	14.27(3)	14.70(2)	14.28(3)	14.37(4)	14.18(3)	14.32(3)	14.57(5)
26	Perthite D	.....	.....	.....	14.34(1)	.....	.....	.....
27	Perthite E	.....	.....	.....	14.37(1)	.....	.....	.....
28	Cryptozoön B	.....	.....	.....	.....	.....	14.21(3)	.....
29	Perthite F	.....	.....	.....	.....	14.25(1)	14.34(1)	.....
30	Feldspar B	.....	.....	.....	.....	14.15(1)	14.34(1)	.....
31	Perthite G	.....	.....	.....	.....	14.15(1)	14.31(1)	.....
32	Perthite H	.....	.....	.....	.....	.....	.....	14.58(2)
33	Perthite J	.....	.....	.....	.....	.....	.....	14.51(2)
34	Perthite K	.....	.....	.....	.....	.....	.....	14.46(2)
35	Perthite L	.....	.....	.....	.....	.....	.....	14.48(2)
	Average.....	14.27	14.67	14.29	14.37	14.18	14.31	14.52

column headed by the series number there customarily appear six values—in a few instances there are less than six—which are the isotope ratios of the six specimens used in that series of runs. The number in parenthesis indicates the number of runs made on that individual specimen during the series. The value for the ratio given for any individual specimen is the arithmetic mean of the values obtained on the specimen for that given number of runs. At the bottom of each vertical column appears a number which is the average of the series of runs of the six specimens.

Examination of the data reveals that *within a single series of runs* the largest value for the mean isotope ratio does not ordinarily differ from the smallest value by more than 1 percent. Within

three different series (3A, 5A, and 7B), however, are found differences greater than 1 percent, yet smaller than 1.3 percent. It should be emphasized that these figures do not do justice to the degree of accuracy that was obtained insofar as a direct comparison between the isotope ratio of the specimens is concerned. For during the time of making a series of runs, slight fluctuations were observed (these fluctuations will be discussed presently) and are reflected in these figures. By interchecking the specimens with the control sample at the proper time, readings with an average deviation of a single observation of about ± 0.04 for the K^{39}/K^{41} ratio could be attained. Thus the accuracy in comparing the isotope ratio of any six specimens was well within 1 percent—perhaps within 0.5 percent. Within this accuracy, the relative abundance of isotopes in all the specimens examined—whether they were kelp-glasses, fossils, or rocks of different geologic age—never varied from that of the control sample.

Though the potassium isotope ratio within any series of runs was constant within experimental error, there were noted definite fluctuations of the ratio under different conditions of the apparatus or of the emitters on different days. Usually the series of runs here presented were made at approximately daily intervals. When, after a one-day interval, a subsequent series of runs was taken on the same six specimens, the isotope ratios of all specimens would not vary from each other by more than 1 percent, yet the ratio now observed might differ by as much as 3 percent from its value the preceding day. During the interim the vacuum was never broken although the pumps were always shut off and the pressure went up to about 10^{-3} mm during the night. After breaking the vacuum and introducing six fresh platinum filaments with glasses fused onto them, the isotope ratio of the six new specimens would not vary from each other by more than 1 percent, yet it might differ by as much as 2 percent from that of the previous series. Figure 5 shows how the ratios varied with the different series of runs taken over a period of about six weeks. Series 1 through 8B were made regularly at almost daily intervals over a period of three weeks. These series appear to exhibit a trend of an increase in the isotope ratio during the three-weeks period. After series 8B was made, three days elapsed, during which the pressure in the apparatus was 10^{-3} mm of mercury. Series 8C was then obtained, after which the apparatus stood at a pressure of 10^{-3} mm for three more days before the new specimens on which series 9A was made was put into the apparatus.

It is interesting to note that in one isolated case the conditions suddenly changed so that a large fluctuation was witnessed during one series of runs (9B). Before the writer had time to complete this series the ratio abruptly changed from a value of about 14.63 to about 14.29. Accordingly, the remainder of the determinations on that day were treated as a separate series, namely 9C, inasmuch as it was apparent that whatever caused the fluctuations had instantaneously appeared here. It should be emphasized

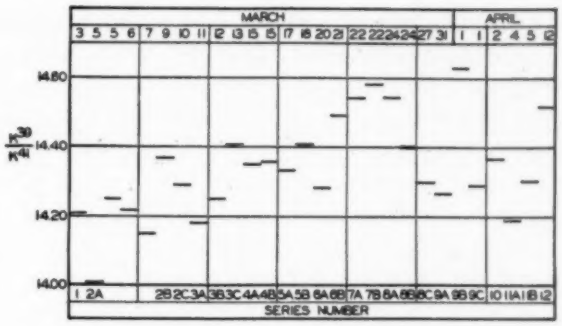

FIG. 5. Comparison of values of the K^{39}/K^{41} isotope ratio taken over a period of six weeks.

TABLE III. K^{39}/K^{41} isotope ratios for specimens used in the preliminary work.

Fil. No.	Day*	Specimens		Fil. No.	Day	Specimen
		Leucite A	Macrocystis B			Leucite A
1		13.60(2)	13.53(5)	5		14.06(4)
2	1A	14.15(9)	14.05(3)			Leucite B
	1B	13.91(7)	13.78(5)	6	1	13.66(3)
	23	13.91(2)	13.75(3)		2A	14.03(5)
	24	13.96(5)	13.96(4)		2B	13.94(3)
	26	14.06(6)	14.03(4)		3A	14.12(3)
	27	14.06(4)	14.06(3)		3B	14.12(3)
	28	14.06(2)	14.06(7)		4	14.25(3)
			Perthite A		5A	14.28(3)
3	1A	14.31(7)	14.28(3)		5B	14.28(3)
	1B	14.22(4)	14.22(2)		6A	14.22(3)
	7A	..	14.38(3)		6B	14.09(3)
	7B	..	14.00(2)		7A	14.22(3)
	8	..	13.91(3)		7B	14.22(3)
			Leucite B			Macrocystis B
4	1A	13.78(3)	13.78(6)	7	1	13.44(1)
	1B	13.87(2)	13.81(5)		2	13.46(4)
				8		14.33(3)

Specimen	Ratio	Specimen	Ratio
Cryptozoön A	13.59(2)	Laminaria	13.59(3)
	13.67(3)		
Nereocystis A	13.63(3)	Pelagophycus	14.51(3)

* A means afternoon; B, evening.

that in this instance the isotope ratio of all the specimens spontaneously changed. This case was the only observed example of such a large fluctuation occurring within a series of runs at the time of observation.

Three consecutive series of runs, which were purposely left out of Table II to help condense it, were made between series 2A and 2B on the specimen Perthite A only. The values of the isotope ratio obtained, in proper order, were 14.25 (7), 14.22 (3), 14.15 (5), and are included in Fig. 5 for completeness.

One part of the fossil Cryptozoön C (specimen 37) was included in series of runs 11A and 11B, and another part of the same fossil was included in series 12. No measurable ion current was registered, however, this fact probably being due to excessive leaching of the specimen. Satisfactory potassium ion emission was obtained from two fossil specimens, *Cryptozoön proliferum* Hall A and *Cryptozoön undulatum* Bassler B, by merely powdering the specimens and putting them on the filaments in the usual manner. Within the 1 percent accuracy obtainable, the isotope ratio of both fossils was found to be the same as that of the rock control sample. These results on the fossils do not agree with those of Brewer and Baudisch,[30] who reported—for the same species—isotope ratios lying about 2 percent below Brewer's normal value of 14.20 to 14.25.

It is noteworthy that in the preliminary investigations, before the rotating filament mechanism and Wilson seal were introduced into the apparatus, somewhat lower values of the isotope ratio than those presented in the above tables were generally observed. Table III gives the observed ratios in this preliminary work. Those specimens bearing the same filament number in the table were placed together in the apparatus when the two-filament mechanism was used. All other specimens in the table were placed alone into the apparatus.

If we give each series of runs in Tables IIA, IIB, and IIC equal weight, the arithmetic mean of the values of the isotope ratio is 14.35. Similarly the arithmetic mean of the values in Table III is 13.88. An average of these two figures, considering them of equal weight, gives 14.12 as a kind of "average" isotope ratio for all the runs made. In this case, the "average" is

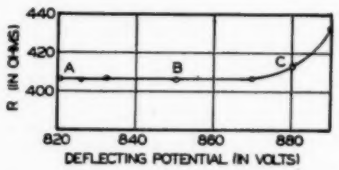

FIG. 6. Effect of changes in deflection potential upon resistance *R*.

rather meaningless except insofar as it helps to give a notion of the absolute value of the isotope ratio. The writer is of the opinion that the value 14.12 is within 2 percent of being the correct absolute value of the potassium isotope ratio. This result is in good agreement with that of Brewer, who gives 14.20 to 14.25 as the normal ratio.[31]

The surprisingly small amount of potassium that is apparently necessary in the crystal lattice of a mineral to yield a satisfactory ion current is worthy of comment from a petrographic standpoint. Specimen 19, consisting of dominant plagioclase feldspar and only a very minor amount of microcline, was a satisfactory emitter of potassium ions. Specimens 23 and 30 were lacking in any visible potash mineral and were comprised wholly of plagioclase insofar as could be determined with the aid of a petrographic microscope. Yet they proved to be good potassium ion-emitters. The explanation is that some potassium ions, in spite of their difference in size from sodium and calcium ions, have gone into the crystal lattice of the plagioclase to form a mix crystal. Heating the crystal sets the potassium free.

III. Discussion of Fluctuations

While the fluctuations do not hinder the *comparison* of the isotope ratio of different specimens to within 1 percent error, they nevertheless prevent the attainment of a greater accuracy than about 2 percent for the absolute relative abundance of the isotopes.

A. Possible Causes Inherent in the Apparatus

To show that the fluctuations could not be due to pre-separation of the isotopes due to stray magnetic field, a number of runs were made during which the deflecting potential was changed

[31] A. K. Brewer, J. Chem. Phys. **4**, 350 (1936); J. Am. Chem. Soc. **58**, 365 (1936); J. Am. Chem. Soc. **61**, 1597 (1939).

(see Fig. 6). The definite up-swing of the curve for the value of R corresponds to a decrease in the K^{39}/K^{41} value. The decrease of isotope ratio in region C of the curve means that the K^{39} ions were the first ones to be cut off by the edge of slits S_4 as the increasing deflecting potential swung the ions around in a path of decreasing radius. There was, therefore, a slight enrichment of the K^{39} ions on the inner edge of the beam coming through the electrostatic deflecting plates. As the ions were swept over to the other side of slit S_4 by decreasing the deflecting potential, a corresponding enrichment of the K^{41} on that side was not reflected in a down-swing of the curve in region A. The electrometers were not sufficiently sensitive to register such a small increase in the K^{41} ions, this increase being only about 1/14 as great as the increase of K^{39} ions in region C. The wide, level plateau in region B indicates that essentially no pre-separation was present within the main body of the ion beam.

Rather large changes in the current flowing through the two compensating electromagnets failed to give any measurable change in the isotope ratio. Hence, variations of current through these magnets could not have been the cause of the fluctuations.

There is a possibility of a slight pre-analysis effect due to the stray magnetic field over the 29-mm distance that the ions traveled from the filament to the region of compensating field. However, it is impossible that it could produce a large, spontaneous change such as was observed between Series 9B and 9C.

No change in the isotope ratio was observed when the accelerating potential was given a value lying 100 volts on either side of the 5700-volt value that was customarily used. Because the accelerating potential would never by itself vary by as much as 100 volts, its variations are ruled out as a cause of the fluctuations.

Before every series of runs, the two electrometers were always charged and left in this condition for a few minutes to ascertain that there were no measurable leakages over the surface of the amber bushings or in the leads from the apparatus to the electrometers.

Periodic checks of the ratio of the capacity of the two condensers used in the null electrical circuit were made throughout the seven months of measurements and indicated that the ratio never varied by more than two parts in a thousand from the average value of 1.298. In order to test the leakage from one condenser plate to the other because of ionization in the condensers, those plates leading to the electrometers were grounded while the respective voltages ordinarily used to balance the total number of incoming ions were impressed on the opposite plates; then the electrometers were disconnected from ground and the amount of drift observed. During the 30 seconds of time ordinarily taken for a single reading, the amount of leakage amounted to less than 1 mm scale-deflection of the electrometer from its original position. This small amount is within the limit of accuracy of reading the scale during a run. Hence, variations due to the changing capacities of the condensers or leakage across the condensers could not cause the large fluctuations observed.

The results obtained whenever experiments were tried to determine the effect of a change in pressure on the isotope ratio are insufficient to conclude whether any consistently definite change may indeed exist from this cause. Inasmuch as the main purpose of the present investigation is to compare the ratios among kelps and among rocks of different geologic age, these experiments were treated as incidental, but would have been carried on somewhat further, had not the exigencies of war necessitated bringing this work to a close at the present time. The results of various runs made on successive days on the same specimen do suggest an increase in the isotope ratio—as has already been pointed out. A similar tendency was observed in the preliminary work, as is best exemplified by the series of runs made on Leucite A, Leucite B, and *Macrocystis B* (see Table III). The tendency was not always present, however. Indeed, the isotope ratio of Perthite A, for example, tends to decrease markedly.

It has already been noted that the isotope ratios of the specimens examined in the preliminary work tended to be considerably lower in value than the ratios obtained after the introduction of the Wilson seal. It is believed that the Wilson seal limited the vacuum conditions so that pressures less than 10^{-5} mm of mercury were not attained after its introduction. Because of a faulty relay—which could not be repaired or

replaced at this time—the exact pressure conditions were unfortunately not known during the latter part of the work.

It has been shown by Sherwin[32] that the chance of neutralization of a positive ion in passing through a gas depends on the velocity of the ion. As the energy of the two potassium isotopes was the same, the velocity of the lighter isotope is 2.5 percent greater than the heavier isotope and consequently might be weakened by absorption at a different rate from that for the light isotope. Sherwin's results on hydrogen give a change of cross section for neutralization of less than one part in 100 for this difference of velocity. In terms of the original intensity I_0, the intensity of the bundle after going 60 cm (the approximate distance of travel through the present apparatus) at a pressure of 10^{-4} mm is $I=I_0e^{-n\sigma\cdot 60}$, where $n=3.55\times10^{12}$ and $\sigma=0.3\times10^{-16}$ cm^2. Thus

$$I=I_0\exp\left[-6\times10^{-3}\right]=I_0(1-6\times10^{-3}).$$

Thus the weakening of the potassium ion bundles in the 60 cm used, even at the very high pressure of 10^{-4} mm, would have been less than one percent. Since a difference of one part in 100 in the one percent is far below the possibility of observation, any residual gases are incapable of causing a measurable difference in the isotope ratio due to a difference in rate of neutralization.

B. Causes Inherent in the Emitters

Causes inherent in the emitters offer a likely explanation of the fluctuations. It is conceivable that various hydrocarbons that are always present in the apparatus may form a coating on the filaments and change the ratio of the ions being emitted from the heated glass ion source. In his investigation of the isotope effect in the evaporation of lithium, potassium, and rubidium from thermionic sources over a period of time, Brewer[33] observed a change in the abundance ratio for lithium, but none for potassium or rubidium. In view of the change of the isotope ratio of lithium over a period of time, it seems not unreasonable that under some circumstances there might occur a similar isotope effect with the other alkali metals. With the particular potassium aluminosilicates used in the present investigation, it may be possible that the potassium experienced such an isotope effect in being emitted from the glasses.

Of all the possible causes for the fluctuations that have been advanced in the above discussion, it seems that the most probable one lies in some kind of surface phenomenon of the emitter—a phenomenon which permits different amounts of the two potassium ions to evaporate at different times.

GEOLOGICAL CONSIDERATIONS AND DISCUSSION

In the laboratory the artificial separation of isotopes can be carried out in many ways. In a search, therefore, for a plant, animal, or rock in which the relative abundance of the isotopes of some element might vary, one logically explores the naturally occurring processes which might conceivably effect the separation of the isotopes in some manner similar to well-established laboratory methods. It is to be emphasized that the requirement of such a process is that it is recurrent or that it comes in cycles, which, given time enough, will effect the separation.

Because there is generally a great degree of physical mixing of all elemental constituents during the *extrusive* manifestations of vulcanism, there is little likelihood that any measurable separation of the isotopes is effected during the formation of extrusive rocks. There is a possibility that the equilibrium[34]

$$\underset{\text{gas}}{S^{34}O_2}+\underset{\text{ions}}{HS^{32}O_3^-}\rightleftarrows\underset{\text{gas}}{S^{32}O_4}+\underset{\text{ions in solution}}{HS^{34}O_3^-}\qquad \alpha=1.015$$

may be present within molten volcanic lava, yet it is difficult to see how the separation effect could be cumulative enough to make measurable differences in the isotope ratio of the sulfur.

Nor is it probable that the *intrusive*, or *plutonic*, manifestations of vulcanism have effected a measurable separation. Professor Bowen[35] has pointed out that in the cooling masses of magma, in order to produce important results in the way of fractional crystallization, the molecular flow of diffusion of substance, which would be selective to the materials participating in it, must play a negligible role in comparison with the factors involving the relative movement of crystals and liquid. He points out that this relative movement

[32] C. W. Sherwin, Phys. Rev. **57**, 814 (1940).
[33] A. K. Brewer, J. Chem. Phys. **4**, 350 (1936).
[34] T. I. Taylor, Science **89**, 177 (1939).
[35] N. L. Bowen, *The Evolution of the Igneous Rocks*, (Princeton Press, 1928), p. 22.

may take place under the influence of gravity during the early stages and under the influence of deformative forces during the middle and late stages of crystallization. The process is probably inadequately cyclic ever to produce a measurable separation by gravitation—even under ideal conditions of crystal settling, when comparatively little movement of the crystals take place. Yet it will be of interest—particularly when more accurate mass spectrographs are built—to investigate those igneous rocks whose formation is ascribed partly to gravitative settling, such as are those from the Sudbury district of Canada[36] and the Bushfeld Complex of South Africa.[37]

Mineralizers are those components of magmatic solutions which, because of their low molecular weight, or catalytic action, or for any other reasons, exert a large influence on the other components of the magma. The mineralizers include water, fluorine, boron, and chlorine. It is not known at the present time what physical condition the mineralizers are in when they are most influential, but it is probable that they are partly in the vapor state at the pressure and temperature conditions encountered in contact metamorphism and in the formation of pegmatites. If one of the isotopes of boron or chlorine is more ready to enter into combination than the other isotope, we might expect to find one side of a bed having minerals with more of this isotope than those on the other side.

Diastrophism would aid the above-mentioned phases of vulcanism only by forming cracks and other openings through which gases or liquids could flow, and pockets where separation of a very local nature might be carried on. These would be minor and relatively unimportant.

It is the process of gradation that offers the best prospects in a search for a naturally occurring separation of the isotopes by geologic processes. For here lies a number of physical processes which may be adequately recurrent or, because they are operative over great lengths of time or distance, may be very effective. One of these phenomena is base exchange, by means of which certain elements in a mineral may be exchanged or replaced by the ions of other elements in solution. This type of replacement is very common, particularly in the case of soil formation, and is effected by gradational agents such as ground water, running water in streams, or oceanic waters. The rocks which best exhibit base exchange are zeolitic rocks and clays. Taylor,[34] in collaboration with Urey, has already obtained "appreciable changes" in the isotope ratio of lithium by chemical exchange with sodium zeolites which show the following equilibrium:

$$Li^{+}+Na\ Zeolite \rightleftarrows Li\ Zeolite+Na^{+}.$$

In this instance one isotope of lithium replaces the sodium in the zeolite better than the other lithium isotope. By allowing a solution of sodium chloride to pass slowly through a 10-cm column of potassium-bearing, zeolitic greensand, Brewer[38] found that the greensand was impoverished preferentially of the K^{39} isotope. He suggests that this effect could occur in nature where base exchange processes are operative. The base exchange taking place in zeolitic rocks is commonly of the type:

$$Ca^{++}+Na\ Zeolite \rightleftarrows Ca\ Zeolite+Na^{+}$$

in which the calcium ions in solution go into the crystal lattice where the sodium was originally. In the process it is likely that the isotopes of calcium go into the zeolite at slightly different rates. In the event that calcareous ground water were to run for many miles along an aquifer containing porous volcanic material—and hence probably zeolitic rocks—a substantial and possibly measurable separation of the calcium isotopes could be effected. The isotope effect would be one of lateral gradation.

Because clay deposits are more widespread than zeolitic rocks, base exchange in the clays is in some respects more far-reaching than in the zeolites. As pointed out by Kelley,[39] there are several elements that can be replaced in the clays, and there is a definite replacing power of the common cations in the order: $Na<K<Mg<Ca<H$. Thus, sodium has less replacing power than potassium, potassium less than magnesium, and so forth. In addition—in the case of the bentonite clays, which have the highest base exchange capacity of all the clays—

[36] A. P. Coleman, Econ. Geol. **19**, 569 (1924).
[37] R. A. Daly and G. A. F. Molengraaff, J. Geol. **32**, 33 (1924).
[38] A. K. Brewer, J. Am. Chem. Soc. **61**, 1597 (1939).
[39] W. P. Kelley, "Base Exchange in Relation to Sediments," *Recent Marine Sediments* (Thomas Murby and Company, London, 1939), p. 455.

ions of magnesium, iron, or both of these elements in solution may go into the crystal lattice of clay minerals and replace the original aluminum.[39] The exchange processes probably proceed at different rates that depend on the isotopes involved. Therefore, ground water which percolates long distances down inclined beds of bentonite in a direction parallel to the bedding may possibly effect a measurable separation of the isotopes of some of the above elements involved in base exchange. The widespread occurrence of bentonite deposits in the western United States makes the possibility of such a separation rather favorable. The separation would be one of lateral gradation; and therefore sampling could be done on the same bed at different localities.

Experiments have as yet been unable to show any isotope separation effect on a column of material migrating through a substance like gelatine.[40] It has been suggested by Lindemann[41] that the head of the column would be richer in the lighter isotope. If success is ever attained in the laboratory, it would be of interest to investigate diffusion (or Liesegang) banding in rocks for an isotope effect. As demonstrated in the experiments of Liesegang and as explained by Oswald, the phenomenon of diffusion banding in rocks is a solution phenomenon. It is the result of rhythmic supersaturation of a solution permeating through a "solid" or colloidal substance.[42]

The phenomenon of replacement is so widespread in rocks that it will be well some day to review the whole process in terms of established chemical equilibrium relations.

One can only speculate as to the exact nature of the chemical equilibria that were present in the great inland seas and marine basins of the geologic past. However, the conditions which were influential in forming the great sedimentary salt beds and the limestone beds could not have been greatly unlike those existing on earth today. During the thousands of years of evaporation necessary to produce the thick deposits of salt, there were doubtlessly in operation the processes of free evaporation, ionic migration, gravitative settling, fractional crystallization, and chemical exchange.

[39] F. W. Aston, *Mass Spectra and Isotopes* (Longmans, Green and Company, New York, 1939), pp. 244–61.
[41] F. A. Lindemann, Proc. Roy. Soc. **A99**, 103 (1921).
[42] E. S. Hedges, *Liesegang Rings and Other Periodic Structures* (Chapman and Hall, Ltd., London, 1932), p. 52.

Robinson and Briscoe[43] have shown that in subjecting ammonium bromide to prolonged fractional crystallization involving about 2700 crystallizations, the isotope ratio of the bromine in the "head" fractions did not differ from that in the "tail" fractions by 1 percent. It is probable, therefore, that no measurable separation was effected by fractional crystallization in ancient salt basins.

Lewis and Macdonald[44] have demonstrated the separation effect of lithium amalgam as it passed through a long, narrow column of lithium chloride solution. In this case the lighter lithium isotope was carried down preferentially and accumulated at the foot of the column. It is doubtful that organisms, even in isolated bodies of water, could give the same result as the amalgam with measurable isotope effects.

Just as there exists in the present-day seas the equilibrium

$$\underset{\text{gas}}{C^{13}O_2} + \underset{\text{ion}}{HC^{12}O_3^-} \rightleftarrows \underset{\text{gas}}{C^{12}O_2} + \underset{\text{ion in solution}}{HC^{13}O_3^-} \qquad \alpha = 1.014$$

in which the heavier isotope prefers to form the ion,[34] so within the ancient seas there was probably maintained the same equilibrium. The lime-secreting organisms that used the HCO_3^- ion in their metabolism would, therefore, have their organic parts enriched in C^{13}. If their organic remains later accumulated to form a limestone deposit, this enrichment should be reflected in a lower C^{12}/C^{13} isotope ratio for that limestone as compared with other rocks. It is interesting to note that the Grenville limestone examined by Nier and Gulbransen[45] did indeed show an enrichment of the C^{13} isotope by as much as 3 percent.

Professor Dempster[46] suggests the possibility of there being a separation effect in the case of long, narrow stalactites. In this case the purely chemical equilibrium (not emphasizing isotopic equilibrium) is as follows:

$$\underset{\text{calcite}}{CaCO_3} + H_2CO_3 \rightleftarrows \underset{\text{in solution}}{Ca(HCO_3)_2}.$$
$$\Updownarrow$$
$$H_2O + CO_2$$

[43] P. L. Robinson and H. V. A. Briscoe, J. Chem. Soc. London **127**, 138 (1925).
[44] G. N. Lewis and R. T. Macdonald, J. Am. Chem. Soc. **58**, 2519 (1936).
[45] Nier and Gulbransen, J. Am. Chem. Soc. **61**, 697 (1939).
[46] Personal communication from Professor Dempster.

The cyclic deposition and redissolving which takes place might tend to leave the heavier calcium isotopes at the top of the stalactite, whereas the lighter ones might preferentially migrate in solution to the bottom and be deposited there. It would be of interest to make isotope determinations on long pencil stalactites in particular.

In this paper the writer has not attempted to discuss the many biological processes which may later be found to offer excellent opportunities for separation of isotopes. Thirty-five years ago Balch[47] commented on the little-known fact that plants such as kelp, although growing in an oceanic medium where sodium abounds, are nevertheless able to assimilate the much less-abundant potassium to the extent of 30 percent by weight of their ash as compared with 10 percent sodium. It will not be surprising, therefore, if plants and animals are later found to show great preferential assimilation of isotopes as well as of elements. The results of the present investigation indicate, however, that though a plant may show a great preference for an element, it need not show a correspondingly great preference for any individual isotope of that element.

CONCLUSIONS

1. It has been found that the naturally occurring minerals that prove excellent thermionic emitters of potassium ions include orthoclase, microcline, muscovite, perthite, and microcline-perthite. It is believed that further study will show that many other naturally occurring potassium-bearing alumino-silicates are equally good emitters.

2. An examination of the most common Pacific kelps indicates that their potassium isotope ratio does not vary by more than 1 percent from that of rocks. In this respect the writer was unable to verify the results of Brewer.

3. An examination of two species of Cryptozoön fossils of Upper Cambrian age shows no difference in their potassium isotope ratio, within 1 percent error, from that of rocks. This result does not agree with that reported by Brewer and Baudisch on the same two species of fossils.

4. An examination of rocks of different geologic age, from Early pre-Cambrian to Tertiary, shows no measurable change in the potassium isotope ratio within the 1 percent accuracy obtainable.

5. The observed fluctuations of the isotope ratio are apparently due to isotope effects of the ion source.

6. With the laboratory methods of artificial separation of isotopes as a guide, an examination of the geologic processes has been made in an attempt to suggest where further evidence might be found that a measurable isotopic separation has been effected in rocks. Apart from biological processes, the geologic process of gradation appears likely to afford the best physical means of separating isotopes naturally. The phenomenon of base exchange in the zeolites and bentonite clays offers the best possibility of finding a measurable separation.

7. Chemical equilibrium within the ancient seas, coupled with the agency of lime-secreting organisms, may account for the enrichment observed by Nier of Grenville limestone in the C^{13} isotope.

ACKNOWLEDGMENTS

The author is deeply appreciative of the privilege of conducting this research under the immediate supervision of Professor A. J. Dempster. He is grateful not only for permission to use Professor Dempster's mass spectrograph and laboratory, but also for the ever-ready council and advice so kindly and generously given by Professor Dempster. He wishes to express his appreciation to Professor N. L. Bowen, whose kind help was given in the work incident to the preparation of the glasses and who permitted the use of the petrology laboratory of the University of Chicago. He wishes to express his thanks to Dr. H. E. Duckworth for teaching him the technique of operating the mass spectrograph. He is deeply indebted to the following for supplying him with specimens: Professors Bastin, Bowen, Fisher, Rigg, Berman, Goodman; Doctors Wohnus, Marble, Ellsworth, Goldring; Messrs. Spence, Chappers. Appreciation is expressed to Professor E. S. Bastin, Dr. A. E. Shaw, and Mr. Robert Smalley for several helpful suggestions and to other members of the Physics and Geology Departments of the University of Chicago for their interest and help.

[47] Balch, Ind. and Eng. Chem. 1, 777 (1909).

PHYSICAL REVIEW VOLUME 64, NUMBERS 9 AND 10 NOVEMBER 1 AND 15, 1943

Development of Electromagnetic Theory for Non-Homogeneous Spaces

BENJAMIN LIEBOWITZ
Trubenizing Process Corporation, New York, N. Y.
(Received July 21, 1943)

It is well known that any attempt by usual methods to extend classical electromagnetic theory to non-homogeneous spaces meets with the difficulty of wave equations which contain more than one component of the electromagnetic vectors or potentials. It is shown here that this difficulty can be overcome, so far as deriving separated wave equations is concerned, by introducing a Riemannian space whose line element $ds^2=h^2(du_1^2+du_2^2+du_3^2)$ is adjusted to the variable inductivity ϵ by means of the formula $h^2=1/\epsilon$. In addition, it has been found necessary to introduce an auxiliary scalar which is related to h by means of a differential equation, *viz.*, Eq. (11). The wave equations which are derived have essential singularities both at the origin and at infinity, for any reasonable choice of h. Simple electrostatic cases are discussed and then some cosmological implications of such a theory are brought out.

THE entire superstructure of electromagnetic theory is practically restricted to (a) space which is everywhere homogeneous, or (b) space subdivided by a finite number of boundaries into spaces each of which is homogeneous, or (c) space in which the inductivity as a function of the coordinates varies so slowly that the homogeneous approximation may be used. In all these cases Maxwell's circuit equations lead to a separate wave equation for each vector component or potential component. But if, for example, the specific inductive capacity of space is an arbitrary continuous function of the coordinates, i.e., if

$$\epsilon\equiv\epsilon(x, y, z), \tag{1}$$

then, as is well known, the wave equations obtained from the circuit equations by the usual methods contain more than one component and, on that account, are unworkable.

This restriction to homogeneous spaces can be lifted, that is, separate wave equations for each component can be derived, by the expedient of introducing a Riemannian space whose line element is "adjusted" to the variable inductivity. The justification and implications of using a Riemannian space in this way will be discussed in a later section.

We shall use the simplest conditions and means suitable for the purpose, and shall therefore assume the magnetic permeability of space to be constant; in the Gaussian units employed here, this constant is unity. Moreover, we shall regard the time as occupying the same privileged position it has in pre-relativity physics, and choose as our line element

$$ds^2=h^2(du_1^2+du_2^2+du_3^2) \tag{2}$$

where $h\equiv h(u_1u_2u_3)$ is independent of the time. The "adjustment," it turns out, consists simply in putting

$$h^2=1/\epsilon. \tag{3}$$

To effect the desired separation of the components in the final wave equations, it has been found necessary to introduce an auxiliary function of the coordinates $\Omega\equiv\Omega(u_1u_2u_3)$, which is related to h by Eq. (11) below. The appearance of this function in all the wave equations (except that for the scalar potential) is probably connected with our use of a 3-dimensional line element (2) instead of a 4-dimensional, which would have placed at our disposal another function besides h, *viz.*, the coefficient of dt^2. For our immediate purposes the introduction of Ω does not constitute a disadvantage.

Under the limitations here imposed, we can carry out all the necessary operations in generalized 3-dimensional curvilinear coordinates without making explicit use of the tensor calculus. The necessary formulation is given, for example, in Stratton's book,[1] page 44 (except that no equations, such

[1] J. A. Stratton, *Electromagnetic Theory* (McGraw-Hill Book Company, Inc., New York, 1941).

as given on page 49, relating the curvilinear coordinates to *Euclidian* space are applicable). For instance, the conditions for permitting the tensor curl[2] to be used as a vector are satisfied in this formulation.

We shall first deduce a wave equation for one of the components, say E_1, of the electric vector **E**. Starting with Maxwell's equations

$$\nabla\times\mathbf{E}+\frac{1}{c}\frac{\partial\mathbf{B}}{\partial t}=0,\quad \nabla\times\mathbf{H}-\frac{1}{c}\frac{\partial\mathbf{D}}{\partial t}=4\pi\mathbf{J},\quad \nabla\cdot\mathbf{B}=0,\quad \nabla\cdot\mathbf{D}=4\pi\rho,\quad \mathbf{D}=\epsilon(u_1u_2u_3)\mathbf{E},\quad \mathbf{B}=\mu\mathbf{H},\tag{4}$$

we take $\mu=1$ and introduce an auxiliary vector **F** defined by

$$\mathbf{E}=\Omega\mathbf{F}/h,\tag{5}$$

where $\Omega\equiv\Omega(u_1u_2u_3)$ is independent of t. (The constant c is to be regarded solely as the ratio of units; the "velocity of light" is given in this theory by $hc=c/\sqrt{\epsilon}$). Taking the curl of the first circuit equation we obtain:

$$\nabla\times\nabla\times\frac{\Omega\mathbf{F}}{h}+\frac{\epsilon}{c^2}\frac{\Omega}{h}\frac{\partial^2\mathbf{F}}{\partial t^2}+\frac{4\pi}{c}\frac{\partial\mathbf{J}}{\partial t}=0.\tag{6}$$

We now form

$$\left(\nabla\times\nabla\times\frac{\Omega\mathbf{F}}{h}\right)\cdot\mathbf{i}_1=\frac{1}{h^2}\left\{\frac{\partial}{\partial u_2}\frac{1}{h}\left(\frac{\partial}{\partial u_1}\Omega F_2-\frac{\partial}{\partial u_2}\Omega F_1\right)-\frac{\partial}{\partial u_3}\frac{1}{h}\left(\frac{\partial}{\partial u_3}\Omega F_1-\frac{\partial}{\partial u_1}\Omega F_3\right)\right\}.$$

Carrying out the indicated operations and making some obvious additions and subtractions, we obtain:

$$\left(\nabla\times\nabla\times\frac{\Omega\mathbf{F}}{h}\right)\cdot\mathbf{i}_1=\frac{1}{h^2}\left\{\frac{\Omega}{h}\sum\frac{\partial^2F_i}{\partial u_1\partial u_i}-\frac{\Omega}{h}\sum\frac{\partial^2F_1}{\partial u_i^2}+\sum\frac{\partial F_i}{\partial u_1}\left(\frac{1}{h}\frac{\partial\Omega}{\partial u_i}-\frac{\Omega}{h^2}\frac{\partial h}{\partial u_i}\right)+\sum\frac{\partial F_1}{\partial u_i}\left(\frac{\Omega}{h^2}\frac{\partial h}{\partial u_i}-\frac{2}{h}\frac{\partial\Omega}{\partial u_i}\right)\right.$$
$$\left.+\frac{1}{h}\frac{\partial\Omega}{\partial u_1}\sum\frac{\partial F_i}{\partial u_i}-\frac{1}{h^2}\frac{\partial\Omega}{\partial u_1}\sum F_i\frac{\partial h}{\partial u_i}+\frac{F_1}{h^2}\sum\frac{\partial\Omega}{\partial u_i}\frac{\partial h}{\partial u_i}\right\}.\tag{7}$$

We now form

$$\frac{\partial}{\partial u_1}\nabla\cdot\mathbf{D}=\frac{\partial}{\partial u_1}\nabla\cdot\frac{\epsilon\Omega\mathbf{F}}{h}$$

and solve the resulting equation for

$$\sum\frac{\partial^2F_i}{\partial u_1\partial u_i},$$

which results in

$$\sum\frac{\partial^2F_i}{\partial u_1\partial u_i}=\frac{h^2}{\epsilon\Omega}\frac{\partial}{\partial u_1}\nabla\cdot\mathbf{D}-\frac{h^2}{\epsilon\Omega}\frac{\partial}{\partial u_1}\frac{\epsilon\Omega}{h^2}\sum\frac{\partial F_i}{\partial u_i}-\sum\frac{\partial F_i}{\partial u_1}\left(\frac{1}{h}\frac{\partial h}{\partial u_i}+\frac{1}{\epsilon\Omega}\frac{\partial}{\partial u_i}\epsilon\Omega\right)$$
$$-\sum F_i\left(\frac{1}{h}\frac{\partial^2h}{\partial u_1\partial u_i}+\frac{h^2}{\epsilon\Omega}\frac{\partial}{\partial u_1}\frac{\epsilon\Omega}{h^2}\frac{\partial h}{\partial u_i}+\frac{1}{\epsilon\Omega}\frac{\partial^2}{\partial u_1\partial u_i}\epsilon\Omega+\frac{h^2}{\epsilon\Omega}\frac{\partial}{\partial u_1}\frac{1}{h^2}\frac{\partial}{\partial u_i}\epsilon\Omega\right).\tag{8}$$

Substituting this in (7), we have

$$\left(\nabla\times\nabla\times\frac{\Omega\mathbf{F}}{h}\right)\cdot\mathbf{i}_1=\frac{1}{h^2}\left\{\frac{h}{\epsilon}\frac{\partial}{\partial u_1}\nabla\cdot\mathbf{D}-\frac{\Omega}{h}\sum\frac{\partial^2F_1}{\partial u_i^2}-\sum\frac{\partial F_1}{\partial u_i}\left(\frac{2}{h}\frac{\partial\Omega}{\partial u_i}-\frac{\Omega}{h^2}\frac{\partial h}{\partial u_i}\right)+\frac{F_1}{h^2}\sum\frac{\partial\Omega}{\partial u_i}\frac{\partial h}{\partial u_i}+R\right\}.\tag{9}$$

[2] Levi Civita, *Absolute Differential Calculus* (Blackie and Son, Ltd., London, 1927), p. 162.

All terms containing components in addition to F_1 have been collected in R, where

$$R=\sum\frac{\partial F_i}{\partial u_1}\left(\frac{1}{h}\frac{\partial\Omega}{\partial u_i}-\frac{2\Omega}{h^2}\frac{\partial h}{\partial u_i}-\frac{1}{h\epsilon}\frac{\partial}{\partial u_i}\epsilon\Omega\right)-\left(\frac{h}{\epsilon}\frac{\partial}{\partial u_1}\frac{\epsilon\Omega}{h^2}-\frac{1}{h}\frac{\partial\Omega}{\partial u_1}\right)\sum\frac{\partial F_i}{\partial u_i}-\sum F_i\left(\frac{\partial\Omega}{\partial u_1}\frac{\partial h}{\partial u_i}\cdot\frac{1}{h^2}\right.$$

$$\left.+\frac{\Omega}{h^2}\frac{\partial^2 h}{\partial u_1\partial u_i}+\frac{h}{\epsilon}\frac{\partial h}{\partial u_i}\frac{\partial}{\partial u_1}\frac{\epsilon\Omega}{h^3}+\frac{1}{h\epsilon}\frac{\partial^2}{\partial u_1\partial u_i}\epsilon\Omega+\frac{h}{\epsilon}\frac{\partial}{\partial u_1}\frac{1}{h^2}\cdot\frac{\partial}{\partial u_i}\epsilon\Omega\right). \quad (10)$$

We make the first term on the right of (10) vanish by putting $h^2=a/\epsilon$. The constant a is chosen as unity in order that the final wave equation shall degenerate to the ordinary wave equation for $\epsilon=1$.

Now we introduce an undetermined function $g(u_1u_2u_3)$; putting G_{1i} for the coefficient of F_i in R, form the expression

$$\frac{R}{h^2}-\frac{\partial g}{\partial u_1}\nabla\cdot\mathbf{D}=-\frac{1}{h^2}\sum\frac{\partial F_i}{\partial u_i}\left(-\frac{1}{h}\frac{\partial\Omega}{\partial u_1}+\frac{h}{\epsilon}\frac{\partial}{\partial u_1}\frac{\epsilon\Omega}{h^2}+\epsilon\Omega\frac{\partial g}{\partial u_1}\right)-\frac{1}{h^2}\left\{G_{11}F_1+G_{12}F_2+G_{13}F_3\right.$$

$$\left.+\frac{\partial g}{\partial u_1}\left[F_1\left(\frac{\partial}{\partial u_1}\epsilon\Omega+\frac{\epsilon\Omega}{h}\frac{\partial h}{\partial u_1}\right)+F_2\left(\frac{\partial}{\partial u_2}\epsilon\Omega+\frac{\epsilon\Omega}{h}\frac{\partial h}{\partial u_2}\right)+F_3\left(\frac{\partial}{\partial u_3}\epsilon\Omega+\frac{\epsilon\Omega}{h}\frac{\partial h}{\partial u_3}\right)\right]\right\}.$$

Putting the coefficient of $\Sigma(\partial F_i/\partial u_i)=0$, we find $g=4h$ plus an arbitrary constant which we equate to zero. Putting the terms in F_2 and F_3 (but not in F_1) equal to zero, we find the required relation between Ω and h, *viz.*

$$\frac{1}{\Omega}\frac{\partial^2\Omega}{\partial u_i\partial u_j}-\frac{1}{h}\frac{\partial^2 h}{\partial u_i\partial u_j}+\frac{1}{h^2}\frac{\partial h}{\partial u_i}\frac{\partial h}{\partial u_j}=0 \qquad \begin{matrix} i\neq j \\ i,j=1,2,3. \end{matrix} \quad (11)$$

If h and Ω are functions of r only, $(r^2=u_1^2+u_2^2+u_3^2)$, this becomes

$$\frac{1}{\Omega}\left(\Omega''-\frac{\Omega'}{r}\right)-\frac{1}{h}\left(h''-\frac{h'}{r}\right)+\left(\frac{h'}{h}\right)^2=0. \quad (11a)$$

We now have left

$$\frac{R}{h^2}=4\frac{\partial h}{\partial u_1}\nabla\cdot\mathbf{D}-\frac{F_1}{h^2}\left[G_{11}+4\frac{\partial h}{\partial u_1}\left(\frac{\partial}{\partial u_1}\epsilon\Omega+\frac{\epsilon\Omega}{h}\frac{\partial h}{\partial u_1}\right)\right]=4\frac{\partial h}{\partial u_1}\rho-\frac{F_1}{h^3}\left(\frac{\partial^2\Omega}{\partial u_1^2}-\frac{\Omega}{h}\frac{\partial^2 h}{\partial u_1^2}+\frac{\Omega}{h^2}\left(\frac{\partial h}{\partial u_1}\right)^2\right).$$

All components other than F_1 have thus been eliminated from R and hence from $(\nabla\times\nabla\times\Omega\mathbf{F}/h)\cdot\mathbf{i}_1$. Introducing this value of R into Eq. (9) and the resulting Eq. (9) into the first component of Eq. (6), and rearranging, we get finally our wave equation for F_1:

$$\sum\frac{\partial^2 F_1}{\partial u_i^2}-\frac{1}{c^2}\frac{\partial^2 F_1}{\partial t^2}-F_1\left[\frac{1}{h\Omega}\sum\frac{\partial\Omega}{\partial u_i}\frac{\partial h}{\partial u_i}+\frac{1}{h}\frac{\partial^2 h}{\partial u_1^2}-\frac{1}{\Omega}\frac{\partial^2\Omega}{\partial u_1^2}-\left(\frac{1}{h}\frac{\partial h}{\partial u_1}\right)^2\right]+\sum\frac{\partial F_1}{\partial u_i}\frac{\partial}{\partial u_i}\log\frac{\Omega^2}{h}$$

$$=\frac{h^3}{\Omega}\left(\frac{4\pi}{c}\frac{\partial J_1}{\partial t}+4\pi h\frac{\partial\rho}{\partial u_1}+16\pi\frac{\partial h}{\partial u_1}\rho\right). \quad (12)$$

For spherically symmetrical cases, i.e., for $h\equiv h(r)$, $\Omega\equiv\Omega(r)$, this becomes:

$$\sum\frac{\partial^2 F_1}{\partial u_i^2}-\frac{1}{c^2}\frac{\partial^2 F_1}{\partial t^2}+\frac{1}{r}\frac{d}{dr}\log\frac{\Omega^2}{h}\sum u_i\frac{\partial F_1}{\partial u_i}-F_1\left(\frac{d}{dr}\log\Omega\frac{d}{dr}\log h-\frac{1}{r}\frac{d}{dr}\log\frac{\Omega}{h}\right)$$

$$=\frac{h^3}{\Omega}\left(\frac{4\pi}{c}\frac{\partial J_1}{\partial t}+4\pi h\frac{\partial\rho}{\partial u_1}+16\pi\frac{\partial h}{\partial u_1}\rho\right). \quad (12a)$$

Introducing the electric vector $E_1=\Omega F_1/h$, we find the wave equation for E_1 is (for $h\equiv h(r)$ etc.),

$$\sum\frac{\partial^2 E_1}{\partial u_i^2}+\frac{h'}{rh}\sum u_i\frac{\partial E_1}{\partial u_i}+\frac{2}{r}\left(\frac{h'}{h}-\frac{\Omega'}{\Omega}\right)E_1-\frac{1}{c^2}\frac{\partial^2 E_1}{\partial t^2}=h^2\left(\frac{4\pi}{c}\frac{\partial J_1}{\partial t}+4\pi h\frac{\partial\rho}{\partial u_1}+16\pi\frac{\partial h}{\partial u_1}\rho\right). \tag{12b}$$

The first derivatives can be eliminated by introducing another vector $\mathfrak{E}$ given by

$$\mathfrak{E}=h^{\frac{1}{2}}\mathbf{E},$$

for which the wave equation is

$$\sum\frac{\partial^2\mathfrak{E}_1}{\partial u_i^2}+\left(\frac{h'}{rh}+\frac{1}{4}\left(\frac{h'}{h}\right)^2-\frac{1}{2}\frac{h''}{h}-\frac{2}{r}\frac{\Omega'}{\Omega}\right)\mathfrak{E}_1-\frac{1}{c^2}\frac{\partial^2\mathfrak{E}_1}{\partial t^2}=h^{5/2}\left(\frac{4\pi}{c}\frac{\partial J_1}{\partial t}+4\pi h\frac{\partial\rho}{\partial u_1}+16\pi\frac{\partial h}{\partial u_1}\rho\right). \tag{12c}$$

From Eq. (12b) we may obtain the meaning of the expression "velocity of light." Let us suppose that in some region ϵ (or h) varies slowly so that we may neglect the derivatives of h and Ω. Let us consider a plane wave traveling in the u_2 direction and write $ds=hdu_2$. Then Eq. (12b) reduces to

$$h^2\frac{\partial^2 E}{\partial s^2}-\frac{1}{c^2}\frac{\partial^2 E}{\partial t^2}=\frac{4\pi h^2}{c}\frac{\partial J}{\partial t}+4\pi h^4\frac{\partial\rho}{\partial s}$$

or

$$\frac{\partial^2 E}{\partial s^2}-\frac{\epsilon}{c^2}\frac{\partial^2 E}{\partial t^2}=\frac{4\pi}{c}\frac{\partial J}{\partial t}+\frac{4\pi}{\epsilon}\frac{\partial\rho}{\partial s}.$$

This is identical in form with the ordinary wave equation for a medium with constant inductivity and shows that the measured velocity of light is hc or $c/\sqrt{\epsilon}$, in regions where h does not vary too rapidly.

To derive corresponding wave equations for the vector and scalar potentials, the vector potential $\mathbf{A}$ is introduced as usual by

$$\mathbf{B}=\nabla\times\mathbf{A},\quad \mathbf{A}=\mathbf{A}_0-\nabla\psi,$$

where ψ is an arbitrary function of the coordinates. Introducing this into the first circuit equation of (4) we have, as usual,

$$\nabla\times\left(\mathbf{E}+\frac{1}{c}\frac{\partial\mathbf{A}}{\partial t}\right)=0\quad\text{or}\quad\mathbf{E}=-\nabla\varphi-\frac{1}{c}\frac{\partial\mathbf{A}}{\partial t},$$

so that

$$\nabla\times\nabla\times\mathbf{A}+\frac{\epsilon}{c}\frac{\partial}{\partial t}\nabla\varphi+\frac{\epsilon}{c^2}\frac{\partial^2\mathbf{A}}{\partial t^2}=4\pi\mathbf{J} \tag{13}$$

and

$$-\nabla\cdot\mathbf{D}=\nabla\cdot\epsilon\nabla\varphi+\frac{1}{c}\frac{\partial}{\partial t}\nabla\cdot\epsilon\mathbf{A}=-4\pi\rho. \tag{14}$$

Instead of using the usual relationship

$$\nabla\cdot\mathbf{A}+\frac{1}{c}\frac{\partial\varphi}{\partial t}=0$$

between the scalar and vector potentials, we shall use

$$\nabla\cdot\epsilon\mathbf{A}+\frac{\epsilon^2}{c}\frac{\partial\varphi}{\partial t}=0. \tag{15}$$

The justification for this will be given presently.

Introducing (15) into (13) and (14) we find

$$\nabla\times\nabla\times\mathbf{A}-\epsilon\nabla\left(\frac{1}{\epsilon^2}\nabla\epsilon\cdot\mathbf{A}\right)+\frac{\epsilon}{c^2}\frac{\partial^2\mathbf{A}}{\partial t^2}=4\pi\mathbf{J}, \tag{16}$$

$$\nabla\cdot\epsilon\nabla\varphi-\frac{\epsilon^2}{c^2}\frac{\partial^2\varphi}{\partial t^2}=-4\pi\rho. \tag{17}$$

Expanding $\nabla\cdot\epsilon\nabla\varphi$ in Eq. (17) and using Eq. (3), we obtain for our scalar potential the following wave equation

$$\sum\frac{\partial^2\varphi}{\partial u_i^2}-\frac{1}{h}\sum\frac{\partial\varphi}{\partial u_i}\frac{\partial h}{\partial u_i}-\frac{1}{c^2}\frac{\partial^2\varphi}{\partial t^2}=-4\pi h^4\rho. \tag{18}$$

If h is a function of r only, this becomes

$$\sum\frac{\partial^2\varphi}{\partial u_i^2}-\frac{1}{hr}\frac{dh}{dr}\sum u_i\frac{\partial\varphi}{\partial u_i}-\frac{1}{c^2}\frac{\partial^2\varphi}{\partial t^2}=-4\pi h^4\rho. \tag{18a}$$

We now introduce the auxiliary vector $\mathbf{Q}$ defined by

$$\mathbf{A}=\Omega\mathbf{Q}/h \tag{19}$$

into Eq. (16), along with (15) and (3). Carrying out the expansion of $(\nabla\times\nabla\times\Omega\mathbf{Q}/h)\cdot\mathbf{i}_1$ as before, and using (11), we obtain finally the wave equation for the first component of the auxiliary vector:

$$\sum\frac{\partial^2Q_1}{\partial u_i^2}-\sum\frac{\partial Q_1}{\partial u_i}\left(\frac{1}{h}\frac{\partial h}{\partial u_i}-\frac{2}{\Omega}\frac{\partial\Omega}{\partial u_i}\right)+Q_1\left[\frac{1}{\Omega}\frac{\partial^2\Omega}{\partial u_1^2}+\left(\frac{1}{h}\frac{\partial h}{\partial u_1}\right)^2-\frac{1}{h}\frac{\partial^2h}{\partial u_1^2}-\frac{1}{h\Omega}\sum\frac{\partial\Omega}{\partial u_i}\frac{\partial h}{\partial u_i}\right]-\frac{1}{c^2}\frac{\partial^2Q_1}{\partial t^2}=-\frac{4\pi h^3J_1}{\Omega}. \tag{20}$$

It will be noted that the left side of this equation is exactly the same as the left side of Eq. (12); that is to say, where there are no currents or charges, the electric vector and the vector potential are propagated according to the same law, as we should expect.

The scalar potential, it will be noted, is not propagated according to the same law as the vectors. In Eq. (18) we can eliminate the first derivatives by introducing a modified scalar potential Φ defined by

$$\varphi=h^{\frac{1}{2}}\Phi \tag{21}$$

which yields

$$\sum\frac{\partial^2\Phi}{\partial u_i^2}+\Phi\left(\frac{1}{2h}\sum\frac{\partial^2h}{\partial u_i^2}-\frac{3}{4h^2}\sum\left(\frac{\partial h}{\partial u_i}\right)^2\right)-\frac{1}{c^2}\frac{\partial^2\Phi}{\partial t^2}=-4\pi h^{7/2}\rho. \tag{22}$$

If h and Ω are functions of r only, then the last equation becomes

$$\sum\frac{\partial^2\Phi}{\partial u_i^2}+\left(\frac{1}{2h}\frac{d^2h}{dr^2}+\frac{1}{rh}\frac{dh}{dr}-\frac{3}{4h^2}\left(\frac{dh}{dr}\right)^2\right)\Phi-\frac{1}{c^2}\frac{\partial^2\Phi}{\partial t^2}=-4\pi h^{7/2}\rho. \tag{23}$$

Our justification for Eq. (15) follows the usual lines (see Stratton,[1] page 24). We may assume that particular solutions of Eqs. (16) and (17) exist; let us call them $\mathbf{A}_0$ and φ_0. Now, from $\mathbf{B}=\nabla\times\mathbf{A}$, we can choose $\mathbf{A}=\mathbf{A}_0-\nabla\psi$, since the curl of the gradient vanishes. This results in two expressions for $\mathbf{E}$, and in order that they shall agree, we must have $\varphi=\varphi_0+(1/c)(\partial\psi/\partial t)$. Inserting these more general expressions for $\mathbf{A}$ and φ in Eq. (15), we obtain

$$\nabla\cdot\epsilon\nabla\psi-\frac{\epsilon^2}{c^2}\frac{\partial^2\psi}{\partial t^2}=\nabla\cdot\epsilon\mathbf{A}_0+\frac{\epsilon^2}{c}\frac{\partial\varphi_0}{\partial t}, \tag{24}$$

the left side of which is identical with the left side of (17). Hence, we can satisfy Eq. (15) by first choosing $\mathbf{A}_0$ and φ_0 as particular solutions of (16) and (17) and then choosing

$$\mathbf{A}=\mathbf{A}_0-\nabla\psi, \quad \varphi=\varphi_0+\frac{1}{c}\frac{\partial\psi}{\partial t},$$

where ψ is a particular solution of (24). In actual practice, of course, these steps are unnecessary; having obtained solutions $\mathbf{A}$ and φ of the wave equations, it is only necessary to test them to see if they satisfy Eq. (15).

With the derivation of these wave equations, the first objective of this paper has been achieved. We now consider a few simple electrostatic cases and some implications of the theory.

In spherical coordinates, Eq. (18) for the scalar potential becomes:

$$\frac{1}{r^2}\frac{\partial}{\partial r}\left(r^2\frac{\partial\varphi}{\partial r}\right)+\frac{1}{r^2\sin\theta}\frac{\partial}{\partial\theta}\left(\sin\theta\frac{\partial\varphi}{\partial\theta}\right)+\frac{1}{r^2\sin^2\theta}\frac{\partial^2\varphi}{\partial\psi^2}$$
$$-\frac{1}{h}\left(\frac{\partial h}{\partial r}\frac{\partial\varphi}{\partial r}+\frac{1}{r^2}\frac{\partial h}{\partial\theta}\frac{\partial\varphi}{\partial\theta}+\frac{1}{r^2\sin^2\theta}\frac{\partial h}{\partial\psi}\frac{\partial\varphi}{\partial\psi}\right)-\frac{1}{c^2}\frac{\partial^2\varphi}{\partial t^2}=-4\pi h^4\rho. \quad (25)$$

First, for a single particle, let ρ be zero everywhere except in a small region at the origin, and let φ be independent of θ and ψ. Then, except for the small region around the origin, Eq. (25) reduces to

$$\frac{d^2\varphi}{dr^2}+\left(\frac{2}{r}-\frac{h'}{h}\right)\frac{d\varphi}{dr}=0,$$

which becomes on integration

$$\frac{1}{h}\frac{d\varphi}{dr}=\frac{\text{const}}{r^2}.$$

But $(1/h)(d\varphi/dr)$ is the gradient of φ in this case, and that in turn is the electric vector $\mathbf{E}_r$. Putting the constant of integration equal to the charge e, we have Coulomb's law which, we see, is unchanged, no matter what the form of h may be. But the situation with respect to energy is changed, i.e., the energy of a point charge need not be infinite as it is in homogeneous spaces. The total energy of a point charge is

$$W=\frac{1}{8\pi}\int\int\int \epsilon E_r^2 h^3 r^2\sin\theta d\theta d\psi dr=\frac{e^2}{2}\int_0^\infty\frac{h dr}{r^2}.$$

Now, one of the possible choices for ϵ which we will discuss below is $\epsilon=e^{2\alpha/r}$, or $h=e^{-\alpha/r}$; using this form here we get

$$W=e^2/2\alpha.$$

If we demand that this energy shall equal the rest energy of the electron, we get for α the classical radius of the electron, *viz.*, $e^2/2mc^2$. However, all this is incidental and not even appropriate for the general purposes of the theory, in which we shall consider other forms for h and, more particularly, in which we shall wish to make α independent of the charge and proportional to the mass of a particle instead of inversely proportional thereto.

Let us consider now the case of an electrostatic dipole; in this case φ is independent of ψ, and, except for the small regions where charge exists, Eq. (25) can be written:

$$\frac{\partial^2\varphi}{\partial r^2}+\left(\frac{2}{r}-\frac{1}{h}\frac{\partial h}{\partial r}\right)\frac{\partial\varphi}{\partial r}=-\frac{1}{r^2}\left[\frac{1}{\sin\theta}\frac{\partial}{\partial\theta}\left(\sin\theta\frac{\partial\varphi}{\partial\theta}\right)-\frac{1}{h}\frac{\partial h}{\partial\theta}\frac{\partial\varphi}{\partial\theta}\right],$$

or

$$\frac{\partial}{\partial r}\left(\frac{r^2}{h}\frac{\partial\varphi}{\partial r}\right)=-\frac{1}{\sin\theta}\frac{\partial}{\partial\theta}\left(\frac{\sin\theta}{h}\frac{\partial\varphi}{\partial\theta}\right).$$

But $(1/h)(\partial\varphi/\partial r)=E_r$ and $(1/hr)(\partial\varphi/\partial\theta)=E_\theta$, hence

$$\frac{1}{r}\frac{\partial}{\partial r}(r^2E_r)=-\frac{1}{\sin\theta}\frac{\partial}{\partial\theta}(E_\theta\sin\theta),$$

and this is satisfied by the usual expressions for the electric force due to a doublet, *viz.*, $E_r=k\cos\theta/r^3$, $E_\theta=k\sin\theta/2r^3$ (Stratton,[1] p. 175). But, although the *expressions* for the electrostatic forces are unchanged, it should be borne in mind that the actual radial distance is not r but $\int h dr$.

A limitation which experience imposes on ϵ is that it shall be sensibly unity at large distances from an atomic nucleus and that it shall increase (as we shall see) as the nucleus is approached. But very close to or within the nucleus ϵ is not bound by convention; we may allow h to become negative or imaginary if that serves a valid purpose, and in such cases we can probably find justification, if need be, for cutting off the integration. But above all, there is no necessity at this stage of the theory for considering point charges at all. There seem to be opportunities here for constructing a theory of nuclear forces and of forces which can hold an electron together; this would rid us of the infinite energy difficulty at its source.

While there is considerable latitude in the choice of the function h, it is nevertheless restricted by phenomenological considerations other than those already mentioned and also, to be sure, by the practical consideration that it must lead through Eq. (11) to a function Ω which, when inserted in the wave equations, will not make them too difficult or unworkable. In order to aid in finding the simplest pairs of functions h and Ω which satisfy (11), that equation may be written as

$$\frac{\partial^2 U}{\partial u_i\partial u_j}+\frac{\partial V}{\partial u_i}\frac{\partial V}{\partial u_j}=0\quad(i\neq j),\tag{26}$$

where $U=\log(\Omega/h)$ and $V=\log\Omega$. If h is a function of r only Eq. (26) becomes

$$U''-\frac{U'}{r}+V'^2=0\quad\text{or}\quad\frac{U'}{r}=-\int\frac{V'^2}{r}dr.\tag{26a}$$

With the aid of this equation I have found the following comparatively simple pairs of functions

$$h=\exp[-\alpha/r+\alpha^2/8r^2],\quad\Omega=\exp[-\alpha/r];\quad h=\exp[-\alpha/3r+\alpha^2/8r^2],\quad\Omega=r^2\exp[\alpha/r];$$
$$h=\exp[-\alpha/r^4],\quad\Omega=r^2\exp[i(6\alpha)^{\frac{1}{2}}/r^2].$$

None of these leads to simple wave equations; only one gives finite energy to a point charge. For $h=e^{-\alpha/r}$, I find the following series for Ω:

$$\Omega=b_0\left\{1-\frac{\alpha}{r}+\frac{3}{8}\left(\frac{\alpha}{r}\right)^2-\frac{3}{40}\left(\frac{\alpha}{r}\right)^3+\frac{3}{320}\left(\frac{\alpha}{r}\right)^4\cdots\right\}.$$

This would be usable for atomic theory only if it would be permissible to cut the series off after the first few terms on the ground that α is so small that higher powers can be neglected outside the nucleus. Whatever choice we may make for h, it must take the form $1-(\alpha/r^n)$ in the large distance approximation, with n real and positive. For further discussion, we assume $n=1$.

So far we have considered the form of h for a single particle. In the case of two particles whose relative motion is either zero or very small, we must impose the condition that a distance ds measured in the frame of reference of one particle shall equal the measurement obtained in the frame of refer-

ence of the other particle. To meet this condition we shall assume that the h for two particles is the product of the h's of the individual particles considered as infinitely separated. If we denote by h_i the "independent" h for the ith particle, then for n particles we have

$$h=\prod_1^n h_i. \tag{27}$$

Herein, it appears, lie the possibilities mentioned for nuclear theory.

In the macroscopic approximation, (27) becomes

$$h=1-\sum\frac{\alpha_i}{r_i}, \tag{27a}$$

where the sum must be a very small quantity in ordinary space. Hence, for the velocity of light we have

$$V=hc=c-c\sum\frac{\alpha_i}{r_i}. \tag{28}$$

The summation in (28) extends over all particles in the universe. There is no *a priori* reason for assuming it to be the same throughout the universe. Moreover, if the motions between the particles are not entirely negligible, then V may vary in time at a given point, and it is conceivable that the velocity of light may not even be wholly isotropic at a given point; if such anisotropy exists, it may vary with time and with position. In this discussion I have naturally had in mind the results which Dayton C. Miller obtained in his protracted observations with the Michelson-Morley apparatus.

Theoretical physicists speak of frequencies where spectroscopists speak of wave numbers. If we take the latter viewpoint literally, that is, if we regard the primary feature of a spectral line as its wave-length unaffected by the local V at the point of origin, this length will be subject to change with change in V as the light ray travels through the universe. On such an assumption, we may interpret the nebular red shift as indicating that the velocity of light is greater in our region of space than in the distant regions surrounding us.

This theory could not have been born if Riemannian spaces had not been previously introduced into physics by the theory of relativity. On the other hand, our ideas were conceived without benefit of invariance. In its present state, therefore, this theory must explain phenomena in its own right, so far as it can, without calling on the relativity theory. For example, we must interpret the deflection of light rays near the sun's limb as an electromagnetic phenomenon arising from the change in the inductivity of the space surrounding the sun in accordance with Eq. (28) (compare reference 2, page 402–3). It is on this ground that we have regarded it as necessary that h shall decrease (ϵ shall increase) as an atom is approached. The "gravitational" red shift of light from the sun is to be similarly understood.

The writer has long felt that the limitations imposed on the classical theory by the restriction to homogeneous space left some of its greatest potentialities unexplored. For instance, the failure of the classical theory in atomic domains may possibly be due to just this restriction. Our theory began as an attempt to understand atomic phenomena in terms of an extended classical theory, but in the course of development it seems to have spread itself all over the universe. Just now we shall make but one comment on the applications of the theory to atomic phenomena, *viz.*, that in its light every atom can conceivably be endowed with a permanent system of electromagnetic wave fields which will not radiate itself away—a conception which was impossible under the old restrictions.

The next task, therefore, is to determine whether or not, with suitable choice of h, non-radiating solutions of the wave equations actually exist which are everywhere finite, and possess finite energy. This task is difficult because all the wave equations have essential singularities both at the origin and at infinity.[3]

[3] Added in proof: It may be pointed out that Mathieu's equation, when suitably transformed, also has irregular points at the origin and infinity. See A. Erdélyi, Math. Zeits. **41**, 653ff. (1936).

PHYSICAL REVIEW VOLUME 64, NUMBERS 9 AND 10 NOVEMBER 1 AND 15, 1943

The Joule Effect in Air

H. D. BAKER*
Department of Physics, University of Wisconsin, Madison, Wisconsin
(Received December 24, 1941)

Previous methods used in determining the magnitude of the Joule effect are reviewed and their significance discussed. Essential requirements on apparatus and the technique necessary for measuring reliably this effect to within 0.1 percent are analyzed. The construction of and operational technique for a set of apparatus built to these requirements are described. Sample data on air are given and compared with other values in the literature. It is concluded that with indicated improvements in detail, the method developed here will achieve precision and reliability to within 0.1 percent.

I. INTRODUCTION

THE Joule effect may be visualized in terms of an "armchair" experiment. Imagine a vessel with thermally non-conducting and mechanically rigid walls, divided into two compartments by a partition. Suppose that a gas is admitted into one compartment, and the other is evacuated. If the partition is removed, the gas will undergo what is known as a "free expansion" in which no external work is done and no heat transfer with the environment takes place. Then in the statement of the first law,

$$\Delta U = Q - W, \tag{1}$$

$Q=W=0$; and hence ΔU, the change in the internal energy, is also zero.

If, during this expansion, internal energy shifts take place between the various degrees of freedom or energy levels in the gas, one may expect a corresponding change in temperature to result. An example of such an internal energy shift would be that corresponding to work done against the intermolecular forces. This temperature change is measured by what is known as the "free expansion" or "Joule" coefficient. Thus:

$$\eta = \left(\frac{\partial T}{\partial v}\right)_u, \tag{2}$$

and

$$\eta' = \left(\frac{\partial T}{\partial p}\right)_u. \tag{3}$$

Other measures of the "Joule effect" are,

$$\lambda = \left(\frac{\partial u}{\partial v}\right)_T = -\left(\frac{\partial u}{\partial T}\right)_v \left(\frac{\partial T}{\partial v}\right)_u = -C_v\eta, \tag{4}$$

$$\lambda' = \left(\frac{\partial u}{\partial p}\right)_T = -\left(\frac{\partial u}{\partial T}\right)_p \left(\frac{\partial T}{\partial p}\right)_u = -(C_p - pv\alpha)\eta', \tag{5}$$

where α is the coefficient of volume expansion.

There are several reasons why it is desirable to know the values of η, η', λ and λ' with the greatest possible precision. First, since these quantities are zero for ideal gases, the finite values for real gases serve to measure the departure of real gases from the ideal condition.[1] Second, these quantities are connected with the virial coefficients which, in turn, are associated with the law of molecular attraction.[2] Third, these quantities enable one to measure the value of the Kelvin ice point.[3]

II. EXPERIMENTAL METHODS

Attempts to measure $(\partial T/dv)_u$ have followed two general methods. Joule (1843)[4] and later Regnault, permitted the gases after expansion to come to thermal equilibrium with the walls of the containing vessel. Their hope was to infer the change in temperature of the gas on expansion from the subsequent change in temperature of the entire system including the vessel and a surrounding water bath. Actually the heat capacity of the system, roughly 1000 times that of the gas alone, so reduced this final temperature

* Now at Department of Mechanical Engineering, Columbia University, New York, New York.

[1] A. L. Clark, Trans. Roy. Soc. Can. [3] **28**, 293–311 (1924).
[2] J. O. Hirschfelder, R. B. Ewell, and J. R. Roebuck, J. Chem. Phys. **6**, 205 (1938).
[3] J. R. Roebuck and T: A. Murrell, in *Temperature, Its Measurement and Control in Science and Industry* (Reinhold Publishing Corporation, New York, 1941), p. 65.
[4] J. S. Ames, *The Free Expansion of Gases* (Harper & Bros., New York, 1898).

change as to make it undetectable with the instruments at their disposal.

Hirn,[5] Cazin,[6] and Keyes and Sears[7] attempted to measure the change in temperature of the gas before it came to equilibrium with the containing vessel. Hirn and Cazin attempted to make the gas serve as its own thermometer. Keyes and Sears used a special platinum resistance thermometer. Results by the second method vary, but are usually high by a large factor. These may be explained by assuming energy interchange with the vessel during expansion. When the expansion occurs through a valve, apparently the predominating effect is the dissipation of kinetic energy of streaming into heat which is conducted through the valve. When the gas is released by the shattering of a glass partition, the kinetic energy conferred upon the fragments affects the result in the same way. The experiment thus fails to satisfy the adiabatic condition. Seventy-five years of work have not brought a solution to this difficulty.

Measurements of $(\partial u/dp)_T$ have followed two methods, both of which involve letting the gas come to equilibrium with the containing vessel. In Washburn's method[8] carried out by Rossini and Frandsen[9] the system includes a water bath as Joule's did. The wall of the second chamber is, however, omitted; the expansion occurs into the atmosphere through a long tube immersed in the bath. These modifications reduce the heat capacity of the system by about one-half, and approximately double the pressure drop, i.e., for the same mass of gas and the same initial pressure. By means of measured electrical energy injected into the bath during expansion the experiment is made nearly isothermal. The constancy of temperature is indicated by a highly sensitive platinum resistance thermometer. It is essentially the 250-fold greater sensitivity of this thermometer over that used by Joule which makes this method capable of yielding quantitative results, whereas that of Joule did not.

For the case of this experiment the first law may be written,

$$u(P_2, T)-u(P_1, T)=\frac{Q-W}{n}-\frac{\Delta U}{n}\ \text{(metal)} \quad (6)$$

where Q is the electrical energy input, W is the mechanical work done against the atmosphere, n is the number of moles of gas, ΔU (metal) is the increase in internal energy experienced by the vessel during the expansion, and $u(P, T)$ is the molar intrinsic energy of the gas.

By holding P_2 and T constant one obtains $u(P_2, T)-u(P_1, T)$ for a series of values of P_1, and this is plotted against P_1. The slopes of such curves then are the values obtained for $(\partial u/\partial p)_T$.

Rossini and Frandsen estimate their results to be accurate to within $\pm 2\frac{1}{2}$ percent. Since this accuracy depended on the determination of bath temperatures to within 0.0001°C, the method does not appear susceptible of any appreciably greater degree of accuracy.

In the present method the system consists merely of the gas itself and two thin metal shells, as shown in Fig. 1. The shells are constructed for minimum heat capacity. The system at maximum working pressure has thus a heat capacity only about fifteen times greater than that of the contained gas, instead of 1000 times as in the case of Joule. With this heat capacity ratio the change in temperature which would

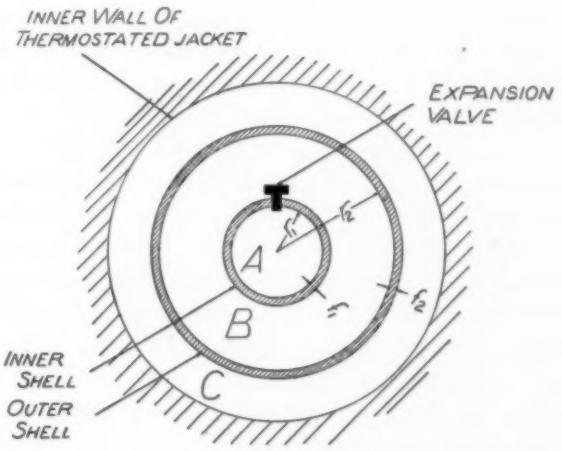

FIG. 1. Diagram of system. A is inner chamber containing n_1 moles of air at pressure P_1 before expansion; B is outer chamber containing n_2 moles of air at pressure P_2 before expansion; C is insulating layer of air at pressure P_0. Pressure in A and B after expansion is P_3.

[5] G. A. Hirn, *Exp. Anal. et Exp. de la Th. Mec. de la Chaleur* (Paris, 1875), third edition.
[6] A. Cazin, Phil. Mag. **40**, 81 (1870).
[7] F. B. Keyes and F. W. Sears, Proc. Nat. Acad. Sci. **11**, 38 (1925).
[8] E. W. Washburn, Bur. Stand. J. Research **9**, 521 (1932).
[9] F. D. Rossini and M. Frandsen, Bur. Stand. J. Research **9**, 733 (1932).

result if an expansion could occur under adiabatic conditions would be about 1½°C.

III. THEORY OF PRESENT APPARATUS

The design of the present apparatus was governed by three general objectives.

First, it was necessary that the heat capacity of the shells relative to that of the contained gas be a minimum.

Second, it was necessary that transfer of heat between the system and its surroundings during the equilibrating period be a minimum, and that means be devised to measure and correct for such flow as could not be prevented.

Third, it was necessary that heat absorbed or liberated by the shells upon alteration of their stress be minimized, and that means be devised to correct for such heat exchange as could not be prevented.

In regard to the first condition, a vessel of small relative mass was attained, primarily through use of a material of high tensile strength, combined with a design devoid of massive fittings, such as flanges, etc. Since the heat capacities per unit volume of most suitable materials do not differ greatly, this property did not feature particularly in the reasoning. The spherical form was found to be optimum, and was adopted; there were two concentric shells. See Fig. 1 and Fig. 2. It was noted that nothing was to be gained in regard to the first objective by going either to very large or to very small shells. Because of a combination of desirable properties Invar was chosen as a material and was used at stresses up to an elastic limit of about 45,000 lb./in.^{2}.

Since gas densities at any given pressure increase with decreasing temperature the ratio of gas mass to vessel mass (and hence of thermal capacities) will tend to be higher. The apparatus will hence tend to be more sensitive when one is working at low than when working at relatively high temperatures. Also when the pressure drops are relatively large, $u(P_2, T)-u(P_1, T)$ in the gas is, in general, larger without the mass of the shells being greater. Thus, when one is working at relatively large pressure drops, the apparatus tends also to be more sensitive.

To achieve the second objective various measures were found suitable. Thus to minimize

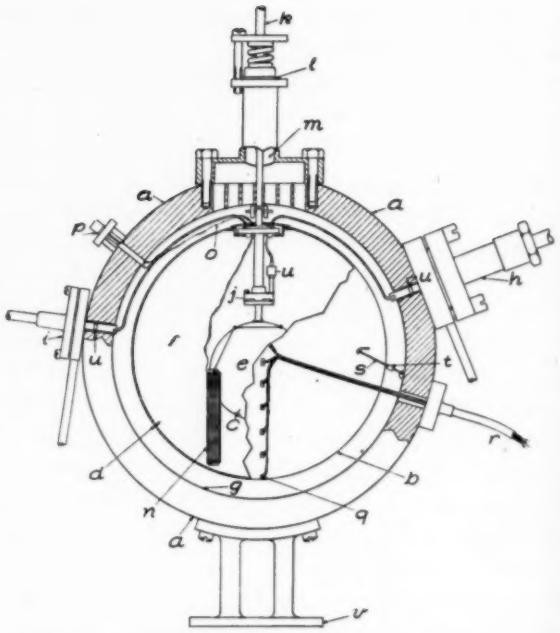

FIG. 2. Vessel and central mounting plate assembly. *a*—central mounting plate; *b*—vessel; *c*—inner shell; *d*—outer shell; *e*—inner chamber; *f*—outer chamber; *g*—jacket surface; *h*—inlet valve; *i*—outlet valve; *j*—expansion valve; *k*—forked valve stem; *l*—ground metal seal; *m*—passage to vacuum system; *n*—heater coil; *o*—heater leads; *p*—battery and potentiometer connection; *q*—thermopile junctions; *r*—thermopile leads; *s*—guy wires; *t*—turnbuckle; *u*—union; *v*—insulating support.

the heat transfer to the surroundings during the equilibrating period, it was necessary to minimize both the rate of transfer and the duration of this period.

In regard to the latter it was inferred from various calculations that this period would be shorter for a smaller vessel than for a large one. Since, however, the quantity of working substance decreases with the size of the vessel, other things being equal, and small spurious quantities of heat, such as that generated in opening the valves, tend to become magnified in importance, it was not deemed advisable to reduce the size below a certain minimum. For this the equilibrating period was about ninety minutes.

To minimize the rate of transfer, conduction, convection, and radiation were dealt with separately. Since all three depend on the temperature difference, the outer shell was surrounded by a jacket maintained at a temperature near that of the shell.

Conduction was minimized by as nearly as possible eliminating all heat paths through solids

from the vessel to the surroundings. Thus, the shells were supported by six fine piano wires (0.005″ diam.). Electrical connections were made through long, fine wires of low conductivity material (manganin). Tubes for conveying the working substance, i.e., the gas to and from the vessel, were long, fine, and of low conductivity material (1/64″ and 1/32″ diam. stainless steel).

Convection and gaseous conduction were to have been eliminated by maintaining a high vacuum in the space between the outer shell and the jacket. Actually this was not achieved in the present work; however convection was greatly reduced by the absence of any appreciable temperature gradients in the space. Making the shells spherical with one shell inside the other minimized the surface exposed to radiation and convection transfer.

Radiation transfer was further reduced by making the jacket spherical, concentric, and near to the outer shell, and by providing a high reflection coefficient on the opposing surfaces.[10] (The jacket surface was of polished silver; the outer shell of polished Invar.)

To measure the heat actually transferred, it was assumed that the transfer would take place according to the equation,

$$\Delta q = e \int_{t_1}^{t_2} \Delta T dt \qquad (7)$$

where, t = time; ΔT = average temperature difference between the jacket and the outer shell; e = emission constant. Since ΔT was never more than 1°C this assumption was probably not seriously in error.

In order to measure ΔT as a function of t during the equilibrating period, twenty-four thermoelectric junctions were distributed over the exterior surface of the outer shell. These were in series, while the corresponding junctions were in the jacket flow. The jacket was assumed to be of uniform temperature.

To determine the emission constant, e, an electric heater symmetrically disposed was provided within the shells. At a constant wattage ΔT would become constant, resulting in a constant galvanometer deflection. It was not necessary to convert the latter to degrees centigrade. The constant e was simply taken as a ratio of the steady power input to the magnitude of the resulting galvanometer deflection.

There is a tendency for ΔT to be very large during the period immediately following expansion. The gas expands from the space within the inner shell to the space between the two shells. Hence the temperature in the outer chamber rises and that in the inner chamber drops. Such gas as remains within the inner shell has then undergone a semi-adiabatic expansion doing work on the gas packed into the outer chamber.

For air at 20°C and a doubling of volume on adiabatic expansion this rise in temperature in the outer space might be as much as 85°C. For larger expansion ratios this peak temperature decreases. If the substance is one for which $(\partial T/\partial v)_u$ is negative, it may be possible to find an expansion ratio for which the decrease in temperature due to the Joule effect just offsets this tendency to adiabatic rise in temperature. For air this is feasible; however, it works for but one initial pressure. In the present work, where other initial pressures were used, this transient rise was still appreciable.

In regard to the third objective there are three modes by which heat exchange might occur between the gas and the shell materials. These are heat of plastic deformation, heat of adsorption, and heat due to the thermoelastic effect.

Heat of plastic deformation[11] is eliminated by keeping all stresses in the shells below the elastic limit of the material. The spherical form, resulting in nearly homogeneous stress, facilitates this.

A change, during an experiment, of the quantity of gas adsorbed upon the inner surface of the shells would involve heat transfer. This effect is probably small at nearly constant temperature and moderate pressures.[12] Experiments with varied adsorbing areas would yield corrections for this error.

Thermoelastic energy shifts between potential and heat energy, when materials are strained, are known to be appreciable,[13] and such shifts will

[10] M. Fishenden and O. A. Saunders, *The Calculation of Heat Transmission* (H. M. Stationery Office, London, 1932), pp. 28–29.

[11] W. S. Farren and G. L. Taylor, Proc. Roy. Soc. London, **A107**, 423 (1925).

[12] K. Fischbeck, H. Mass, and H. Meissenheimer, Zeits. f. physik. Chemie **A171**, 385 (1934).

[13] K. T. Compton and D. B. Webster, Phys. Rev. **5**, 159 (1915).

unavoidably take place in the inner and outer shells. As far as the writer can determine, previous data and computation formulae on this effect have been limited to the one-dimensional case.[13] These formulae involve certain dubious approximations, and experimental determinations differ from one another by several percent.[13] The magnitude of this error is thus left in doubt.

To remove this doubt an exhaustive theoretical analysis has been made.[14] The three-dimensional case was treated. Quantitative estimate was made of possible discrepancies due to all assumptions made.

Kelvin's formula,[15]

$$\Delta q = -\frac{T}{J}\left[\frac{\partial(\Delta w)}{\partial T}\right]_T, \tag{8}$$

was used as the basis for this analysis. Here Δq is the heat absorbed by, and Δw the work done upon, a body when strained isothermally at temperature T. Kelvin made no approximations and limited application only by stipulating reversability.

The quantity $[\partial(\Delta w)/\partial T]_T$ was expressed in the form of a Taylor's expansion in three dimensions. It was found that successive orders of terms after the second in this expansion decrease by a factor which for most metals is of order 10^2 to 10^3. Hence those beyond the quadratic were neglected. The formula arrived at was

$$\frac{\Delta q}{\Delta v} = \frac{T}{J}\Bigg\{ s[X_x+Y_y+Z_z] + \frac{\sigma}{E}\left[\frac{1}{E}\frac{\partial E}{\partial T} - \frac{1}{\sigma}\frac{\partial \sigma}{\partial T} + \frac{(1-3\sigma+5\sigma^2)s}{\sigma(1-2\sigma)}\right] \times (X_xY_y+X_xZ_z+Y_yZ_z) + \frac{1}{2E}\left[-\frac{1}{E}\frac{\partial E}{\partial T} + \frac{(1-6\sigma+2\sigma^2)s}{1-2\sigma}\right] \times (X_x^2+Y_y^2+Z_z^2)\Bigg\}, \tag{9}$$

where $J = 4.185\times10^7$ ergs/cal. mechanical equivalent of heat, s = the linear coefficient of thermal expansion, X_x = direct stress in the x direction, Y_y = direct stress in the y direction, Z_z = direct stress in the z direction, σ = Poisson's ratio, E = Young's modulus, and T = Kelvin temperature.

Trial calculations were made with the following assumed values: $\sigma = 0.3$ for steel and annealed Invar, $E = 2.01\times10^{12}$ dynes/cm^2 for steel, $E = 1.44\times10^{12}$ dynes/cm^2 for annealed Invar,[16] $s = 13.22\times10^{-6}$ (deg. C)$^{-1}$ for steel, and $s = 1.7\times10^{-6}$ (deg. C)$^{-1}$ for annealed Invar.[17] $(1/E)(\partial E/\partial T) = -24\times10^{-5}$ (deg. C)$^{-1}$ for steel,[18] $(1/E)(\partial E/\partial T) = 48.2\times10^{-5}$ (deg. C)$^{-1}$ for annealed Invar,[16,18] $(1/\sigma)(\partial\sigma/\partial T) = 1.3\times10^{-5}$ (deg. C)$^{-1}$ for steel,[18] $(1/\sigma)(\partial\sigma/\partial T) = 35.1\times10^{-5}$ (deg. C)$^{-1}$ for annealed Invar,[19] $X_x = Y_y = 27.6\times10^{-8}$ in dynes/cm^2 (40,000 lb./in.^{2}), $Z_z = 0$, and $T = 273$°K.

For a thin, spherical, annealed Invar shell, Eq. (9), with the above values, reduces to

$$\Delta q = \pm 5.1\times10^{-13} pr^3T - 2.3\times10^{-23}\times(p^2r^4T/f), \tag{10}$$

where p is the increase in internal pressure, f the wall thickness, and r the mean radius, c.g.s. units.

It is found that the linear term is much larger than the sum of the quadratic terms in Eq. (9), i.e., 120 times for steel, four times for Invar. At higher stresses this ratio decreases. The calculation assumes that Hooke's law holds. Investigation shows that the change in Eq. (9), made by assuming the elastic constants to be linear functions of the strain is, for most metals, of the order of magnitude of the quadratic terms in s. The terms in s are greatly reduced for Invar.

The discrepancies due to elastic hysteresis effects are not calculated. These were studied experimentally on the actual shells used.

Where the vessel consists of two concentric shells, the expansion taking place from the inner shell to the annular space between, each shell in turn confines the gas. As the gas leaves the inner shell the stress change there is one of decrease; whereas it is an increase for the outer shell. It is

[14] H. D. Baker, Doctor's Thesis, Library of the University of Wisconsin, Madison, Wisconsin, 1938.

[15] W. T. Thomson (Lord Kelvin), Math. Phys. Pap. **1**, 297 (1882).

[16] G. K. Burgess, Circ. Bur. Stand. No. 58, "Invar and related Nickel steels" (June 22, 1923), p. 90.

[17] See reference 17, p. 59.

[18] G. H. Keulegan and M. R. Houseman, Bur. Stand. J. Research **10**, 289 (1933).

[19] P. Chevenard, Traveaux et Memoires de Bur. Int. des Poid et Mes. **17**, 51 (1927), Fig. 21.

easily shown that for shells whose walls are "thin" the total linear effect in Eq. (9) is equal in magnitude for both shells. The two effects should then almost exactly cancel one another provided the shells are made from the same sample of material and similarly annealed.

It is found that the ratio of the magnitude of this first-order term to the energy magnitude of the quantity dealt with in the Joule effect is independent of the actual size of vessel. It is smaller, however, at lower working temperatures and larger expansion ratios. Large pressure drops are to be achieved by using the highest practical pressure in the inner chamber and the largest feasible expansion ratio. For Invar the magnitude of this linear term is minimized. It is advisable to take advantage of these means of reducing the relative and absolute magnitude of the linear term. This tends to lessen the error due to deviation from exact cancellation which may result from imperfect similarity of the two shells.

The magnitude of the quadratic terms is small. It may be computed as a correction with sufficient accuracy by using the second term of Eq. (10).

IV. THE APPARATUS

The preceding principles were applied in the apparatus shown in Figs. 1 and 2. The shells, $2\frac{1}{2}''$ diam., 0.021″ wall, and $6\frac{3}{4}''$ diam., 0.009″ wall, respectively, were made from the same sample of sheet Invar spun into hemispheres. This material possessed, besides a very small coefficient of thermal expansion S, the other required properties. It did not, however, possess the desired high thermal conductivity. To avoid oxidation the annealing, intermediate between spinning operations, was done in an atmosphere of hydrogen. The walls were reduced to uniform thickness with carborundum cloth.

A lapped seam, only slightly greater than the wall thickness and evidently of at least equal strength, was made by grinding male and female tapers to a glove fit and silver soldering. During soldering the spherical shells were filled with hydrogen; the exterior was protected by molten *fluxine*. The exterior surface of the outer shell was polished.

Before assembly of the outer shell about it, the inner shell was stretched 100 times at its yield point (100 atmos.). Volume-pressure plots measured the hysteresis effect as 0.17 joule per cycle. For air, the resulting error would not exceed 0.04 percent. Both shells were seasoned three years at 75°F.

The expansion valve between the inner and outer chambers consisted of a brass disk lapped smooth and flat carried on an airtight flexible diaphragm. A No. 3–48 screw pressed this disk against an equally flat Invar valve seat. On repeated closings the surfaces shaped themselves to mate. It has not proved possible to detect leakage past such a valve.

The inner shell had a heat capacity about three times that of the air it confined at its elastic limit; while the total heat capacity of both shells, including the valve mechanism, was only about fifteen times that of the air used in an experiment.

Six 0.005″ diam. steel piano wires with turnbuckles trussed the shells in place. The inner chamber was supplied through a 0.009″ inside diam., 0.003″ wall tube, while the outer chamber emptied through a 0.025″ inside diam., 0.005″ wall tube, both of stainless steel.

Valves in the inlet and outlet lines, necessarily without cavities, which would be parts of the two chambers, were of the same style as the expansion valve. Because these are outside the vessel their construction could be more rugged. The high pressure valve had a perforated diaphragm and packed stem, not entirely satisfactory. The diaphragm should have been airtight and adequately strong.

It was arranged for air from a storage cylinder to be filtered through a wad of oily cotton and then passed to the inner chamber through a tube cooled by liquid air. This was assumed to remove dust and condensable material. A two-liter ballast tank immersed in the main bath served to stabilize pressure as initial equilibrium was approached in the inner chamber. Pressure was measured by a Bourdon gauge with 1 mm dial graduations representing lb./in.^{2}. The usual gear drive had been replaced by a continuous metal belt, eliminating the periodic errors common in such gauges. This gauge was calibrated on an American Gauge Tester Type 1300, and on a Crosby Steam and Valve Company tester.

The central mounting plate, Fig. 2, carried all

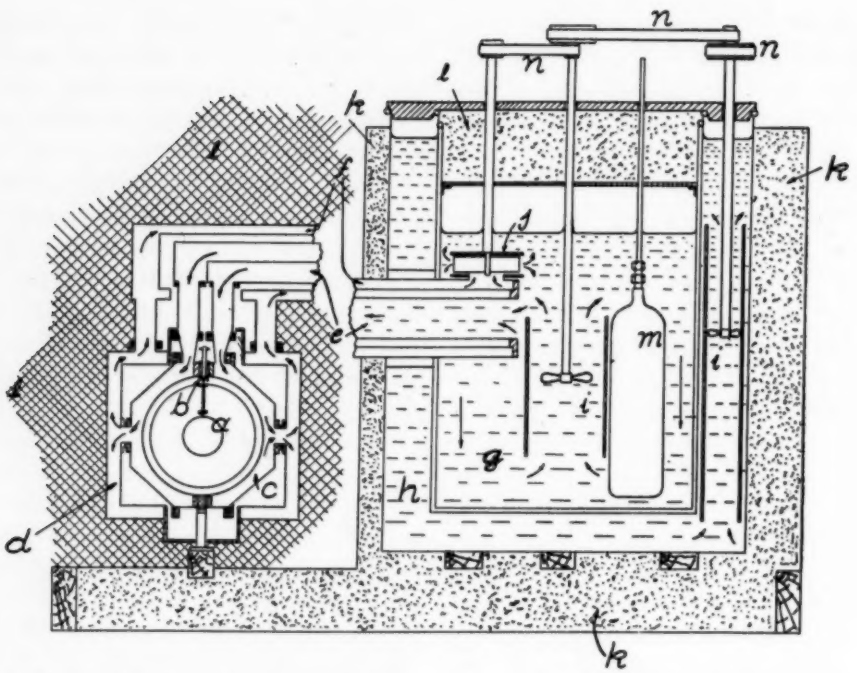

FIG. 3. Jacket and bath assembly. *a*—vessel; *b*—forked valve stem; *c*—vacuum jacket; *d*—outer jacket; *e*—flow to jacket; *f*—return flow; *g*—main bath; *h*—outer bath; *i*—propeller tubes; *j*—centrifugal circulating pump; *k*—ground cork; *l*—loose cotton; *m*—gas ballast tank; *n*—drive belts.

elements, mechanical, pneumatic, and electrical, running to the shells. The shells could thus be completely installed before the jacket was assembled about them. A stem running through this plate carried a fork to operate the expansion valve. A flat ground monel shoulder on this stem pressed against a flat ground base on the brass mounting plate. Ordinary stopcock grease proved to be an adequate vacuum seal.

The jacket was spherical, double-layered, and fed by circulation maintained from a ten-gallon, constant temperature bath. Complexity of function prevented its immersion within the bath, Fig. 3. Its inner surface was silver plated and polished. To prevent an uncontrolled change in temperature along the pipe line, this duct, 2½″ diam., was surrounded by, but insulated from, the return flow. To avoid temperature disturbance due to turbulence, the pump, of special centrifugal design, was located at the end of the return flow.

The bath was arranged for electrical heat input along the outer surface through which heat was also removed, across the air gap to an outer ice bath. The heater was equipped with a toluene bulb and Gowy regulator.[20] In the present work ice was used in the inner bath also. An ordinary propeller tube stirred each bath.

The space between the outer shell and jacket was arranged to be evacuated to about 10^{-6} mm mercury. The present preliminary work was, however, done at atmospheric pressure.

A thermopile measured the mean difference between the jacket and the outer shell temperatures. This contained 24 series connected junctions of manganin and constantan wire, No. 38 B & S gauge, distributed along two vertical great circles. These were in thermal contact with, but electrically insulated from, the outer shell. The other set of junctions was immersed in the jacket flow. The actual temperature of the jacket fluid was measured relatively to an ice point by a 12 junction thermopile of the same materials.

The metals, manganin and constantan, were chosen for their high mechanical strength, their low thermal conductivity, their high thermoelectric power, and their low temperature coefficient of resistance. A galvanometer was chosen

[20] Gowy, J. de Phys. **6**, 479 (1897).

of such sensitivity as to keep deflections on a 90 cm scale.

Unavoidably cramped conditions made insulation, adequate to resist dampness, difficult to achieve. The high humidity prevailing during the present set of readings gave rise to small, steadily drifting e.m.f.'s, probably electrolytic, and resulted in the largest error to which this work was subject.

A 6500-ohm manganin wire heater was symmetrically mounted within the vessel. The wiring was such that it was possible (see Fig. 4) to measure the resistance of this heater and the potential across its terminals without dismounting anything. The heater leads, while of negligible thermal path, have resistance small in comparison to heater resistance. The heater was used to measure the emission constant e.

All resistances (Fig. 4) and the standard cell were carefully compared with certified units. The volume of the chambers was measured by weighing against certified weights when filled with distilled water at controlled temperature. The elastic constant of the inner shell was measured. The heat capacity of both shells was found to be 0.125 cal./g deg. C.[21]

V. PROCEDURE IN A MEASUREMENT

The thermostat was set into operation and the bath circulation established. Careful tests for leaks were made. The resistance of the heater was measured. When the reading of the galvanometer in the jacket-vessel thermopile circuit became steady, it was noted, and a current of a few milliamperes started in the heater. When the galvanometer reading again became steady, it was noted again along with the current through, and the potential difference across, the heater. Then the heater current was stopped. The indicated shift in the galvanometer reading measured the rise in outer shell temperature above the jacket necessary to dissipate the steady electrical energy input. The ratio of heat input to the galvanometer deflection gives the emission constant e.

The heater was then shut off, the ballast tank filled to the chosen pressure and put in communication with the inner chamber. After a sufficient quantity of purified air had been passed through both chambers, the expansion valve was closed, the outer chamber remaining open to the atmosphere. When thermal and pressure equilibrium had been reached, the barometer and the Bourdon gauge were both read. The temperature of the jacket was also read. Both valves leading to the vessel were closed, the expansion valve was opened, and readings begun simultaneously on the galvanometer and on a clock. When (usually after about 90 minutes) the galvanometer reading showed the outer shell to be at jacket temperature, readings were stopped. It was assumed that thermal equilibrium within the outer shell had also been reached at this time. The jacket temperature was then read once more, and another determination of the emission constant made. The whole procedure required about 10 hours.

VI. REDUCTION OF DATA

The galvanometer readings were plotted against time. The area under the curve was measured with a planimeter and multiplied by the emission constant e. This product gave the

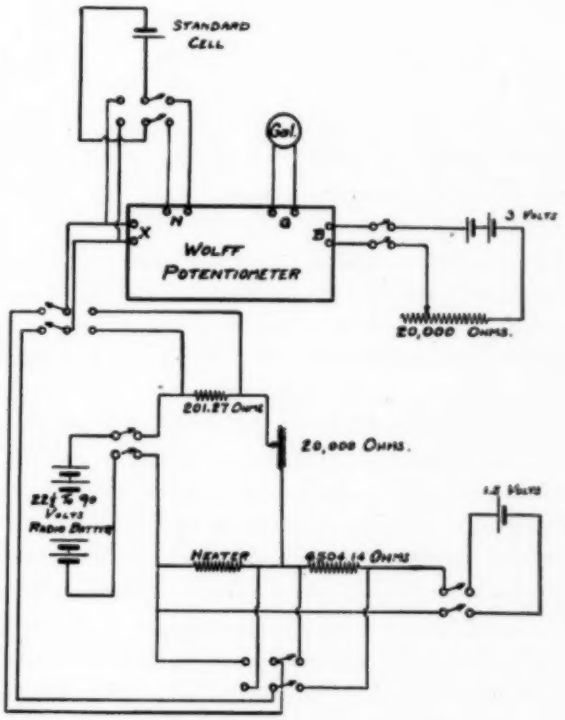

FIG. 4. Diagram of heater circuit.

[21] International Nickel Company.

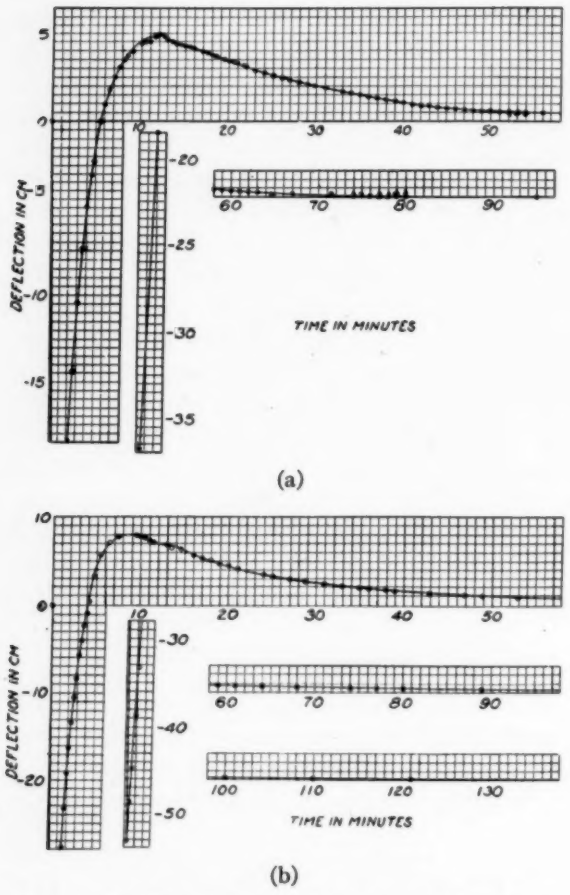

FIG. 5. Readings taken during first and fourth runs. Times in minutes from instant expansion valve is opened are plotted horizontally. Deflections in centimeters on galvanometer in thermocouple circuit are plotted vertically. Positive deflections correspond to vessel temperatures below jacket temperature; negative, above. (a) Data for the first run. (b) Data for the fourth run.

total heat transferred from the jacket to the system composed of gas and two shells.

The jacket temperature readings at the two equilibrium situations were taken to be the vessel temperatures, respectively. The heat necessary to restore the system to its initial temperature was computed by multiplying this temperature shift by the heat capacity of the shells and contained air.

Estimate of thermoelastic heat absorbed by the shells was based on Eq. (10). It was found that the magnitude of the linear term was only about 1.0 to 2.0 percent of the magnitude of energy involved in the Joule effects. The inner and outer shells were thin, made from the same sample of material, heat treated and aged in just the same way, and designed to achieve very nearly homogeneous stress in each case. Hence it was regarded a legitimate conclusion that this linear effect would cancel in the two vessels to within a very small fraction of its own magnitude. The resulting error is regarded as negligible in the present experiment.

The quadratic effect, which does not cancel, was computed as a small correction.

The amount of work done by the inner shell on the air was taken to be one-half the pressure drop times the dilatation, and similarly with the outer shell. The work done by the outer shell on the atmosphere was taken to be the pressure times the dilatation of the outer shell. The measured values of the dilatations of the inner shell were used. The dilatations of the outer shell were computed from those of the inner shell by the formula,

$$\Delta V_2=(r_2^4/r_1^4)\cdot(f_1/f_2)\cdot(P_3-P_0)/(P_1-P_2)\Delta V_1, \quad (11)$$

where

ΔV_1 = dilatation of the inner shell under pressure (P_1-P_2), Fig. 1.

ΔV_2 = dilatation of the outer shell under pressure (P_3-P_0).

Upon opening the expansion valve, n_1 moles originally in the inner chamber experience a drop in pressure, P_1-P_3, while the n_2 moles of the gas originally in the outer chamber experience a rise in pressure, P_3-P_2. The average value of λ' over the pressure range was assumed to be given by

$$\lambda'=\left(\frac{\partial u}{\partial P}\right)_T=\frac{\Delta U}{n_1(P_3-P_1)+n_2(P_3-P_2)}. \quad (12)$$

ΔU is the corrected value of the energy required to maintain constant temperature on expansion. Thus,

$$\Delta U=e\int_{t_1}^{t_2}\Delta T dt+W(\text{elastic})+Q(\text{to restore initial temp.})+Q(\text{thermoelastic}). \quad (13)$$

The effective molecular weight of air was taken to be 29.

VII. RESULTS

In the present work this sequence was repeated four times. The second run was invalidated by evidence of leakage in the valve packing while closing just before expansion, the third by evidence of drifting spurious e.m.f.'s in the thermopile. During the first and fourth runs the behavior of the apparatus appeared good in all respects. The data taken are shown plotted in Figs. 5 (a) and (b). Results are detailed in Table I.

Comparison figures are given in Table II.

VIII. CONCLUSION

The values found for λ', while probably no more precise than those previously obtained by other means, checked sufficiently well with these to establish the soundness of the present method. The errors were indicated not as fundamentally inherent in the method, but rather as common types—i.e., electrical insulation and air leaks, readily eliminated by standard methods. Other refinements are obvious, such as: thermostating the bath above room temperature to prevent moisture condensation disturbing both the jacket temperature and the electrical insulation; evacuating the space around the vessel, evacuating the outer chamber before expansion; using the highest pressure the vessel is capable of; and using a piston gauge to measure this pressure.

With these improvements perfected, there appears no obstacle to measuring λ' and λ reliably to within one-tenth of one percent. For helium and hydrogen the error would probably be greater, for carbon dioxide, less.

TABLE I. Details of results.

Quantity	Run 1	Run 4	Units
Miscellaneous			
Area under curves Fig. 5(a) and 5(b)	41.4	138.6	cm min.
Emission constant e	0.131	0.174	cal. min.$^{-1}$ cm^{-1}
Initial pressure, inner chamber	28.26	55.40	atmos.
Ditto, outer chamber	0.97	0.97	atmos.
Final pressure	2.40	3.78	atmos.
Dilatation of inner shell	0.144	0.294	cm^3
Ditto, outer	0.932	1.884	cm^3
Initial temperature	0.057	0.056	deg. C
Ditto, final	0.059	0.063	deg. C
Thermal capacity of vessel	37.00	37.00	cal. (deg. C)$^{-1}$
Ditto, contained air	1.33	2.11	cal. (deg. C)$^{-1}$
Energy Quantities			
Heat absorbed from surroundings	5.423	24.116	cal.
Work performed by the inner shell on the air during expansion	0.048	0.194	cal.
Ditto, outer shell	−0.016	−0.064	cal.
Work performed on the vessel by the atmosphere	−0.022	−0.044	cal.
Net heat liberated by the thermoelastic effect [second term, Eq. (10)]	0.012	0.048	cal.
Heat to restore initial temperature of vessel	−0.074	−0.259	cal.
Ditto, contained air	−0.003	−0.015	cal.
Total	5.368	23.976	cal.
Results			
Energy attributed to the Joule effect, ΔU by Eq. (13)	5.368	23.976	cal.
Quantity of air initially in inner chamber, n_1	0.1676	0.3253	moles
Ditto, outer, n_2	0.1038	0.1042	moles
Total air	0.2714	0.4295	moles
Pressure drop, experienced by n_1	25.86	51.62	atmos.
Ditto, rise, n_2	1.43	2.81	atmos.
λ' computed by Eq. (12) with above data	−5.367	−6.082	joules mole^{-1} atmos.$^{-1}$

TABLE II. Comparisons with other investigations.

λ' for air in joules mole^{-1} atmos.$^{-1}$	Temperature deg. C	Pressure range atmos.	Kind of data	Reference
−6.495	0.0	1.0	Measurements of Joule-Thomson coeff.	[a]
−6.453	0.0	20.0	Measurements of Joule-Thomson coeff.	[a]
−6.345	0.0	60.0	Measurements of Joule-Thomson coeff.	[a]
−5.82	28.0	0 to 40	P.V.T. measurements	[b]
−6.08	28.0	0 to 40	Calorimetric measurements	[b]
−5.367	0.06	2.4 to 28.3	Calorimetric measurements	Present work
−6.082	0.06	3.8 to 55.4	Calorimetric measurements	Present work

[a] J. R. Roebuck, Proc. Am. Acad. **64**, 334 (1930).
[b] See reference 9 in text.

IX. ACKNOWLEDGMENTS

I wish to express my wholehearted gratitude to Professor J. R. Roebuck to whom this method is due, and whose constant encouragement, criticism, and advice made its realization possible. I wish also particularly to commend E. V. Floyd who built apparatus and took readings by this method many years ago. Although his work was regarded as neither elaborate enough nor sufficiently certain to justify separate publication,[22] it served as an invaluable precedent in the present research.

I wish also to thank Mr. Robert Davies and Mr. Bernard Moss for careful assistance in the checking of calculations, Mr. Stanley Naysmith for many valuable suggestions, and Dr. M. W. Zemansky for effective help with the manuscript.

[22] J. R. Roebuck, Proc. Am. Acad. **64**, 312 (1930).

Fifth Meeting of the American Society for X-Ray and Electron Diffraction

ANN ARBOR, MICHIGAN, JUNE 7–11, 1943

THE fifth meeting of the American Society for X-Ray and Electron Diffraction was held at the University of Michigan, Ann Arbor, Michigan, June 7–11, 1943. Since this Society is an Associated Society of the American Institute of Physics, and since, moreover, the papers presented lie generally in the editorial field of *The Physical Review*, it appears appropriate and useful to publish their abstracts in the Review.

ABSTRACTS OF PAPERS PRESENTED AT THE FIFTH MEETING OF THE AMERICAN SOCIETY FOR X-RAY AND ELECTRON DIFFRACTION

1. Design of X-Ray Equipment. I. FANKUCHEN, *Brooklyn Polytechnic Institute, Brooklyn, New York.*

Because many new manufacturers are planning to produce x-ray diffraction tubes and equipment at this time, it was thought advantageous to review some of the desirable characteristics of x-ray diffraction equipment. Tubes, high tension sources, cameras, and auxiliary equipment were considered. Tubes should be designed so that the target is in a metallic grounded end of the tube. This makes it possible to bring grounded cameras in contact with the windows. Rectification of some sort is suggested. The table on which the tube is mounted should be large enough to mount Weissenberg goniometers or other large equipment and should be capable of being "cleaned up" to present a clear flat surface. Camera design on commercial apparatus should be brought up to date, suggested changes being in slit design, film mounting, and new camera types—focusing cameras, for example—should be made. Single crystal apparatus with stationary film should also be made commercially available, and goniometer head mountings should be standardized.

2. Design of Powder Cameras, J. C. M. BRENTANO, *Northwestern University, Evanston, Illinois.*

The desiderata which a powder camera for routine requirements should satisfy are: (a) ease of evaluation of the powder pattern which requires that the distances on the film should be proportionate to the deflection angles 2θ; (b) a wide angular range should be covered with one single exposure; (c) relative intensities should be independent of the particular shape of the specimen or of its absorption coefficient; (d) short exposure times. Point (c) arises out of the requirements of the identification method. Point (d) which is irrelevant for structure analysis is important where x-ray methods are on a competitive field with other analytical procedures. The Debye-Hull method complies with (a) and (b), it is unfavorable for (c) except by diluting the specimen to a point where the exposure times become excessively long. It is also unfavorable for (d) because of the necessity of using narrow beams. Wide angle beams can be used when the powder particles are located on a surface which satisfies the property that rays deflected from any point through a given angle establish between two points an object to image relation. For a point source such a surface is a toroid which has as generatrix the arc of a circle which goes through the origin and the point of collection of the diffracted beam. The properties of this surface have been discussed by the writer.[1] Approximations to this surface which will satisfy a range of θ values are obtained either by disposing the powder in form of a cylindrical ring which forms an equatorial band to the toroid,[2] or by a cylindrical strip taken longitudinally to the toroid.[3] Both these devices give large intensities. Neither satisfies condition (a). While the longitudinal strip is more favorable with regard to point (b), the equatorial strip satisfies (c) when used with an ionization method. Both are unfavorable under (c) for photographic recording. By rotating a powder surface in conjunction with a diaphragm the focusing condition of the toroid can be satisfied in succession for a film disposed round the axis of rotation of the powder surface.[4] This arrangement complies with (a), (b), and (c). By making use of a surface of double curvature incident beams of considerable angular aperture can be used.[5] Reasonably sharp lines can then be obtained covering an angular range 2θ of 110° without rotating diaphragm with very short exposure times. The back reflection method for which beams with small angular apertures generally are used can be developed into a very rapid method by making it conform with the requirements of the focusing condition. The photographic film is arranged on a cylinder while the powder is in a spherical holder. With this arrangement I could take records in the large angle region with exposures of the order of 2 ma hours. This arrangement does not conform with (a), but the operation of correction is that of the stereographic projection. It does only approximate condition (c). In a general way with geometrically similar cameras and slit systems, intensities and sharpness are both independent of the camera size. The additional spreading of the lines due to the penetration into the layer and diffusion in the photographic film have a lesser relative effect with large cameras. Two kinds of calibration are carried out. One is intended to correct for errors of machining. It is generally easier to avoid faults by careful designing than to correct them by calibration since the limit of mechanical accuracy exceeds that of measuring distances on a film. The other

type of calibration refers to faulty positioning of the individual powder specimen. These corrections are very relevant; they require the admixture of a standardizing substance and increase the exposure times. We found it convenient to reduce the necessity for such corrections by using jigs in preparing the specimens. The non-uniform contraction of the photographic film and the Ross and Eberhard effects make it more desirable to place fiducial reference marks on the film rather than to locate the film by means of one-sided shadow marks. The full use of large aperture beams depends on suitable tubes with which it is possible to approach the anticathode much closer than with the commercial tubes at present available. Use could also be made of tubes with greater output with correspondingly increased cathode spots.

[1] J. C. M. Brentano, Arch. Sci. Phys. Nat. **44**, 66 (1917).
[2] J. C. M. Brentano, Arch. Sci. Phys. Nat. [6] **1**, 550 (1919).
[3] H. Seeman, Ann. Phys. **59**, 455 (1919); H. Bohlin, *ibid.* **61**, 421 (1920).
[4] J. C. M. Brentano, Proc. Phys. Soc. **37**, 184 (1925).
[5] J. C. M. Brentano, Proc. Phys. Soc. **49**, 61 (1937).

3. X-Ray Studies of Preferred Orientations. C. S. BARRETT, *Carnegie Institute of Technology, Pittsburgh, Pennsylvania.*

The practical importance of preferred orientations lies in their relation to the variation of properties with direction in engineering materials. In sheet metals, for instance, preferred orientation is one of the causes of directionality that may lead to failure of the sheets when they are being drawn or pressed. Beneficial orientations have been induced in steel used for transformer cores so that electrical transformers of today are better and cheaper than those of a few years ago. Investigators in this field have found it convenient to describe the observed orientations by naming the crystal axes or planes that lie parallel to the principal axes of strain in the metal. This use of "ideal orientations" is, however, somewhat arbitrary and incomplete, and for the most part is displaced by the use of "pole figures" which are stereographic projections of the distribution of crystal axes in space. A pole figure is constructed from a series of x-ray photographs of a specimen tilted in a series of angular positions, or from a film exposed in an oscillating-crystal, oscillating-film camera of special design. Particular care must be taken when constructing the pole figure of a metal with large grains, for the x-ray photographs may not contain enough spots to show small degrees of preferred orientations. It is sometimes advisable to substitute optical goniometer measurements on individual grains for the usual x-ray technique. The origin of preferred orientations has received much study and may be said to be rather well understood in the case of cold-worked metals, but remains very little understood in the case of recrystallized metals. Orientations in iron and steel after uniaxial compression and after rolling illustrate the complexities that may be encountered. Grains possessing certain original orientations remain pseudo-single crystals after the most severe deformation, while others subdivide into "deformation bands" that rotate individually to different final positions. More complex forms of distortion may also be encountered in some grains of rolled material, with the result that the entire pole figure may be reproduced within a single deformed grain. Aluminum, as well as many other metals, also exhibits deformation bands. G. I. Taylor's theory of the origin of the preferred orientation in aluminum after compressive deformation has been tested and found to be in reasonable accord with the statistical behavior of the grains although it fails to predict the direction of rotation of many of the individual grains. Inhomogeneous flow probably accounts for the discrepancy. Preferred orientations after recrystallization may resemble those in the cold-worked metal from which they grew, or they may differ, or preferred orientations may be absent. They are controlled by controlling hot-working, cold-working, and annealing schedules, metal purity, alloy composition, and amount of cross-rolling or other deformation. Developments have almost invariably come through cut-and-try methods because few principles are yet known concerning the fundamental mechanism controlling the orientations.

4. The Gold-Silver Tellurides. GEORGE TUNELL, *Geophysical Laboratory, Washington, D. C.*

The gold-silver tellurides, sylvanite, krennerite, and calaverite, constitute a group of minerals closely related chemically and morphologically. Sylvanite and calaverite belong to the monoclinic, and krennerite to the orthorhombic, system. The chemical composition of sylvanite is close to $AuAgTe_4$, the atomic ratio of gold to silver of crystallographically studied material being about 1.15. The chemical composition of krennerite and calaverite may be written $(Au, Ag)Te_2$; in krennerite the atomic ratio of gold to silver in analyses by K. J. Murata of material studied crystallographically by the present writer varies from 4.07 to 3.56, and in calaverite the variation in investigated crystals is from 54.2 to 6.6. The atomic arrangement in all three minerals is such that each gold or silver atom is surrounded by six tellurium atoms on a somewhat distorted octahedron. In sylvanite and calaverite each tellurium atom is surrounded by three gold or silver atoms and three tellurium atoms on distorted octahedra; in krennerite, however, the tellurium atoms are in part surrounded by three gold or silver atoms and three tellurium atoms, in part by one gold or silver atom and five tellurium atoms, and in part by five gold or silver atoms and one tellurium atom, all on distorted octahedra. The structural determinations were carried out by the use of equi-inclination Weissenberg photographs and powder photographs. The three minerals crystallize in three different space groups, but are basically similar structurally. A Fourier analysis was made in each case to confirm the parameter values obtained by the comparison of observed and calculated intensities. Oriented polished surfaces of representative crystals of all three minerals were examined under the reflecting microscope to establish their homogeneity.

5. Diffraction Effects Accompanying Some Ordering Reactions. D. HARKER, *General Electric Company, Schenectady, New York.*

It is found that three stages in the ordering reaction by which the face-centered cubic solid solution of composition

AuCu changes to the tetragonal AuCu structure can be recognized by their x-ray diffraction patterns. They are: (1) the stage during which the (004) reflection of the cubic lattice vanishes (and other intensity changes occur), (2) the stage during which the reflections of the cubic lattice broaden and separate into reflections characteristic of a tetragonal lattice, and (3) the stage during which lines appear whose presence is forbidden by an all-face-centered lattice. These phenomena are explained on the basis of a mechanism of ordering involving the following assumptions: (1) The ordering of a small region in a single crystal of the solid solution gives rise to pressures, tensions, and shears in the neighboring disordered material which induce the formation of other ordered regions near the original one in such orientations as to minimize the total strain in the system. (2) The ordered regions eventually arrange themselves more or less regularly on a simple cubic lattice whose axes parallel those of the solid solution crystal and whose axial length is of the order of a few hundred times as large as the a_0 of the disordered structure. (3) The mutual orientation of the ordered regions is such that all the regions in a layer parallel to one of the {111} planes of the disordered structure have their c axes parallel to one of the original cube edges, and succeeding layers have c axes parallel to the other original cube edges, in rotation. The foregoing structural assumptions are in agreement not only with the x-ray diffraction effects, but also with the microscopic appearance of polished specimens, and the changes of mechanical properties during the reaction. It is proposed to use the x-ray diffraction effects, when possible, as criteria for the identification of an ordering reaction, as distinguished from a precipitation.

6. X-Ray Study of Solid Soap Phases. R. H. FERGUSON, *Procter and Gamble, Ivorydale, Ohio.*

There are four crystalline phases (alpha, beta, delta, omega) which appear in solid soaps, although only three of them exist in the usual commercial bar soaps. Soap properties are influenced by the phases present in the final product and by the related factors of crystal size, coherence, etc. Changes in crystal phase, and to some extent the changes in liquid crystalline and pseudo-crystalline phases, can be followed by means of the x-ray diffraction pattern. The crystalline soap phases are best characterized and identified by certain short spacings, but the long spacings are useful in studying solid solution and hydrate formation.

7. The Relation of Crystal Habit to Space Group. J. D. H. DONNAY, *Hercules Powder Company Experiment Station, Wilmington, Delaware.*

One of the challenging problems of crystallography is the correlation of the external form of crystals with their internal structure. Recent developments in this field are reviewed: the Baumhauer-Ungemach form series in zone development, Peacock's "Harmonic-Arithmetic Rule," the generalization of the Law of Bravais, and the method of space-group determination by morphological analysis. The relationships between crystal habit and space group are fully discussed for the isometric system. The determination of the aspect (and hence, of the possible space groups) is illustrated by the following orthorhombic cases: epsomite and chalcomenite ($P2_12_12_1$); krennerite (*Pbm*); cannizzarite and danburite (*Pnam*); hambergite, scorodite, brookite, strengite, and sulfamic acid (*Pbca* or *Pcab*); hemimorphite (*Imm*); natrolite (*Fdd2*); thenardite (*Fddd*); diaphorite (*Cmma*); stephanite (*Cmc2*); cordierite (*Cmcm*); gallium (*Abma*).

8. X-Ray and Electron Diffraction Examination of Colloidal Materials. W. O. MILLIGAN, *Rice Institute, Houston, Texas.*

In this paper there are summarized the results of recent x-ray and electron diffraction studies on inorganic colloidal materials, such as the hydrous oxides and the colloidal salts. Numerous earlier investigators deduced from older and less direct techniques that many of these colloidal materials consisted of complex compounds or mixtures of series of such complex compounds. Contrary to these earlier views, the application of x-ray and electron diffraction methods leads to the following conclusion concerning the constitution of many inorganic colloids: In general, the hydrous oxides and colloidal salts consist of minute, crystalline particles of simple oxide or hydrated oxide, and simple salts. Numerous colloidal materials have been examined in the form of air-dried gels, moist gels, and as colloidal particles in the sol state. Among the various substances discussed in this paper are the hydrous oxides of aluminum, titanium, iron, vanadium, gallium, scandium, indium, and several rare earths, and colloidal salts such as zeolites, basic cupric sulfates, arsenic trisulfide, copper sulfides, and a number of heavy metal iron cyanides.

9. The Electron Microscope in an X-Ray Diffraction Laboratory. GEORGE L. CLARK AND MARTHA BARNES BAYLOR, *Noyes Chemical Laboratory, University of Illinois, Urbana, Illinois.*

The usefulness of the electron microscope as a supplementary instrument in a laboratory long devoted to x-ray and diffraction investigations is illustrated by a number of examples. One of the principal fields is the correlation of colloidal particle size and shape as directly observed from electron micrographs and as calculated from diffraction patterns. Not only does the electron microscope overlap other methods in range of resolution, but it also affords types of data which are unique to it. It is able to differentiate particle size in the range from 10^{-4} to 10^{-6} cm in materials; This is not possible from x-ray patterns. Details of particle shape and the placement of particles in relation to each other also can be studied directly. Thus, it is applied in the study of carbon blacks, insecticides, limes, pigments, rubber fillers, soils, catalysts, polishing rouges, etc. Absolute measurements from micrographs must still be made with reservations though comparative observations are reliable. The measurement of large protein molecules such as hemocyanin offers confirmatory results to other techniques such as the ultracentrifuge as it has in such studies as the orientation of fibrils within the

animal cell (sperm) as demonstrated previously by x-ray diffraction. Limitations of the electron microscope such as necessity of complete drying, extreme thinness of specimens, disruptive effects of electron beam, etc., must still be recognized though it is certain that some of these will be eliminated through further development of the instrument.

10. Ambiguities in X-Ray Analysis. A. L. PATTERSON, *Department of Physics, Bryn Mawr College, Bryn Mawr, Pennsylvania.*

The structure factor used in x-ray analysis does not depend directly on the positions of the atoms in the lattice but only on the vector distances between the atoms. X-ray analysis taken alone is therefore only capable of determining these distances and can give no other structural information. Two cases[1] were previously known in which the vector distances did not determine the structure. In the present paper it is shown that there are many such cases and a few of the simplest are discussed in detail. Most of these new cases arise from the consideration of arrangements of points on the line in which the distances between the points are integral sub-multiples of the period, but the ambiguous cases are by no means confined to these special locations. It is shown that each of the cases which arise on the line has its counterpart on the plane and in space.

[1] L. Pauling and M. D. Shappell, Zeits. f. Krist. 75, 128 (1930). A. L. Patterson, Nature 143, 939 (1939).

11. X-Ray Techniques in the Quartz Oscillator Industry. W. PARRISH.

12. X-Ray Structural Study of a Series of Related Polyhalides. ROSE C. L. MOONEY, *Newcomb College, New Orleans, Louisiana.*

Though all of the alkali metals and ammonium form tri-halides and higher polyhalides in solution, it has been shown that only ammonium, rubidium, and cesium form solid, unsolvated tri-iodides at temperatures above 25°. These tri-iodides give off iodine on standing, and revert to the mono-iodides. The stability of the compounds increases with increasing cation size. Our x-ray structural study began with the determination of the crystal structure of the isomorphous rubidium and ammonium tri-iodides, and resulted in a measurement of the size and configuration of the tri-iodide anion group. For a more extensive study of the manner in which these complex ions form crystal lattices, a longer and more stable series was required. The work of Dawson, and of Chattaway and Hoyle suggested that the quaternary ammonium salts formed such a series. Our experiments have corroborated the fact that a series of solid, unsolvated tri-iodides, stable to high temperatures, can easily be prepared from the mono-iodides of alkyl-substituted ammonium. Penta-iodides of tetramethyl and of tetraethyl ammonium have also been prepared in stable crystalline form. The existence of such compounds has been considered hypothetical by some workers. As a preliminary to x-ray study, quantitative analyses of the products were made, first by Miss A. A. Reitdijk, University of Leiden, and recently by Miss Lillian Naihaus, Newcomb College. Since the samples to be tested were dry, stable crystals, straightforward methods of iodine determination were used to find the percentage of iodine. Having determined, from the crystal structure of ammonium and rubidium tri-iodides, that the tri-iodide anion is a linear group with a spacing of 2.85A between iodines, the series of tri-iodides formed by the quaternary ammonium cations were investigated by x-rays. Each of these salts, namely, the tetramethyl, tetraethyl, tetrapropyl and tetrabutyl ammonium tri-iodides has a different space group. The tetramethyl and tetraethyl tri-iodide crystals are orthorhombic (the tetraethyl being pseudo-tetragonal, and erroneously reported as tetragonal in Groth); the tetrapropyl ammonium tri-iodide is monoclinic, and the tetrabutyl ammonium tri-iodide is triclinic. Though the symmetry of the lattice is thus changed by the introduction of increasingly larger cation groups, the essential features of the tri-iodide structure remain the same; that is to say, the cation groups occupy planes which are interleaved with planes containing tri-iodide groups. Only the end iodines are co-ordinated with the cations, the central iodine being isolated. An interesting monovalent cation group, tetraphenyl arsonium, first made by Blicke, and further studied by Willard and his associates, forms a tri-iodide so stable and so insoluble as to be useful in detecting small concentrations of iodine. A complete structure determination has been made of the iodide and of the tri-iodide of tetraphenyl arsonium. The structures of two "mixed" trihalides have been determined; the tetramethyl ammonium dichloriodide and ammonium chlorobromoiodide. The iodine occupies the central position in the linear groups in each case. The determination of the structure of potassium tetrachloriodide resulted in the measurement of the first pentahalide anion group. Here the central iodine forms four co-planar bonds extending toward chlorines at the corners of a square. The iodine-chlorine distances are 2.34A. The structure studies of the penta-iodides of tetramethyl and of tetraethyl ammonium have not yet been completed. The indications are that the iodines are associated in a penta-iodide group.

13. Recent Developments in the Electron Microscope. V. K. ZWORYKIN AND J. HILLIER, *RCA Manufacturing Company, Camden, New Jersey.*

During the past year, considerable development work has been done on the various optical components of the electron microscope. The effect on the specimen illumination of the electron gun focusing has been calculated. The results show that for some adjustments of the electron gun, the condenser of a conventional microscope exerts practically no control over the illuminating beam. The resolving power of an electron microscope objective has been investigated thoroughly with and without a physical limiting aperture. It was found that for heavy specimen particles the resolving power was roughly twice as good with a limiting aperture as it was without. The best resolving power obtained was 24A. The distortion of the final image

caused by the projection lens errors has been investigated, and methods for greatly reducing this distortion have been found. A small magnetic electron microscope has been developed. The resolving power obtained at present exceeds 50A. This instrument uses no condenser lens while the objective and projection lenses are incorporated in a single magnetic circuit excited by a single regulated current supply. Internal photography is used although, because of the small volume, no air locks are necessary.

14. An Evaluation of the Sector Technique as Applied to the Diffraction of Electrons by Gases. S. H. BAUER, *Cornell University, Ithaca, New York.*

After working for some time with a rotating sector interposed in the path of a diffracted beam of electrons, for purposes of eliminating the steep decline in the background portion of the pattern, we found that although it is a simple matter to obtain sharpened maxima and minima, the technique becomes troublesome if accurate, intensity measurements are desired. Full development of this procedure is therefore justifiable only when structures cannot be determined by means of the visual technique. For those cases which we desire to investigate, namely internal rotation in molecules and mixtures of gases, the components of which react with one another, accurate radial distribution functions are needed and hence reliable intensity measurements must be made. Further, it can be shown that for small values of $s(=4\pi(\sin\theta/2)/\lambda)$, computation of the diffraction pattern can be made only roughly unless the molecular form factors are known. These also can be estimated to the necessary accuracy using the sector technique . The apparatus we developed is briefly described, and we indicate the modifications which need to be made in existing electron diffraction units to permit the use of a rotating sector. Methods of correcting for extraneous radiations, the question of sector construction, and the host of errors which creep into the procedure are discussed. The consequence of such a careful analysis for each particular molecule is a diffraction pattern with a flat background; the molecular form factor is immediately obtained. In cases of known structures the intensities of the peaks then permit one to deduce the variation of coherent and incoherent scattering factors for atoms to very low values of s, data which cannot be obtained from x-ray diffraction studies. Accurate radial distribution curves may then be constructed, and in the case of mixtures the final pattern may be analyzed into the patterns produced by the individual components.

AUTHOR INDEX TO ABSTRACTS OF PAPERS PRESENTED AT THE FIFTH MEETING OF THE AMERICAN SOCIETY FOR X-RAY AND ELECTRON DIFFRACTION

Barrett, C. S.—No. 3
Bauer, S. H.—No. 14
Baylor, Martha Barnes (see Clark, George L.)—No. 9
Brentano, J. C. M.—No. 2

Clark, George L. and Martha Barnes Baylor—No. 9

Donnay, J. D. H.—No. 7

Fankuchen, I.—No. 1
Ferguson, R. H.—No. 6

Harker, D.—No. 5
Hillier, J. (see Zworykin, V. K.)—No. 13

Milligan, W. O.—No. 8
Mooney, Rose C. L.—No. 12

Parrish, W.—No. 11
Patterson, A. L.—No. 10

Tunell, George—No. 4

Zworykin, V. K. and J. Hillier—No. 13

Letters to the Editor

PROMPT publication of brief reports of important discoveries in physics may be secured by addressing them to this department. The closing date for this department is the third of the month. Because of the late closing date for the section no proof can be shown to authors. The Board of Editors does not hold itself responsible for the opinions expressed by the correspondents. Communications should not in general exceed 600 words in length.

On a Stellar Model Built in Complete Accordance With Bethe's Formula of Energy-Generation

N. R. SEN AND U. R. BURMAN
Department of Applied Mathematics, University of Calcutta, Calcutta, India
October 11, 1943

BETHE'S scheme of energy-generation within stars of the main sequence type, produced by the so-called "carbon-cycle" requires a temperature of about 20 million degrees. Such stars should have small convective cores within which it is natural to suppose that nearly the whole energy-generation takes place.

The general trend has hitherto been to impose surface conditions on the star, in the shape of assigning the observed values of L (luminosity), M (mass), and R (radius), and to integrate the stellar equations of equilibrium from the boundary inwards. Proceeding in this line, Blanch, Lowan, Marshak, and Bethe[1] have worked out a model for the sun, but although a convective core with almost the entire energy generated inside it has been obtained, the total luminosity is in disagreement with the energy-generation formula by a factor 100.

The problem can be attempted from the other side. A preliminary investigation has been made to find what types of core, with a central temperature of 20 million degrees, a H_2-content (X) of 35 percent, a He-content (Y) zero, and average molecular weight unity, strictly conform to Bethe's formula. Two cores are to be distinguished, namely, a convective core within which the transfer of energy is mainly by convection, and an energy core within which the whole of the energy is generated according to Bethe's formula. It is found that for a central density $\rho_c < 31$ g/cm³, there is no convective core, the transfer of energy being entirely by radiation; for ρ_c between 31 and 51 g/cm³, there is a convective core, but generally this is smaller than the energy core; for $\rho_c \geqslant 51$ g/cm³ the model is entirely convective (there being no radiative envelope). These remarks apply to cores only when no attention is paid to the surface conditions of the star.

The significant value of ρ_c which gives a convective-radiative model true to the surface conditions $\rho \to 0$, $T \to 0$, simultaneously, is ~ 47 g/cm³. The energy core then is slightly greater than the convective core. The model worked out with Bethe's formula has the following characteristics:— $M \sim 2\times10^{33}$ g, $R \sim 6\times10^{10}$ cm, $L \sim 3\times10^{33}$ ergs/sec., $T_c = 2\times10^{7}$ K, $\rho_c \sim 47$ g/cm³, $X = 0.35$, $Y = 0$. Further the convective core, within which 94 percent of the total energy is generated, encloses about 10 percent of the total mass, and occupies nearly 17 percent of the radius of the star. The remaining 6 percent of the energy generated within the radiative envelope has not been ignored in course of integration. This model, in spite of its close agreement with the sun in respect to the mass, differs from it in respect to radius and luminosity by 20 percent and 15 percent, respectively, but it is in perfect agreement with Bethe's energy-generation formula. The luminosity may, however, be made to agree more closely with the solar value by a slight increase in the value of T_c, the composition remaining unaltered, but the significant value of ρ_c will in that case be expected to be a little lower than 47 g/cm³. It will be noted that for given composition and central temperature there exists (if at all) one and only one central density, furnishing a significant solution (Vogt-Russel theorem). The general characteristics described above are typical of central temperatures near about 20 million degrees.

In the present calculations radiation pressure has been neglected, and Kramers' opacity formula with Strömgren's table of guillotine factors has been used. Further Bethe's formula has been taken in the form[1] $\epsilon = 3\times10^{21}\cdot X\cdot\rho\cdot\zeta^{2}e^{-\zeta}$, where $\zeta = 152/\tau^{\frac{1}{3}}$, τ being in millions of degrees.

[1] Blanch, Lowan, Marshak, and Bethe, Astrophys. J. **94**, 37 (1941).

A Note on the Mesotron Temperature Coefficient

F. A. BENEDETTO, S.J.*
Department of Physics, Fordham University, New York, New York
October 23, 1943

IN a previous paper[1] it was indicated that in computing average atmospheric temperatures for the purpose of obtaining the mesotron temperature coefficient (α), the *mass* average temperature $T = \int\theta dp/\int dp$ is to be preferred to the *spacial* average temperature $\bar{\theta} = \int\theta dh/\int dh$. From a comparison[2] of various temperature coefficients determined from spacial average, mass average, and temperatures *at* various levels, it will be observed that the temperature coefficient for large columns of air (12 to 16 km), as obtained by the spacial average method, is considerably higher than that obtained by the mass average method, whereas for small columns the difference between the two methods is relatively not so great.

The two values of particular interest for this note are the values $\alpha = 0.40\pm0.02$ percent per degree C obtained by using ground temperatures, and $\alpha = 0.46\pm0.03$ when mass temperatures of the lower 4/5 atmosphere are used. These values, obtained by vertical counter train, are considerably higher than those obtained by non-directional ionization chambers, and hence it was decided after overhauling the apparatus to repeat the counter measurements. For the period of January to August, 1943, by using mass average temperatures of the 4/5 fraction, we obtained $\alpha = 0.49\pm0.08$, which is substantially in agreement with our earlier values.

Rossi[3] lists values of α as obtained by counter trains and by ionization chambers, and it appears significant

that two of the three observations of Barnóthy and Forró using counter trains give values for α of 0.42 and 0.46, respectively. The discrepancy between the observations by counter train and by ionization chamber may be due to one or more of the following considerations:

(1) The greater screening in the telescopes affords better discrimination against the soft, zero temperature coefficient, electron component, and therefore the telescope records greater percentage variations than does the less shielded ionization chamber.

(2) For a given local temperature the ionization chamber records fluctuations of cosmic-ray intensity due to variations of temperature over large surrounding areas; under certain conditions these fluctuations may depress the value of the "true" temperature coefficient.

(3) Rathgeber[4] suggests that the mesotron spectrum is principally composed of a hard component $\sim 3\times 10^9$ ev originating at altitudes of 17 km or greater, and a softer component $\sim 2\times 10^8$ ev originating at 6 km or lower. On this assumption it can be shown that oblique rays will have a smaller temperature coefficient than vertical rays. The altitude of the 100−50 mb isobars ($\sim$16−20 km) is practically constant, and hence the hard mesotrons originating at or above these levels are insensitive to temperature variations. The percentage of hard mesotrons being greater for oblique rays, the total percentage variation registered by ionization chamber will be smaller and hence will lead to a smaller value for α than that obtained by vertical counter train. It would certainly appear worth while to make a comparative investigation of the temperature effect by the use of vertical and inclined counter trains.

Grateful acknowledgment is made to Professor V. F. Hess for valuable suggestions, to Professor W. F. G. Swann of the Bartol Foundation, and to the Penrose Fund of the American Philosophical Society for aid in repairs.

* Now at St. Mary's College, St. Marys, Kansas.
[1] V. F. Hess and F. A. Benedetto, Phys. Rev. 60, 610 (1941).
[2] F. A. Benedetto, G. O. Altmann, and V. F. Hess, Phys. Rev. 61, 266 (1942).
[3] B. Rossi, Rev. Mod. Phys. 11, 296 (1939).
[4] L. Rathgeber, Phys. Rev. 61, 210 (1942).

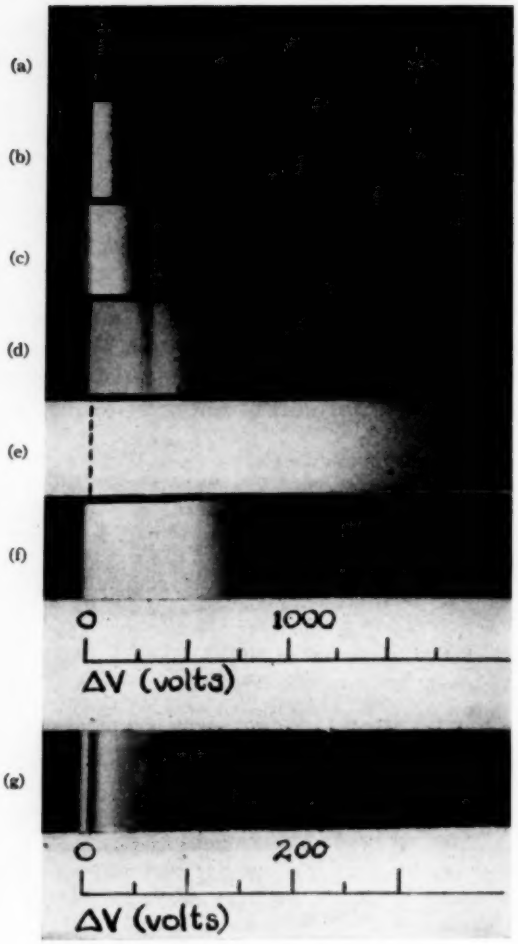

FIG. 1. Velocity distribution of electrons. (a) Specimen—collodion membrane; incident electron energy—47.5 kev; exposure—0.1 second; emulsion—Eastman Tri-X Panchromatic. This analysis shows the line due to the electrons which have been transmitted with their original velocity and a continuous distribution of electrons which have lost small amounts of energy in inelastic collisions with electrons of outer shells; most probable energy loss, 24 ev. (No attempt was made in the testing of the instrument to obtain precision measurements though the values obtained are all within ±5 percent of the values predicted from x-ray data.) (b) Specimen—evaporated beryllium film on collodion; inc. electron energy—47.5 kev; exp.—0.5 sec.; emulsion—Tri-X Panchromatic. Line due to the *K* level of Be appears at 135 ev. (c) Specimen—collodion membrane; inc. electron energy—47.5 kev; exp.—0.5 sec. (printed light); emulsion Tri-X Panchromatic. Line due to *K* level of C appears at 290 ev. (d) Specimen—collodion membrane; inc. electron energy—28.0 kev; exp.—3 min.; emulsion—Tri-X Panchromatic. Lines due to the *K* levels of C, N, and O appear at 290, 400, and 550 ev, respectively. (e) Specimen—evaporated aluminum film on collodion; inc. electron energy—28.0 kev; exp.—40 min.; emulsion—medium lantern slide. The weak line due to the *K* level of Al is indicated at 1600 ev. (f) Specimen—evaporated film of iron on collodion; inc. electron energy—28.0 kev; exp.—10 min.; emulsion—medium lantern slide. Line due to the *L* level of Fe appears at 730 ev. (g) Specimen—iron film; inc. electron energy—28.0 kev; exp.—2 sec.; emulsion—medium lantern slide; photographic enlargement—30×. Negative was translated parallel to line during print exposure to eliminate photographic grain. A line, presumably due to an *M* level of Fe, appears at 57 ev. A second line appears at 44 ev, but has not yet been identified.

On Microanalysis by Electrons

JAMES HILLIER
RCA Laboratories, Princeton, New Jersey
November 3, 1943

RECENTLY, using 7.5-kilovolt electrons and an electron-velocity analyzer of a focusing half-circle magnetic type, G. Ruthemann[1-3] has investigated the velocity distribution in the electrons transmitted by thin collodion membranes. He found that the number of electrons suffering discrete energy losses of 298, 400, and 546 ev corresponding to the excitation of the *K* level of C, N, and O was sufficient to produce observable peaks in the velocity distribution curve.

In the present work it has been the intention of the author to investigate the possibility of extending the detection of this phenomenon to heavier elements and of using it for making an elemental analysis of extremely small regions of electron microscope specimens. In the instrument[4] designed for the purpose a minute area of the specimen is irradiated by an electron probe formed by a

two-stage magnetic lens system. The electrons transmitted by the irradiated area of the specimen are focused by a third magnetic lens so that the probe is reformed at the slit position of a homogeneous field magnetic analyzer of the half-circle type. The analyzed velocity distribution is recorded photographically. By turning off the deflecting field of the analyzer and properly adjusting the probe, the instrument is converted immediately into an electron microscope of the shadow type,[5] by means of which the area of the specimen being analyzed can be accurately located and identified. In its present stage of development the apparatus can be used with 15- to 50-kilovolt electrons; the analyzer gives a measured resolving power of $\Delta V/V$ of 1/4300 while the resolving power of the probe is approximately 0.3μ. The regulation of the power supplies is slightly better than that of a conventional magnetic electron microscope enabling exposures of as long as one hour to be made.

In testing the instrument the work of Ruthemann has been repeated with higher electron velocities. The velocity losses due to the excitation of the K levels of carbon, nitrogen, and oxygen were observed in thin collodion membranes; that of nitrogen being barely detected (Fig. 1c, 1d). In the case of light elements the exposure time was a fraction of a second for the photographic emulsions and the electron beam intensities used. The K-level excitations of beryllium, aluminum, and silicon have been detected, but the last two were found to be quite weak and to require exposure times of around half an hour on Eastman Medium Lantern Slides (3 minutes on Eastman Kodak Tri-X Panchromatic) (Fig. 1b, 1e). The K-level excitation of iron could not be detected, but the L level was quite sharp and strong (Fig. 1f). A line, presumably due to an M-level excitation, was also observed in a short exposure on the iron specimen (Fig. 1g). In all of these tests thin films of the sample material were used. Qualitatively the velocity analysis obtained appeared to be independent of the probe diameter. The quantity of material irradiated in each of the above tests was between 10^{-14} and 10^{-16} g.

The author wishes to thank Dr. V. K. Zworykin, Associate Director of RCA Laboratories, for his active interest and many suggestions. The analyses of beryllium and silicon were obtained by Dr. R. F. Baker.

[1] H. Voges and G. Ruthemann, Zeits. f. Physik **114**, 709–718 (1939).
[2] G. Ruthemann, Naturwiss. **29**, 648 (1941).
[3] G. Ruthemann, Naturwiss. **30**, 145 (1942).
[4] Tentatively named, "Electron Microanalyser."
[5] H. Boersch, Zeits. f. tech. Physik **20**, 346–350 (1939).